INSTITUTE OF CHEMICAL TECHNOLOGY PRAGUE

Faculty of Chemical Engineering

Department of Chemical Engineering

MASTER THESIS

STUDY OF THE RIVULET TYPE FLOW OF THE LIQUID ON THE INCLINED PLATE

Author: Bc. MARTIN ISOZ

Supervisor: ***Ing. František J. Rejl, Ph.D.***

Study program: *Process engineering and Informatics*

Area of study: *Chemical engineering, Bioengineering and Mathematical modeling of processes*

Year: **2013**

This thesis was written at the Department of Chemical Engineering of the Institute of Chemical Technology in Prague and at the Institute of Thermal, Environmental and Natural Products Process Engineering of TU Bergakademie Freiberg from July 2012 to May 2013.

I hereby declare that this thesis is my own work. Where other sources of information have been used, they have been acknowledged and referenced in the list of used literature and other sources. I have been informed that the rights and obligations implied by Act No. 121/2000 Coll. on Copyright, Rights Related to Copyright and on the Amendment of Certain Laws (Copyright Act) apply to my work. In p articular, I am aware of the fact that the Institute of Chemical Technology in Prague has the right to sign a license agreement for use of this work as school work under §60 paragraph 1 of the Copyright A ct. I have also been informed that in the case that this work will be used by myself or that a license will be granted for its usage by another entity, the Institute of Chemical Technology in Prague is en titled to require from me a reasonable contribution to cover the costs incurred in the creation of the work, according to the circumstances up to the full amount.

I agree to the publication of my work in accordance with Act No. 111/1998 Coll. on Higher Education and the amendment of related laws (Higher Education Act).

In Prague on .....

Title: Study of the rivulet type flow of the liquid on the inclined plate

Abstract: The industrial importance of distillation and raising popularity of structured packings bring up an immediate need for better understanding of hydrodynamic processes occurring in the packed columns. Because of the both geometrical and behavioral complexity of counter current liquid and gas flows through an element of structured packing, the simplification of the problem to a rivulet flow down an inclined plate was proposed motivating both theoretical and experimental study of such an arrangement. The main goal of the work was to propose yet unexisting simple model for predicting the size of a rivulet gas-liquid interfacial area which is crucial for the mass transfer calculations.

The experiments were performed at TU Bergakademie Freiberg. Using an optical technique, it was possible to study gas-liquid interface during the rivulets flowing down an inclined plate. The software was developed providing a possibility of easy and on site evaluation of the experimental data.

The experimental work was completed by a thorough study of the current state of theoretical understanding of the problematics of liquid spreading. Based on this study, a model for calculation of gas-liquid interfacial area size of a rivulet was proposed.

The derived model was successfully validated against the obtained experimental data and its limits of applicability were found.

Název práce: Studium potůčkového toku kapaliny po nakloněné desce

Abstrakt: Průmyslová důležitost rektifikace, stejně tak jako rostoucí popularita strukturovaných výplní jsou silnými motivátory studia hydrodynamiky tekutin v plněných kolonách. Protiproudý tok kapaliny a plynu skrze segment výplně je systémem s příliš složitým chováním i geometrií na to, aby mohl být studován přímo. V prezentované práci bylo navrženo zjednodušení tohoto problému až na chování toku kapaliny typu potůček po nakloněné desce. V tomto zjednodušení mohla být provedena jak experimentální, tak teoretická zevrubná studie problému vedoucí k návrhu doposavad neexistujicího výpočetně nenáročného modelu pro odhad velikosti mezifázové plochy tekoucího potůčku. Takto odhadnuté velikosti plochy mezifázového rozhraní mohou být dále využity pro výpočty spojené s přestupem hmoty.

Měření byla prováděna na TU Bergakademie Freiberg a byla založena na využití optické techniky umožňující studium mezifázového rozhraní kapalina-plyn potůčku stékajícího po nakloněné desce. V průběhu měření byl také vyvinut software umožňující rychlé zpracování dat přímo v laboratoři.

Experimenty byly doplněny studií současného stavu znalostí problematiky roztékání kapalin. Na základě této studie byl následně navrhnut model pro výpočet velikosti mezifázové plochy potůčku.

Odvozený model byl úspěšně testován oproti získaným experimentálním datům a byly stanoveny meze jeho použitelnosti.

Dedication: I would like to thank my supervisor, Ing. František J. Rejl, Ph.D. for the patience, guidance and support throughout my period of study. Next, I would like to gratefully acknowledge the possibility of spending the summer 2012 at TU Bergakademie Freiberg provided by Prof. Dr.-Ing. habil. Jens-Uwe Repke and the time he reserved for mutual visits and consultations of the studied problematics. Also, I would like to express my gratitude towards M.Sc. André Marek, the author of used experimental apparatus and my guide during my stay at Freiberg. Last, but not at least, I would like to thank all my other coworkers and friends from the Mass transfer laboratory of Chemical engineering department at ICT Prague.

Contents

List of Figures vi

List of Tables ix

1 Introduction 1

2 Theory 2
2.1 Coordinate system and basic notations . . . 2
2.2 Steady rivulet . . . 3
2.2.1 Navier-Stokes equations . . . 3
2.2.2 Model of Towell and Rothfeld . . . 4
2.2.3 Model of Duffy and Moffat . . . 5
2.3 Droplet spreading . . . 7
2.3.1 Basic surface thermodynamics . . . 7
2.3.2 Description of the droplet spreading . . . 8
2.3.3 Huh and Scriven's paradox . . . 9
2.3.4 Spreading dynamics of a drop . . . 10
2.3.5 Proposed calculation method . . . 14
2.4 Rivulet spreading . . . 15
2.4.1 Spreading of a oil stripes on a horizontal substrate . . . 15
2.4.2 Spreading of a point source with neglected contact line effects . . . 16
2.4.3 Contact line movement in case of a spreading rivulet . . . 17
2.5 Calculation of the size of gas-liquid interfacial area of a rivulet . . . 18
2.5.1 Interfacial area size of rivulet with fixed contact lines . . . 18
2.5.2 Interfacial area size of rivulet with moving contact lines . . . 19

3 Experiments 24
3.1 Experimental set up description . . . 24
3.1.1 Measuring technique . . . 24
3.1.2 Carried out experiments . . . 25
3.1.3 Process scheme . . . 25
3.1.4 Experimental set up options and problems . . . 27
3.1.5 Measurement procedure . . . 28
3.2 Measured quantities . . . 28
3.2.1 Gas-liquid interface shape evolution along the plate . . . 28
3.2.2 Size of the gas-liquid interfacial area . . . 29
3.2.3 Local width and height . . . 29
3.2.4 Local mean speed and Reynolds numbers . . . 29
3.2.5 Local contact angles . . . 30

4 Data evaluation program description 31
4.1 Flow cell finding algorithm . . . 33
4.2 Plate finding algorithm . . . 33
4.3 Rivulet distinction and interfacial area size calculation . . . 33

5 Results and Discussion **35**
5.1 Experimental results . . . 35
5.1.1 Experimental study of the gas-liquid interface shape . . . 35
5.1.2 Measured sizes of the gas-liquid interfacial area . . . 38
5.1.3 Measured contact angles . . . 40
5.1.4 Measured widths, heights and their ratio . . . 43
5.1.5 Measured Reynolds numbers . . . 45
5.1.6 Summary of experimental results . . . 47
5.2 Theoretical results and their comparison and fitting to measured values . . . 48
5.2.1 Initial condition for the equation (2.84) . . . 48
5.2.2 The case of silicon oils . . . 48
5.2.3 The case of water . . . 51

6 Conclusions **53**

7 List of symbols **54**

8 Bibliography **57**

A Surface curvature **61**
A.1 Surfaces . . . 61
A.2 Curvature tensor invariants . . . 62

B Young equation derivation **64**

C Derivation of the thin film governing equation **65**
C.1 One dimensional case . . . 65
C.2 Three dimensional case . . . 68

D Data evaluation program documentation **71**
D.1 RivuletExpDataProcessing.m . . . 73
D.1.1 Description of the program . . . 75
D.2 findEdges.m . . . 75
D.2.1 Description of the algorithm . . . 76
D.2.2 Subfunctions . . . 81
D.3 rivuletProcessing.m . . . 84
D.3.1 Description of the algorithm . . . 84
D.3.2 Subfunctions . . . 87
D.3.3 Created files . . . 95
D.4 postProcPlotting.m . . . 99
D.4.1 Description of the algorithm . . . 99
D.4.2 Subfunctions . . . 102
D.5 Other functions . . . 102
D.5.1 treshInflStudy.m . . . 102
D.5.2 fitIFA.m . . . 103

E Experimental results **105**

F Theoretical results **110**

G Contents of the attached DVD **111**

List of Figures

2.1 Used coordinate system with the basics of rivulet spreading notation. α is the plate inclination angle, β and β_m are the apparent and microscopic contact angles, a is the rivulet half width. 2
2.2 Mechanical force balance on the three-phase contact line, graphical interpretation of the Young's equation 7
2.3 Sketch of advancing contact line. In the chosen frame of reference, the contact line is stationary and the solid moves to the right with velocity $\dot{R}$. 9
2.4 Schematic of procedure for continuum modeling, inspired by [5]. 14

3.1 Scheme of used experimental set up. 24
3.2 Liquid circulation scheme. 26
3.3 Front view of the measurement cell - inclined plate. 26

4.1 31

5.1 Comparison of measured rivulet surfaces before (left) and after processing, DC 10 oil, $\alpha = 75\,^\circ$, $Q = 0.18 \cdot 10^{-6} m^3\, s^{-1}$ 35
5.2 Measured profile shapes along the plate for silicon oil DC 05, $\alpha = 60\,^\circ$ and $Q = 0.24 \cdot 10^{-6}\,\mathrm{m^3\,s^{-1}}$. 37
5.3 Comparison of profile shapes of water and tenzids at 15 cm from the plate top for $Q = 5.77 \cdot 10^{-6}$ and $\alpha = 45\,^\circ$. 37
5.4 Measured S_{g-l}, DC 10 oil, influence of the plate inclination angle. Mean values with errorbars are depicted. 38
5.5 Measured S_{g-l}, $\alpha = 52\,^\circ$, different liquids. Mean values with errorbars are depicted. 39
5.6 Comparison of measured apparent contact angles measured from the left side of the rivulet for different liquids, $Q \sim 0.56 \cdot 10^{-6}\,\mathrm{m^3\,s^{-1}}$, $\alpha = 45\,^\circ$. . . . 40
5.7 Measured values of apparent contact angle from the left side of the rivulet for different Q along the plate. DC 05 oil, $\alpha = 45\,^\circ$. Mean values with errorbars are depicted. Liqud flow rates in $Q \cdot 10^{-7}\,\mathrm{m^3\,s^{-1}}$ are specified in graph legend. 41
5.8 Comparison of apparent contact angles measured from the left and right side of the rivulet for different liquids and flow rates. Liquid type and volumetric flow rate in $Q \cdot 10^{-6}\,\mathrm{m^3\,s^{-1}}$ are specified in plot legend. Plate inclination angle is the same for all the data, $\alpha = 45\,^\circ$ 42
5.9 Study of absolute error introduced into calculation by assumption $\tan\beta \approx \beta$ 42
5.10 Mean values of measured rivulet widths along the plate for silicon oil DC 10, $\alpha = 45\,^\circ$. Liqud flow rates in $Q \cdot 10^{-6}\,\mathrm{m^3\,s^{-1}}$ are specified in graph legend. 43
5.11 Mean values of measured rivulet heights along the plate for silicon oil DC 10, $\alpha = 45\,^\circ$. Liquid flow rates in $Q \cdot 10^{-6}\,\mathrm{m^3\,s^{-1}}$ are specified in graph legend. 44
5.12 Rivulet centerline height to width ratio for different liquids. $\alpha = 60\,^\circ$, $Q \sim 0.56 \cdot 10^{-7}\,\mathrm{m^3\,s^{-1}}$. 45

5.13 Comparison of Re_{max}, Re_{l_c} and Re_a for DC 10 oil, $\alpha = 60\,^\circ$ and $Q = 0.57 \cdot 10^{-6}\,\mathrm{m^3\,s^{-1}}$. 46
5.14 Reynolds numbers calculated from $\langle u_{exp} \rangle_i$ and l_c for different liquids and $\alpha = 60\,^\circ$. Liquid types and flow rates in $Q \cdot 10^{-6}\,\mathrm{m^3\,s^{-1}}$ are specified in graph legend. 47
5.15 Comparison of measured and calculated rivulet widths, $2a$, for both silicon oils and different plate inclination angles 49
5.16 Comparison of predicted and measured values of S_{g-l} for fitted l and l equal to threshold of experimental data evaluation procedure. DC 05 oil, $\alpha = 60\,^\circ$ 50
5.17 Comparison of predicted and measured values of apparent contact angle, β. DC 05 oil, $\alpha = 45\,^\circ$, $Q = 4.90 \cdot 10^{-6}\,\mathrm{m^3\,s^{-1}}$ 50
5.18 Comparison of predicted and measured values of S_{g-l} for water, for different plate inclination angles. The fitted parameters were in both cases, $l = 4.3 \cdot 10^{-5}\,\mathrm{m}$, $\Phi = 0.389$ 51
5.19 Comparison of predicted and measured values of S_{g-l} for tenzids, for different plate inclination angles. The fitted parameters were in both cases, $l = 3.3 \cdot 10^{-5}\,\mathrm{m}$, $\Phi = 0.624$ 52

C.1 One dimensional free surface problem 65

D.1 Scheme of the main program window 73
D.2 Scheme of the main program execution process 74
D.3 Preprocessed experimental image, it is clear that flow cell and plate are of completely different graphic nature 76
D.4 Right side of the experimental image with found flow cell. In the magnified area is shown the idea between the sum of dot products. 77
D.5 Scheme of the flow cell finding algorithm 78
D.6 Scheme of the plate finding algorithm 79
D.7 GUI of the program for changing image processing parameters 83
D.8 Scheme of the `rivuletProcessing` function algorithm 86
D.9 Calibration flow cell used for conversion of grayscale values in the images in the film thickness 88
D.10 Main elements identified by the `'simple'` algorithm 91
D.11 Principle of the of the $(g) - (l)$ interfacial area size calculation 92
D.12 GUI of the program for changing experimental set up parameters 95
D.13 Example of file created into *Profiles* folder 97
D.14 Scheme of the `postProcPlotting` function algorithm and corresponding GUI elements 100
D.15 Example of the threshold influence on results study 103
D.16 Example of the current state of the `fitIFA.m` function 104

E.1 Measured profile shapes along the plate for Water (upper) and tenzids, $\alpha = 60\,^\circ$ and $Q = 1.6 \cdot 10^{-6}\,\mathrm{m^3\,s^{-1}}$. 105
E.2 Mean values of measured rivulet widths along the plate for DC 05 silicon oil, $\alpha = 45\,^\circ$. Liquid flow rates in $Q \cdot 10^{-6}\,\mathrm{m^3\,s^{-1}}$ are specified in graph legend. 106
E.3 Mean values of measured rivulet widths along the plate for water, $\alpha = 45\,^\circ$. Liquid flow rates in $Q \cdot 10^{-6}\,\mathrm{m^3\,s^{-1}}$ are specified in graph legend. 106
E.4 Mean values of measured rivulet widths along the plate for tenzids, $\alpha = 45\,^\circ$. Liquid flow rates in $Q \cdot 10^{-6}\,\mathrm{m^3\,s^{-1}}$ are specified in graph legend. 107
E.5 Mean values of measured rivulet heights along the plate for DC 05 silicon oil, $\alpha = 45\,^\circ$. Liquid flow rates in $Q \cdot 10^{-6}\,\mathrm{m^3\,s^{-1}}$ are specified in graph legend. 107

E.6 Mean values of measured rivulet heights along the plate for water, $\alpha = 45\,^\circ$. Liquid flow rates in $Q \cdot 10^{-6}\,\mathrm{m^3\,s^{-1}}$ are specified in graph legend. 108
E.7 Mean values of measured rivulet heights along the plate for tenzids, $\alpha = 45\,^\circ$. Liquid flow rates in $Q \cdot 10^{-6}\,\mathrm{m^3\,s^{-1}}$ are specified in graph legend. 108
E.8 Rivulet centerline height to width ratio for DC 10 silicon oil, $\alpha = 45\,^\circ$. Liquid flow rates in $Q \cdot 10^{-6}\,\mathrm{m^3\,s^{-1}}$ are specified in graph legend. 109
E.9 Dependence of Re_{max} on the plate inclination angle, α, for DC 10 silicon oil. The part of the curve corresponding to measured α's is in the enhanced area. 109

F.1 Comparison of simulated (left) and measured gas-liquid interface of a DC 10 rivulet, $\alpha = 52\,^\circ$, $Q = 0.42 \cdot 10^{-6}\,\mathrm{m^3\,s^{-1}}$. 110

List of Tables

2.1 A list of mechanisms that have been proposed to relieve the dynamical singularity near the contact line along with representative references. Taken from [5]. 10

3.1 Used liquids properties at $T = 298.15$ K 25

5.1 Re_{max} for different fluids and plate inclination angles 46

D.1 List of files of RivuletExpDataProcessing program 71
D.2 Mandatory fields in `handles` when calling `findEdges` 75
D.3 Mandatory fields in `handles` when calling `rivuletProcessing` 85
D.4 Outputs of the `rivuletProcessing` function 85
D.5 Files created during the `rivuletProcessing` function execution 96
D.6 Example of file created in one of the *Height*, *Speed* or *Width* folders 98

1. Introduction

Distillation is the most important and widely used separation process. With the extensive development of the oil industry in the last century the process achieved maturity. Originally performed in the tray columns the performance of vacuum applications was vastly enhanced by invention of structured packing and its widespread usage in 70's and 80's.

Despite considerable effort of chemical engineers in the past 50 years, distillation design is mostly empirical and new units are built mostly on the basis of known performance of the older ones [1]. This approach brings serious problems ever when any change in the process is necessary. Any safety over design of the units is undesirable because of pressure-drop concerns especially in the vacuum applications.

Rigorous modeling of the distillation consists of modeling of the phase equilibrium, hydrodynamics and interfacial transport phenomena. Hydrodynamic behavior of the liquid is important for the generation of the effective interfacial area, which is one of the most important interface transport parameters.

Character of the liquid phase flow can be generally divided into the three different categories [2,3]: (i) film flow, (ii) rivulet flow, (iii) formation and fall of the droplets. Structured packing with their construction from the metal sheets naturally tends to the formation of the films, which is further supported by texture on the surface. Nevertheless, for the lower liquid flows and higher surface tension of the liquid, rivulet type of the flow can be anticipated.

In principle, fluid flow can be modeled using CFD software. The geometry of the structured packing is rather complicated, still [4], and the interaction of the liquid with the solid surface is even more challenging [5]. Dynamic behavior of the surface-liquid-gas interface is not a resolved problem and its modeling is still under the development. Therefore the behavior must be studied experimentally and the constructed models must be carefully verified against the experimental results.

For study of the flow character and liquid spreading the optical methods are most appropriate. These methods cannot be used for the structured packing element and simplification is necessary. An inclined steel sheet has been suggested as a useful simplification for the experimental purposes. Such experimental apparatus has been designed and utilized at the TU Freiberg.

To complete the experimental study, theoretical analysis of the problem of calculation of gas-liquid interfacial size of a rivulet was carried out. The previous solutions to the problem of rivulet flow on an inclined plate made with an assumption of fixed contact lines [6,7] were studied as well as the liquid spreading properties [5,8] and currently available solutions to the rivulet spreading problem [9–12]. Then, the parallel was made between spreading of static shapes in time and spreading of the rivulet along the space and used to obtain an approximative model for rivulet interfacial area size calculation.

At the end, to fulfill the main goal of the work, derived relations were used to fit experimental data.

2. Theory

Up to now, there were many studies on the problem of rectilinear rivulet flow down an inclined plate. However, there are still almost no results published on the subject of the rivulet spreading along it. Although this state is acceptable from the point of view of the rivulet hydrodynamics (mainly because the liquid velocity is much higher in the plate longitudinal direction than in the others), from the point of view of the size of gas-liquid interfacial area calculation, it poses quite a problem, because gas-liquid interfacial area size, S_{g-l}, can change quite radically with the rivulet spreading.

In the first section of this chapter, some of the published models of the steady, uniform rivulet will be presented. In the second, will be described problematic of the droplet spreading on the flat, wetted plate. Then, in the third section, current models for the liquid spreading over an inclined plate will be presented. Finally, in the last part of this chapter, there will be presented an analogy between the spreading of the droplet in time and spreading of the rivulet along the plate.

2.1 Coordinate system and basic notations

Throughout the work, there is always the same coordinate system used (with some exceptions in the Data evaluation program description and documentation parts caused by the „historical“ reasons.

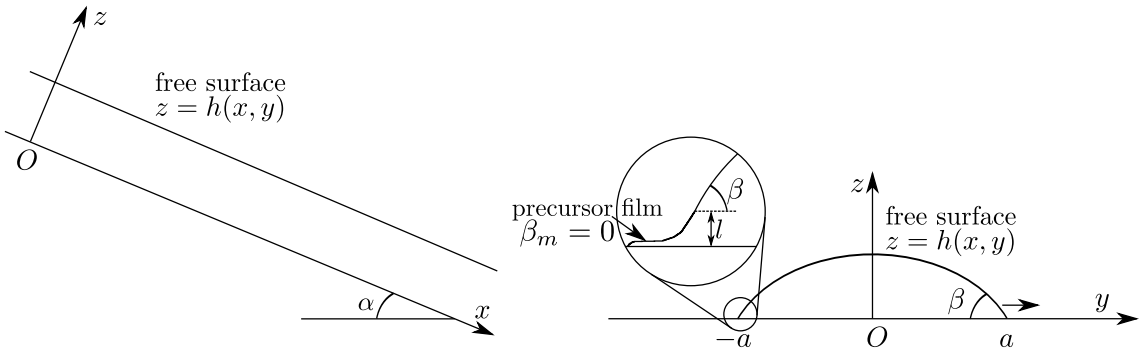

Figure 2.1: Used coordinate system with the basics of rivulet spreading notation. α is the plate inclination angle, β and β_m are the apparent and microscopic contact angles, a is the rivulet half width.

.

For easier orientation in the text, the basic symbols and notation are presented in the following text and in Figure 2.1.

The used coordinate system was Cartesian with x as longitudinal, y as transversal plate coordinates and z coordinate normal to the plate. The velocity elements are noted as u in x, v in y and w in z direction respectively. For description of the rivulet free surface, there was used Monge parametrization [13], $z = h(x,y)$. The letter a then stands for the rivulet half width.

Notation of the plate inclination angle, α and the apparent contact angle of the rivulet, β was established accordingly to [7] and completed by introducing the microscopic contact angle, β_m. The intermediate region length scale [5] was noted as l.

2.2 Steady rivulet

Rivulet flow occurs, when the liquid flow rate is to low to sustain a continuous liquid layer over the whole surface or nearby a spring liquid source [14]. When the liquid flow rate is reduced even more, the rivulet breaks into dropwise flow. Up to now, the problematic of the rivulet flow was already studied extensively, but always with quite severe simplifications.

One group of scientists, represented for example by Towell and Rothfeld [6], Duffy and Moffat [7] and others [15–17] used the assumption of steady (not moving) contact lines, whilst the others did not take the contact lines into account at all (Shetty [9]) or assumed steady, not moving trickle (McHale *et al.* [11]), which has the same geometry as the rivulet but none of its flow characteristics.

On the other hand, although the theoretical description of rivulet flow on the inclined plate is currently far from complete, there are some CFD methods and algorithms providing relatively accurate and not as time consuming modeling possibilities. For details, especially on so called volume-of-fluid (VOF) method, see for example [18–21] and many others.

In the following sections, there will given brief description of the pioneering work of Towell and Rothfeld [6], followed by somehow more thorough notes on Duffy's modification of it [7], motivated by its use in the presented work. The case of spreading rivulet will be studied in section 2.4.

2.2.1 Navier-Stokes equations

$$\rho\frac{D\mathbf{u}}{Dt} = -\nabla p + \mu\nabla^2\mathbf{u} + \rho\mathbf{F} \tag{2.1}$$

The set of well known Navier-Stokes equations (2.1) describing the motion of fluid substances can be, in case of the rivulet flow significantly simplified introducing the following assumptions:

1. Incompressible Newtonian liquid with constant viscosity and surface tension coefficient.
2. Only acting body force ($\rho\mathbf{F}$) is the gravity.
3. One dimensional flow ($v = w = 0$).
4. Steady state.
5. No shear at the gas-liquid interface.

In case of these simplifications, the equations (2.1) can be rewritten as:

$$0 = -\frac{\partial p}{\partial x} + \mu\left(\frac{\partial^2 u}{\partial y^2} + \frac{\partial^2 u}{\partial z^2}\right) + \rho g\sin\alpha \tag{2.2}$$

$$0 = -\frac{\partial p}{\partial y} \tag{2.3}$$

$$0 = -\frac{\partial p}{\partial z} - \rho g\cos\alpha. \tag{2.4}$$

According to the thin film theory [22,23], it is possible to reduce the equation (2.2) to

$$0 = -\frac{\partial p}{\partial x} + \mu\frac{\partial^2 u}{\partial z^2} + \rho g \sin\alpha \tag{2.5}$$

and integrate equations (2.5),(2.3) and (2.4) subject to boundary conditions:

$$\begin{aligned} z &= 0, \quad u = 0 && (2.6)\\ z &= h(y), \quad p - p_{\mathrm{A}} = -\gamma\frac{\mathrm{d}^2 h}{\mathrm{d}y^2} && (2.7)\\ & \qquad \frac{\partial u}{\partial z} = 0 && (2.8)\\ y &= \pm a, \quad h = 0 && (2.9)\\ & \qquad \frac{\mathrm{d}h}{\mathrm{d}y} = \pm\tan\beta && (2.10) \end{aligned}$$

In the equations above, p_{A} stands for atmospheric pressure, μ for the liquid dynamic viscosity, γ for its surface tension coefficient, ρ for its density and g for the gravitational acceleration. The rest of the symbols is explained in the section 2.1.

Please note, that the equation (2.7) is description of the continuity of stresses at free surface, with the viscosity of the air neglected and with an assumption of nearly flat surface, in which case, $\kappa \approx 1/2\nabla^2 h$ (the term of mean surface curvature, κ, is explained more in detail in Appendix A).

The velocity profile in x direction, u, can be obtained easily by integrating the equations above. The resulting relation is then:

$$u(y,z) = \frac{\rho g \sin\alpha}{2\mu}(h(y)z - z^2) \tag{2.11}$$

and expression of the volumetric liquid flow rate is as follows:

$$Q = \int_{-a}^{a}\int_{0}^{h(y)} u(y,z)\mathrm{d}z\mathrm{d}y \tag{2.12}$$

2.2.2 Model of Towell and Rothfeld

Towell and Rothfeld presented their pioneering work on the rivulet flow hydrodynamics [6] in 1966. They divided the problem of finding the shape of gas-liquid interface in three different parts. With capillary length defined as $l_c = \sqrt{\gamma/\rho g\cos\alpha}$, ϱ_0 as radius of mean curvature at rivulet centerline and $\Psi(y) = (h(0) - h(y))/l_c$, they can be denoted as:

1. Limiting case of small rivulet, with small radius of mean curvature and thus

$$l_c/\varrho_0 \gg \Psi. \tag{2.13}$$

2. Limiting case of wide, shallow rivulet, with

$$l_c/\varrho_0 \ll \Psi. \tag{2.14}$$

3. General solution of the problem.

The velocity profile equation (2.11) becomes, using the Ψ function defined above:

$$u(y,z) = (\Psi_0 - \Psi)z - \frac{1}{2}z^2 \tag{2.15}$$

Towell and Rothfeld proposed an equation for the gas-liquid interface based on the mean surface (curve actually, as it is a one dimensional problem) curvature:

$$\frac{\Psi''}{(1+\Psi'^2)^{\frac{3}{2}}} = \frac{l_c}{\varrho_0} + \Psi, \tag{2.16}$$

where $'$ stand for derivation with respect to y. The boundary conditions for this second order differential equation are $\Psi = 0$ and $\Psi' = 0$ at $x = 0$ (assumption of symmetric profile with defined height at centerline).

In the first case, the member Ψ can be neglected on the right side of the equation (2.16) and it can be directly integrated. The shape of the interface is then uniquely defined by liquid flow rate (see i.e. (2.12)) and apparent contact angle, β.

In the second case, it is the term l_c/ϱ_0, that can be neglected and it can be easily shown, that the maximal depth of liquid, $\Psi_0 = 2\sin\beta/2$. After inserting this into equation (2.15), integrating (2.12) and solving the resulting equation, one can obtain, once again, the width of rivulet as function of liquid flow rate and the apparent contact angle.

In the case of general solution for the intermediate region, when none of the terms on the right side of equation (2.16) can be neglected, one can integrate this equation by noting, that

$$\Psi'' = \Psi' \frac{\mathrm{d}\Psi'}{\mathrm{d}\Psi}. \tag{2.17}$$

And rewrite it as

$$\frac{\Psi' \mathrm{d}\Psi'}{(1+\Psi'^2)^{\frac{3}{2}}} = \left(\frac{l_c}{\varrho_0} + \Psi\right) \mathrm{d}\Psi. \tag{2.18}$$

Integrating it one time with initial condition $\Psi' = 0$ at $\Psi = 0$ (which obvious from the initial conditions of the original problem), the following result is obtained:

$$\frac{1}{\sqrt{1+\Psi'^2}} = 1 - \frac{l_c}{\varrho_0}\Psi - \frac{1}{2}\Psi^2. \tag{2.19}$$

This equation can be, through the substitution $\{\hat{\Psi} = l_c/\varrho_0 + \Psi, \hat{\Psi} = l_c/\varrho_0 \text{ at } y = 0\}$, solved for $\hat{\Psi}$, transformed to an elliptical integral for y, reducible to standard forms (for details, see [6] and [24]).

Through this, one obtains implicitly defined shape of the interface, yet it is also uniquely specified by the liquid flow rate and the liquid-solid contact angle. However, this definition of $h(y)$, even though more precise than the others (namely the one for wide, flat rivulet) is not very suitable to be used in other calculations due to its complexity and the fact, that explicit relation cannot be obtained for $h(y)$.

2.2.3 Model of Duffy and Moffat

In their work on steady, uniform rivulet hydrodynamics [7], Duffy and Moffat are solving the same problem as Towell and Rothfeld in [6]. However, they aim to obtain results in a form somehow more useful for later calculations.

Duffy and Rothfeld used for representation of the free surface directly the Monge representation (see Appendix A). In this case, they obtained the velocity field $\mathbf{u} = u(y,z)$ directly as described in equation (2.12).

They concerned themselves with the plate inclination angle, α as defined in Figure 2.1, varying between 0 and π and divided the obtained solution in three parts, for $\alpha \in \langle 0, \pi/2)$(i), $\alpha = \pi/2$(ii) and $\alpha \in (\pi/2, \pi\rangle$(iii) respectively.

As for the shape of the gas-liquid interface, they have taken the assumption of nearly flat rivulet with surface curvature taken as h'', where $'$ stands for derivation with respect

to y. Thus, $h'' = 2\kappa$, with κ as the mean surface curvature defined in Appendix A. This simplification allowed them to obtain explicit solutions for the free interface profile shape for the whole range of studied plate inclination angles. However, always with assumption of the wide, flat rivulet.

The main difference between the three studied cases is in the influence of gravity on the profile shape. In the first case, the gravity tends to flatten the rivulet, in the second, it has no effect on its shape and in the last case, the resulting profile shape is more sharp than segment of circle.

For the brevity in writing the solution, it is useful to define the Bond number as:

$$\mathrm{Bo} = \frac{a}{l_c}, \tag{2.20}$$

Where a is the rivulet half width, as defined in Figure 2.1 and l_c is the liquid capillary length, with the same meaning as in the previous text, only with the $\cos\alpha$ taken in its absolute value.

With this, the pressure field obtained for three cases can be written in the terms,

$$p(z) = p_\mathrm{A} - \rho g \cos\alpha + \tan\beta l_c \Upsilon_p, \tag{2.21}$$

with p_A being the atmospheric pressure and

$$\Upsilon_p = \begin{cases} \coth \mathrm{Bo} & \text{(i)} \\ \mathrm{Bo}^{-1} & \text{(ii)} \\ \cot \mathrm{Bo} & \text{(iii).} \end{cases}$$

Note: For the case (ii), $\alpha = \pi/2$, the Bond number is equal a zero and equation (2.21) is not formally right. However, with an easy modification, one can see, that the effects of $|\cos\alpha|$ are canceled with α limiting to $\pi/2$.

With the following partial non-dimensionalization

$$\bar{h} = \frac{h}{l_c} \tag{2.22}$$

$$\xi = \frac{y}{a}, \tag{2.23}$$

$$\tag{2.24}$$

the equations for the rivulet profile can be given in the following form:

$$\bar{h} = \tan\beta \Upsilon_h, \tag{2.25}$$

with Υ_h defined as:

$$\Upsilon_h = \begin{cases} (\cosh \mathrm{Bo} - \cosh \mathrm{Bo}\xi)/\sinh \mathrm{Bo} & \text{(i)} \\ \mathrm{Bo}(1-\xi^2)/2 & \text{(ii)} \\ (\cos \mathrm{Bo}\xi - \cos \mathrm{Bo})/\sin \mathrm{Bo} & \text{(iii).} \end{cases}$$

For the cases (i) and (iii), the profile shape is defined by the liquid flow rate Q and the contact angle β implicitly, but in the case (ii), the explicit solution can be obtained:

$$p(z) = p_\mathrm{A} + \frac{\gamma}{a}\tan\beta \tag{2.26}$$

$$h(y) = \frac{\tan\beta}{2a}(a^2 - y^2) \tag{2.27}$$

$$h_0 = \frac{a}{2}\tan\beta \tag{2.28}$$

$$a = \left(\frac{105\mu Q}{4\rho g \tan^3\beta}\right)^{\frac{1}{4}} \tag{2.29}$$

Apart of the presented models, the problem of rectilinear rivulet flow was up to now thoroughly studied. From other theoretical works on the subject, one can mention for example [16] or [25] for the flow on an inclined plate, [15] for vertical plate and many others.

2.3 Droplet spreading

Study of wetting and spreading properties of liquids on solids has become one of the classic problems of hydrodynamics, statistical physics and material chemistry. Liquid-on-solid behavior is of key importance for many applications. At large scales, wetting or non-wetting plays an important role in oil recovery and the efficient deposition of pesticides on plant leaves, and also in the drainage of water from highways and the cooling of industrial reactors. On a smaller scale, wetting solutions have been proposed to solve technological problems in microfluidics and nanoprinting, inkjet printing, etc [5]. Other possible application, would be the wetting of package elements in structured packings. However, this last subject has not been, up to authors knowledge, studied at all.

In the following text, first some basics of surface thermodynamics are described, next, the dynamic problem of reaching the equilibrium state in case of small droplet spreading is studied and the famous Huh-Scriven paradox, *not even Herakles could sink a solid*, [26] is mentioned and explained. Finally the problem of matching the interface shape between the microscopic and macroscopic scales is introduced and a dependence of the apparent contact angle, β, on time is given for the spherical geometry (dynamic droplet spreading).

2.3.1 Basic surface thermodynamics

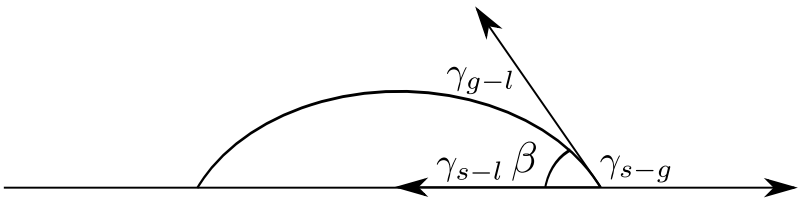

Figure 2.2: Mechanical force balance on the three-phase contact line, graphical interpretation of the Young's equation

.

Let us consider a drop of incompressible, non-volatile, Newtonian liquid on a horizontal solid surface. There are three different phases and therefore three different surface tensions to be considered. The situation schematics is shown in Figure 2.2.

The surface tensions to be considered are: solid-liquid, γ_{s-l}, gas-liquid, γ_{g-l} and solid-gas, γ_{s-g}. The relation between them and the liquid-solid equilibrium, apparent contact angle, β_{eq} is given by Young equation,

$$\gamma_{s-g} = \gamma_{s-l} + \gamma \cos \beta_{eq}, \tag{2.30}$$

where $\gamma = \gamma_{g-l}$, which will simplify the future writing of the problem. The Young equation is schematically derived in Appendix B. For more thorough derivation, see for example [27].

As all three surface tensions are usually not known (and are not measurable with the same accuracy), equilibrium spreading coefficient, Ξ_{eq} is defined for practical use as follows:

$$\Xi_{eq} \equiv \gamma_{s-g} - (\gamma_{s-l} - \gamma) = \gamma \left(\cos \beta_{eq} - 1\right). \tag{2.31}$$

There can be distinguished three different states of wetting. The first one being complete wetting with $\beta_{eq} = 0$, the second so called partial wetting with $\beta_{eq} \in (0,\pi)$ and the

third, no wetting at all with $\beta_{eq} = \pi$. However, the third state, even though theoretically possible does not occurs for any known liquid-solid combination. For the brevity of writing and conformity with the made experiments, in all the following text, the problematic will be reduced to a complete wetting state, ensured by presence of thin, precursor film on the studied surface (which is coherent with an assumption of wetted plate made during the experiments). This corresponds to $\Xi_{eq} \geq 0$.

Because of the limitation to complete wetting, there is no use in study of the static droplet spreading, because at the equilibrium state, the liquid will always form a very thin layer with $\beta_{eq} \to 0$. Thus the following will be limited to study of dynamic droplet spreading on ideally smooth surface (because all of the surface imperfections are assumed to be suppressed by the presence of the thin film underneath the drop. For more profound study of static wetting properties as well as description of surface imperfection effects, see [8] or [5] and many references therein.

2.3.2 Description of the droplet spreading

After the drop is placed on a solid surface, its spreading state is usually far from equilibrium, thus $\beta \neq \beta_{eq}$ or $\Xi_{ie} \neq \Xi_{eq}$, more specifically, for the complete wetting, $\beta \geq \beta_{eq} = 0$ and $\Xi_{ie} \geq \Xi_{eq} = 0$. If the drop is not trapped in some metastable state, the dynamic process is set into motion as it reaches the equilibrium state.

This problem was, up to now, extensively studied both experimentally and theoretically [5]. The most simple case is small (with l_c smaller than its radius, thus negligible gravity effects), viscous drop spreading over the surface which it wets completely.

In this case, the drop shape is well approximated by spherical cap [28], which is the equilibrium shape of its gas-liquid interface. This is expectable, as its ratio of viscous to surface tension forces given by capillary number,

$$\mathrm{Ca} = \dot{R}\frac{\mu}{\gamma} \tag{2.32}$$

is very small ($\mathrm{Ca} \in \langle 10^{-5}, 10^{-3} \rangle$). Here, $\dot{R}$ stands for the change of the droplet radius in time, thus the contact line speed, μ is the liquid dynamic viscosity and γ its surface tension as defined in the previous text.

For the sufficiently flat drop ($h'(r) \ll 1$), its volume can be approximated as:

$$\Omega \approx \pi R^2 h_0 \tag{2.33}$$

and thus the interface shape is given by

$$h(r) = \frac{2\Omega}{\pi R^2}\left[1 - \left(\frac{r}{R}\right)^2\right], \tag{2.34}$$

with r being the droplets radial coordinate [5,8].

When the droplet volume, Ω, is known, the shape of its interface is uniquely defined by its apparent contact angle, β, between the spherical cap and the substrate. For the thin enough droplet, $\beta \ll 1, h'(R) = \tan\beta \approx \beta$, one obtains the following relation for the contact angle:

$$\beta = \frac{4\Omega}{\pi R^3} \tag{2.35}$$

and the apparent contact angle, $\beta(t)$ converges to zero as $1/R(t)^3$, as the drop spreads. However, in these relations, β is expressed through a composed function. Direct dependence of the contact angle on time, commonly known as the Tanner's law was, for the drop,

obtained theoretically by Voinov in 1976 [29] and both theoretically and experimentally by Tanner in 1979 [30] and it can be written, in approximate form, as

$$R(t) \propto t^{\frac{1}{10}} \tag{2.36}$$

Important thing to note is that the speed of spreading does not depend on the in-equilibrium spreading coefficient, Ξ_{ie}, even though it is a measure of total surface energy available to the system. Very schematically, one can state, that it is because the spreading over dry surface (where the spreading coefficient has a role) is in fact two stage process consisting of formation of a thin precursor film which uses up all the energy available through Ξ_{ie} and of the macroscopic spreading itself for which the spreading coefficient has been reduced to its equilibrium value, $\Xi_{eq} = 0$. The situation of spreading is sketched in the enlarged area of Figure 2.1 on page 2.

Furthermore, for finding the power of t in equation (2.36), the dissipation energy (which is at low Ca concentrated to a region close to the contact line) has to be calculated. The problem is, that the viscous energy dissipation rises so sharply near the triple phase line, that the total dissipation formally diverges [5,31]. This obviously poses a difficulty for the hydrodynamic modeling of the spreading process and it will be treated more carefully in the following part of the text.

2.3.3 Huh and Scriven's paradox

It was first pointed out by Huh and Scriven in 1971 [26], that application of the no-slip boundary condition to a flow close to contact line leads to a logarithmically diverging energy dissipation.

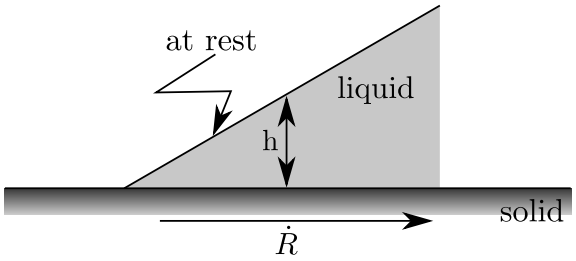

Figure 2.3: Sketch of advancing contact line. In the chosen frame of reference, the contact line is stationary and the solid moves to the right with velocity $\dot{R}$

.

The situation becomes clear, if the frame of reference is chosen as it is shown in Figure 2.3 and the assumption of some finite contact angle $\beta > 0$ between the liquid and solid is made. Thus it follows from the no-slip condition that the fluid at the bottom moves with some constant velocity $\dot{R}$, while the flux through the cross section is zero. Because of the mass conservation, the fluid at the top has to move to the left. Hence, in some distance r from the contact line, the typical vertical velocity gradient is

$$\frac{\mathrm{d}u_r}{\mathrm{d}z} = \frac{\dot{R}}{h(r)}, \tag{2.37}$$

with $h(r) \approx \beta r$ for small β (sufficiently flat drop). As the rate of viscous dissipation per unit volume in a fluid of viscosity μ is $\epsilon \approx \mu(\mathrm{d}u_r/\mathrm{d}z)^2$ [32], by integration $(\dot{R}/h(r))^2$ over the wedge, the estimation of the dissipation per unit time and unit length of contact line is obtained:

$$D_{visc} \approx \mu \int_l^R \left(\frac{\dot{R}}{\beta r}\right)^2 \beta r \mathrm{d}r = \frac{\mu \dot{R}^2}{\beta} \ln\left(\frac{R}{l}\right), \tag{2.38}$$

where R stands for the droplet diameter (but can be in fact any other outer length scale) and l is a small cutoff length implemented to make the integral (2.38) finite. When the standard continuum hydrodynamic no-slip condition is assumed, $l = 0$ and the dissipation logarithmically diverges. Thus the paradox from which comes the phrase *not even Heracles could sink a solid* is stated.

Table 2.1: A list of mechanisms that have been proposed to relieve the dynamical singularity near the contact line along with representative references. Taken from [5].

Mechanism	Authors, year and reference
Mesoscopic precursor film	Hervet and de Genes, 1984 [33]
Molecular film	Eres *et al.*, 2000 [34]
Navier slip	Huh and Scriven, 1971 [26]
Nonlinear slip	Thompson and Troian, 1997 [35]
Surface roughness	Hocking, 1976 [31]
Shear thinning	Weidner and Schwartz, 1993 [36]
Evaporation and condensation	Wayner, 1993 [37]
Diffuse interface	Seppecher, 1996 [38]
Normal stresses	Boudaoud, 2007 [39]

Yet, many liquids are spreading even on dry surfaces. To account for the experimental observations, some microscopic features have to be built into the hydrodynamic description. In Table 2.1, taken from [5], there is as list of different mechanisms proposed to treat the paradox above. At the time, there is no evidence, which would favorize one of the approaches.

Another issue wort mentioning would be the problem of the contact angle, β, dependence on distance from the contact line – microscopic length scale (cuttof length), l, which takes place at inequilibrium state when the equation (2.30) does not hold up. However, as the assumption of the wetted plate is held throughout the work, the microscopic contact angle is, as the free surface of the precursor film is taken to be parallel with the plate, equal a zero (see enlarged area of Figure 2.1 on page 2). The inner region length scale, l, is then kept as adjustable parameter of the models.

For more information on the apparent and microscopic contact angles issue, as well as on the inner length scale size derivation and short range forces that have to be taken into account for microscopic wetting properties estimation, reader is kindly pointed to the reviews of de Gennes [8] and Bonn [5] and to many references therein.

2.3.4 Spreading dynamics of a drop

Most of the analytical descriptions of the spreading dynamics rely on a number of simplifying assumptions [5,8]:

1. The capillary number is small, $\mathrm{Ca} \leq 0.1$.

2. Inertial effects can be neglected. This means, that the viscous length scale, $l_v = \mu^2/\rho\gamma$, is assumed greater than other length scales relevant for the contact line motion.

3. The surfaces are perfect, so there is no contact angle hysteresis.

In the scope of this work, the third assumption is very well defendable, as there is always assumed a microscopic film covering the whole surface of the solid. However, the

other two assumptions have to be taken as they are, because not much is known if they are violated.

The aim of this work is to find a shape of gas-liquid interface of the studied object (which will be for almost all the rest of the section a droplet). This can be done using so called lubrication approximation and the film governing equation,

$$h_t - \frac{1}{3\mu}\nabla\left[\left(h^3 + 3\lambda h^2\right)\left(\rho g \nabla h - \gamma \nabla \kappa\right)\right] = 0. \tag{2.39}$$

For the details on derivation of this equation, see Appendix C or [40]. In the equation above, λ stands for so called Navier slip length introduced to treat the Huh-Scriven paradox (for details see previous section and Appendix C). The term κ is the surface curvature as defined in Appendix A.

Note, that the problem of diverging dissipation energy in vicinity of contact line can be treated not through the introduction of a Navier slip on the substrate, but through any of the methods listed in Table 2.1. Thorough mathematical description of the problem was given by Bertozzi in [41].

As the geometry solved in this section is that of a spherical cap, equation (2.39) can be reduced to its one dimensional form:

$$h_t - \frac{1}{3\mu}\frac{\partial}{\partial r}\left[\left(h^3 + 3\lambda h^2\right)\left(\rho g h_r - \gamma \frac{\partial}{\partial r}\kappa\right)\right] = 0, \tag{2.40}$$

For the possibility of finding an analytical solution to the equation above, a number of simplifications has to be proposed:

1. Effects of gravity can be neglected.
2. The drop is sufficiently flat to assume $\kappa \approx h_{rr}$
3. There is no effect of λ on outer profile solution, $\lambda = 0$.
4. Effects on long range forces on the pressure field are negligible, $p = -\gamma\kappa$
5. Contact lines are in motion perpendicular one to another.

The resulting simplification yields,

$$h_t + \frac{\gamma}{3\mu}\frac{\partial}{\partial r}\left(h^3 h_{rrr}\right) = 0. \tag{2.41}$$

After one spatial integration, one obtains the leading order equation for the droplet profile,

$$3\frac{\mathrm{Ca}}{h^2} = -h'''. \tag{2.42}$$

The prime here denotes spatial derivation with respect to r. Time dependence of the profile is concentrated in the capillary number, Ca.

Notes on the equation (2.42)**:** [5]

1. Everything is expressed through the interface shape, velocity field has been eliminated.
2. Viscous forces diverge as the contact line is approached ($h \to 0$), all other forces are negligible near the three phase line.

3. This equation is scale invariant, solutions being of form $h(r) = lh_{in}(r/l)$, where l is characteristic length set by microscopic effects. Thus the mechanisms to solve the diverging energy problem can be reintroduced in calculations through this length. This will be used in later to patch the macro- and microscopic solutions to the problem of a free interface shape.

4. The sign convention is established so that Ca would be positive for advancing contact line. The case of receding contact line is not covered in this work and reader is referred to the literature [5,8,42]

The equation (2.42) is of a third order with respect to spatial variable, r. To solve it, there are three boundary conditions needed. The first two come from specifying the values of h and h' near the contact line. The third one is then obtained from matching the local solution to the problem geometry dependent macroscopic one.

The problem can be divided into three separated parts

1. Finding universal microscopic solution, h_{in} and its typical length scale, l.

2. Find outer solution, h_{out}, derived from the precise problem geometry and other forces the liquid is subject to.

3. Patch the inner and outer solutions by an intermediate one. If outer and inner length scales are well separated, also this intermediate solution will be universal.

As for the intermediate solution, at some small distance from the contact line, Δr, the curvatures of inner and outer solutions must agree. Thus, in the meaning of nearly flat surface approximation, $h''_{out}(\Delta r) = h''_{in}(\Delta r/l$. But with l to be taken very small,

$$\lim_{l\to 0} h_{in}(\Delta r/l) = 0 \tag{2.43}$$

and this condition, together with the boundary conditions at the contact line uniquely fixes the microscopic solution. The asymptotic solution to the equation (2.42) was, for sufficiently large arguments $\Delta r/l$, given by Voinov [29] and is:

$$h'^3(r) = \beta_m^3 + 9\,\mathrm{Ca}\ln\left(\frac{r}{l}\right). \tag{2.44}$$

Equation (2.44) or some variations of it, is usually referred to as the Cox-Voinov law. In this relation, the microscopic properties are represented by the microscopic contact angle, β_m and the arbitrary length scale. Usually, both of those parameters have to be determined by matching this inner solution to the outer one. However, in the scope of this thesis and with and assumption of wetted plate, $\beta_m = 0$ and the only searched for parameter remains l.

Before the matching will be done, there are four facts that have to be mentioned:

1. The slope of h, thus apparent (or dynamical) contact angle, β, varies logarithmically with the distance from contact line. Therefore, it is impossible to assign unique apparent contact angle to the moving contact line.

2. The dependence of the local profile as defined by the Cox-Voinov law(2.44) on l is logarithmic, hence it is less important than the microscopic contact angle.

3. In the derivation of the equation (2.44), the speed dependence of the profile was eliminated from equation (2.42) using the transformation $h \to \mathrm{Ca}^{1/3}h$. Thus it is not a perturbative result for small Ca.

4. There are several, more general, equivalents to the equation(2.44), for example the results for arbitrary slopes of h given by Voinov [29] or by Snoeijer [43] and the relation for two immiscible fluids with different viscosities given by Cox [44]. However, patching of neither of these solutions can be done purely through the analytical methods and because of this, the added precision was abandoned in favor of lower computational time.

Having found the intermediate scale interface profile, one can proceed to solving the problem as a whole using the found solution as the effective boundary condition. The aim of this part of the text is to find the dependence of the apparent contact angle β on the contact line speed, $\dot{R}$, and ultimately, using the equation (2.35), the dependence of the droplet radius on time. The used matching equation is, according to [5],

$$\beta^3 = \beta_m^3 + 9\,\mathrm{Ca}\ln\left(\frac{Rc}{l}\right) \tag{2.45}$$

To find a resulting, time dependent profile of the drop, one has to add the speed dependent term to the static shape profile, as defined by equation (2.34). The resulting equation would be

$$h_{out} = h_S(r) + \mathrm{Ca}h_D(r) + O(\mathrm{Ca}^2), \tag{2.46}$$

where h_S is spherical cap shape of the static profile (limit of the solution for steady contact line) and h_D is the yet unspecified speed dependent contribution.

The static profile, h_S depends on the time implicitly through its dependence on the drop radius, R. To compare the inner and outer solutions represented by equations (2.44) and (2.46) respectively, one has to at first obtain third power of h'_{out}. Neglecting the terms multiplied by at least second power of Ca, the following is obtained:

$$h'^3_{out} \approx h'^3_S + 3\mathrm{Ca}h'^2_S h'_D \tag{2.47}$$

Substituting it to the (2.44) yields, that h'^3_{out} has logarithmic singularity at $-9\,\mathrm{Ca}\ln(R-r)$ with $r \to R$. Then, from prefactor comparison and using $\beta = -h'_S$ together with equation (2.45), one arrives directly at

$$\ln(Rc) = \lim_{r\to R}\left[\frac{h'^2_S h'_D}{3}\right] + \ln(R-r)\,. \tag{2.48}$$

Inserting the expansion (2.46) into the Cox-Voinov law, (2.44) and intergrating the result once, one finds

$$\left(h''_D + \frac{h'_D}{r}\right)' - \frac{3}{rh_S^3}\int_0^r \frac{\partial h_S(s)}{\partial R} s\mathrm{d}s = 0. \tag{2.49}$$

In equation (2.49), h_S is specified by (2.34), so it is a third order ODE for yet unspecified h_D. The solution is fixed by the following boundary conditions:

1. Condition of the droplet symmetry.

$$r = 0, \qquad h'_D = 0 \tag{2.50}$$

2. Zero height on the contact line.

$$r = R, \qquad h_D = 0 \tag{2.51}$$

3. Zero addition to the integral droplet volume.

$$\int_0^R r h_D \mathrm{d}r = 0 \tag{2.52}$$

Finding h_D from (2.49) subject to the boundary conditions above and using equation (2.48), one easily finds, that for the droplet symmetry, $c = 1/2e^2$. However, as the symmetry dependent constant, c is in order of magnitude 10^{-1} and is influencing the result only through a logarithmic dependence, its exact value is not as crucial for the actual numerical results.

In the case of pre-existing thin film $\beta_m = 0$. Hence substituting for the apparent contact angle, β from the (2.35), equation (2.45) becomes

$$\left(\frac{4\Omega}{\pi R^3}\right)^3 = 9\dot{R}\frac{\mu}{\gamma}\ln\left(\frac{R}{2e^2 l}\right), \tag{2.53}$$

which is, finally the equation from which can be deduced the time dependence of the droplet radius and shape.

Notes on the equation (2.53)

1. The equation was derived for the case of small, nearly flat droplet with negligible effects of gravity (and any other body forces) even on the static, outer itnerface profile shape.

2. Neglecting the logarithmic dependencies and approximating the logarithm by a constant yields $\dot{R}R^9 \propto C \rightarrow R \propto t^{1/10}$, in agreement with Tanner's law (equation (2.36)).

3. For $\beta_m = 0$, l is the only specific feature of the contact line.

4. Cox [44] studied the problem without reference to specific geometry, but the difference between his results and the ones obtained here is, from the engineering point of view, not crucial.

2.3.5 Proposed calculation method

In this part of the text, there is briefly summarized all of the above concerning the problem of simulating the droplets spreading and a simple computing algorithm is proposed.

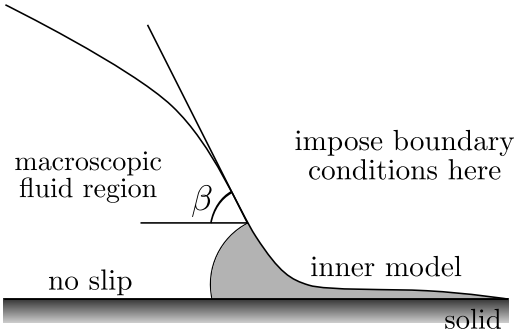

Figure 2.4: Schematic of procedure for continuum modeling, inspired by [5].

.

When calculating the flow dynamics of the problem with moving contact lines, one cannot use the set of standard boundary conditions, because, as it was described before, the no-slip boundary condition will cause the solution to have a singularity at the contact line. However, this influences only very small part of the problem solution. Furthermore, the scales of outer and inner solutions are usually well separated by an inner length scale, l.

This leads to proposition of a general calculation method, independent of a chosen model for resulting the Huh-Scriven paradox (see Table 2.1). Schematic of this method is given in Figure 2.4 and it consists of finding a microscopil scale solution and using it as an effective boundary condition for the macroscopic one.

For the simplest case of a small droplet and a substantial number of simplifying arguments, this procedure is shown and solved analytically in subsection 2.3.4. However, a procedure analogical to this one can be used also for purely numerical CFD models, only with the difference, that the inner length scale, l, is not given by the microscopic properties of the problem, but by the resolution of the computational grid. For more details, reader is pointed towards the literature, for example to [3,19–21].

2.4 Rivulet spreading

The current state of description of the spreading of a rivulet flowing down an inclined plate can be divided in two parts. The first one is the description of the spreading dynamics with neglected contact line effects done by Shetty and Cerro [9]. The second principle is the study of the contact line movement as it was done by Davis [10,12] and his followers.

In the following text, the analysis of spreading of thin stripes of oil will be given very briefly to make a liaison to the previous section. Afterwards, the solution of the problem of Shetty and Cerro will be studied. Finally, the approach of Davis will be briefly sketched.

2.4.1 Spreading of a oil stripes on a horizontal substrate

McHale *et al.* [11] have studied the problematics of the liquid spreading in a manner very close to the one described in a section 2.3, but for the small stripes of viscous, non-volatile oil on a horizontal substrate. The stripes were assumed to be narrow, very shallow (enough to neglect the effects of gravity) and spreading over a horizontal substrate.

By the means of analysis very close to the one presented in 2.3, McHale *et al.* have found a relation for the dependence of contact angle on the time valid for the case of perfectly wetting fluid (or pre-existing precursor film),

$$\beta = \left[\left(\frac{384\Omega}{441L} \right)^{\frac{1}{2}} \frac{\mu J_W}{\gamma(t+c)} \right]^{\frac{2}{7}}, \tag{2.54}$$

with Ω being volume of the spreading stripe, L its length, μ the liquid viscosity, c the integration constant and with J_W derived from the viscous dissipation energy balance and defined as [11]

$$J_W \approx \ln\left(\frac{1}{l}\right) - 1, \qquad l = h_l \cot\left(\frac{\beta}{2}\right) \tag{2.55}$$

where h_l is small finite height, where macroscopic profile crosses over into the precursor film and l is a horizontal distance from contact line at which this occurs. The parallel between l as defined here and microscopic length scale used in subsection 2.3.4 (Spreading dynamics of a drop) is obvious.

One can also, in analogy to subsection 2.3.2 (Description of the droplet spreading), take a stripe volume approximately as

$$\Omega \approx 2aL\frac{h_0}{2}, \tag{2.56}$$

where a is the stripe half width and h_0 is its height at $y = 0$ (with the same coordinate system as stated in 2.1. Using this and assumption of the stripe rectangular base, one

obtains a relation for the stripe interface profile similar to (2.34),

$$h(y) = \frac{3}{4}\frac{\Omega}{aL}\left[1 - \left(\frac{y}{a}\right)^2\right], \tag{2.57}$$

from which the approximate relation for the small apparent contact angle is obtained,

$$\beta = \frac{3}{2}\frac{\Omega}{a^2 L}. \tag{2.58}$$

Substituting (2.58) into (2.54) and using approximation for small β, $cot\beta \approx 1/\beta$ in (2.55), one obtains an implicit relation for the stripe half width as function of time,

$$\frac{3}{2}\frac{\Omega}{a^2(t)L} = \left[\left(\frac{384\Omega}{441L}\right)^{\frac{1}{2}} \ln\left(\frac{3\Omega}{2a^2(t)Lh_l}\right)\frac{\mu}{\gamma(t+c)}\right]^{\frac{2}{7}}. \tag{2.59}$$

Taking the logarithmic members in equation (2.59) as constants, the dependency of the stripe half width on time can be written as

$$a \propto t^{\frac{1}{7}}, \tag{2.60}$$

as it was stated previously in the literature [11,30].

2.4.2 Spreading of a point source with neglected contact line effects

Shetty and Cerro [9] have proposed a study of spreading of point sources over inclined solid surfaces motivated by the effort to understand a hydrodynamics of liquid on structured packings. However, they have chosen completely different approach to the problematic than the one studied in the previous part of the work.

They have completely resigned on the problematic of moving contact lines as they have proposed different basic shape of the interface profile[1]. They stated cross-sectional shape of the free surface to be representable by a (simplified) normal probability distribution,

$$h(x,y) = h_0(x)\exp\left(-\frac{y^2}{2\sigma(x)^2}\right) \tag{2.61}$$

The rivulet is from its beginning assumed shallow, meaning, that there can be defined a small parameter ϑ,

$$\vartheta = \frac{h_0(0)}{2\sigma(0)} \ll 1. \tag{2.62}$$

To shorten the following writing, the standard deviation and peak height at $x = 0$ will be referred to as σ_I, h_{0I}, respectively. The velocity in x and y direction is assumed to be the same order of magnitude as the mean free falling film velocity given by,

$$\zeta = \frac{\rho g \sin\alpha}{3\mu} h_{0I}^2. \tag{2.63}$$

The problem is, with an assumption of nearly flat surface, reduced through partial solving of Navier-Stokes equations and leading order analysis reduced to finding the dependence of the maximal peak height (taken at the rivulet centerline) on the plate longitudinal coordinate, x.

[1] In the text concerning three dimensional cases, the word profile is understood as $z = h(x,y)$ for fixed x and varying y. In respect to the same coordinate system as stated in 2.1

Two approximative asymptotic solutions are obtained. Both derived from the equation

$$\overline{Bo}\bar{h}_0^8 + \bar{h}_0^{14}(\bar{x}) + \frac{3}{16}\frac{\overline{\mathrm{Ca}}}{\vartheta^3}\frac{\mathrm{d}\bar{h}_0(\bar{x})}{\mathrm{d}\bar{x}} = 0, \tag{2.64}$$

with h_0 being non-dimensionalized through h_{0I} and x through $2\sigma_I$. $\overline{Ca}$ stands for capillary number defined through the mean falling film velocity, ζ, as $\overline{Ca} = \zeta\mu/\gamma$ and $\overline{Bo}$ has meaning of a Bond number defined as

$$\overline{Bo} = \frac{27}{6\pi}\frac{\cos\alpha}{\sin^2\alpha}\frac{\mu^2 Q^2}{g\gamma h_{0I}^6} \tag{2.65}$$

In the first asymptotic solution of the equation (2.64), the plate is taken to be in a vertical position ($\alpha = \pi/2$, which causes $\overline{Bo} = 0$. The simplified ODE can be easily integrated and using an initial condition, that $\bar{h}_0 = 1$ for $\bar{x} = 0$, it yields

$$\bar{h}_0(\bar{x}) = \frac{1}{\left(1 + \frac{208\vartheta^3}{3\overline{Ca}}\bar{x}\right)^{1/13}}. \tag{2.66}$$

Similarly, for high plate inclination angles, authors propose to neglect the capillary effects represented by the member $\bar{h}_0^{14}$, integrate the result using the same initial condition as above and obtain

$$\bar{h}_0(\bar{x}) = \frac{1}{\left(1 + \frac{112\vartheta^3\overline{Bo}}{3\overline{Ca}}\bar{x}\right)^{1/7}}. \tag{2.67}$$

As for the intermediate solution for $\alpha \in (0, \pi/18)$, they propose to obtain solution numerically by fitting the data using equation

$$\bar{h}_0(\bar{x}) = \frac{1}{(1 + \Lambda\bar{x})^{1/9}}, \tag{2.68}$$

with Λ being an adjustable parameter.

However, besides some problems in duplicability of the presented results[2], this approach has at least one flaw that makes it unusable for the calculation of the rivulet gas-liquid interfacial area size. The speed of liquid spreading, v, is assumed to be of the same order of magnitude as its speed along the plate, u, although there is not a force effecting the liquid directly in y-direction as there is gravity for x-direction.

2.4.3 Contact line movement in case of a spreading rivulet

Davis [10,12] has studied the problematics of moving contact lines in case of flowing rivulet spreading along inclined plate in the presence of steady gas phase. He did not make an assumption of nearly flat interface and thus have to treat the capillary addition to the pressure field through a mean radius of the surface defined as

$$\frac{1}{\varrho} = \kappa, \tag{2.69}$$

with κ being the mean surface curvature defined and described in Appendix A.

Davis divided the problem into four different cases. At first, he treated the rivulet with fixed contact lines in a manner similar to the one proposed by Towell and Rothfeld [6] or by Duffy and Moffat [7]. Then he proceeded to the moving contact lines, but with fixed

[2]Author of the presented thesis was not able to reproduce these results as the values of $\overline{Bo}$ proposed by authors were between 1.44 and 44.9 and about three orders of magnitude different from the ones obtained by substituting the published values into proposed relations.

contact angles. The third studied case was the one of a smoothly varying contact angle (as a function of contact line speed), meaning the ideal surface and no contact angle hysteresis were assumed. Finally, he briefly discussed the problematics of a contact angle hysteresis.

For the above listed cases (apart from the contact angle hysteresis), Davis proposed suitable boundary conditions and derived the sufficient conditions for the rivulet stability against the break up into flowing droplets.

The results of Davis are very general and of a wide applicability to different problems (as he, for example, did not make any assumptions about the interface shape or gravity effects on the rivulet spreading). However, the cost for this generality is that even in the most simplified case of fixed contact lines no explicit solution for the profile shape is obtained, making the results unusable in chemical engineering practice.

Many of Davis's followers have studied the conditions of the rivulet stability with steady [46–48] and moving [49], but there are no followers developing the contact line movement and the shape of the gas-liquid interface of the rivulet.

2.5 Calculation of the size of gas-liquid interfacial area of a rivulet

The aim of this thesis is to present a method to calculate the size of gas-liquid interfacial area of the case of a gravity driven rivulet flowing down an inclined, wetted, plate in the presence of steady gas phase and to present the model to fit the experimental data with.

The following section is divided in two parts. In the first one, there is briefly sketched the procedure of interfacial area size calculation for the problem of fixed contact lines. Next, the problem is generalized for the contact lines moving accros the wetted plate.

The main assumptions kept throughout this section are:

1. Wide and shallow rivulet, $\varepsilon = h_0(x)/2a \ll 1$.
2. Incompressible Newtonian liquid with constant viscosity and surface tension coefficient.
3. Steady state.
4. No shear at the gas-liquid interface.
5. Effects of the gravity on the shape of the interface are negligible.

2.5.1 Interfacial area size of rivulet with fixed contact lines

For the case of rivulet flowing down a plate of length L inclined to a horizontal by an angle α and with contact lines fixed at $-a$ and a, the calculation of its interfacial area is rather straightforward. Generally one can write following relation for the interfacial area size,

$$S_{g-l} = \int_0^L \int_{-a}^{a} \sqrt{1 + \left(\frac{\partial h(x,y)}{\partial y}\right)^2} \mathrm{d}y\mathrm{d}x. \tag{2.70}$$

Nevertheless, with constant a and x independent h, the above equation simplifies to

$$S^f_{g-l} = L \int_{-a}^{a} \sqrt{1 + h'(y)^2} \mathrm{d}y, \tag{2.71}$$

with the superscript f used to underline the assumption of the fixed contact lines and with prime denoting the derivative with respect to y. Thus the problem of calculation of the S^f_{g-l} is reduced to search for value of the integral in equations (2.70) and (2.71),

the arc length of the transversal profile of the rivulet, for the brevity noted as ς and ς^f, respectively.

With the effects of gravity on the shape of the gas-liquid interface neglected, it can be assumed to be a part of the circle (for details see 2.3.2 and 2.4.1) and the solution of Duffy and Moffat for neglected gravity as presented in 2.2.3 (case (ii)) can be used to specify the rivulet profile shape.

As it follows from equations (2.27) and (2.29) on page 6, the profile shape and thus the rivulet interfacial area size can be uniquely specified by any pair of the three problem parameters, the rivulet half width, a, the liquid volumetric flow rate, Q and the liquid-solid apparent contact angle, β.

Substituting from these equations, one obtains relation for the profile arc length,

$$\begin{aligned} \varsigma^f &= \int_{-a}^{a} \sqrt{1 + \left(\frac{\tan\beta}{a} y\right)^2}\, \mathrm{d}y \\ &= a\left[\sqrt{1+\tan^2\beta} + \frac{1}{2\tan\beta} \ln\left(\frac{\tan\beta + \sqrt{1+\tan^2\beta}}{-\tan\beta + \sqrt{1+\tan^2\beta}}\right)\right] \end{aligned} \tag{2.72}$$

where it is possible to express either a or β from the equation (2.29) for known liquid volumetric flow rate and calculate the size of the gas-liquid interfacial area from

$$S^f_{g-l} = \varsigma^f L. \tag{2.73}$$

2.5.2 Interfacial area size of rivulet with moving contact lines

Even though the surface area of rivulet is calculable directly from numerical solutions of the Navier-Stokes equations with corresponding boundary conditions, such calculations are time consuming and redundantly complex to be used for chemical engineering practice.

In the following text, there is proposed a simple calculation method to be used for fitting the experimental data or to predict some of the rivulet properties behavior. However, at the time the accordance between the purely theoretical results and experimental data is mainly qualitative, which is understandable as the simplifying assumption used to develop the proposed model are very strict. The used assumption are:

1. Incompressible, Newtonian fluid with constant viscosity and surface tension coefficient.
2. Steady state.
3. No shear at the gas-liquid interface.
4. The rivulet is symmetrical along the plate longitudinal axis.
5. Laminar flow, no laminar waves. Absence of waves means, that there are no fluctuation in the liquid‘s volumetric flow rate along the plate.
6. The liquid velocities in directions transversal and normal to the plate are negligible in comparison to the one in its longitudinal direction, $u \gg v \sim w$.
7. Gravity is the only acting body force.
8. The rivulet is shallow enough for the gravity effects on its interface shape to be negligible. Also the contact angles, $\beta = \beta(x)$ are assumed small all along the rivulet.
9. The capillary number defined through the contact line velocity in the y-axis direction is small, $\mathrm{Ca} \leq 0.1$.

10. As of the contact line motion, the inertial effects can be neglected.

11. There is a thin precursor film on the whole studied surface, so there is no contact angle hysteresis and $\beta_m = 0$.

12. The macroscopic and microscopic solutions to the film governing equation, (2.39), are well separated by the intermediate region length scale l.

As of the validity of assumptions listed above, the most problematic ones are the one about negligibility of gravity effects on the rivulet interface shape and the one of no laminar waves on the rivulet.

The problem with gravity effects on the interfacial shape negligibility is that the height of the rivulet for which this assumption is valid is extremely small ($\leq 10^{-4}$ m) [7,22]. This is acceptable for the small, flat droplet on horizontal substrate, but for the rivulet with width of 10^{-2} m it is far stretched.

Assumption of absence of laminar waves on the rivulet can be put into question as these are occurring even for quite low liquid velocities (or correctly defined Reynolds numbers). However, the rivulet stability analysis in face of film waving is far outside of this master thesis scope and can be found for example in [46,50].

With the simplifications as listed above, one can make parallel between spreading of a rivulet along the inclined plate and spreading of static shapes in time.

The problem of finding the interface profile shape, as defined by the thin film governing equation (2.39) is the reduced from two spatial dimensions to one and a search for the right transformation from the time to spatial range.

Furthermore, as it was stated in subsection 2.3.4, based on [5,29,44], if the inner and outer length scale are well separated, both the inner and intermediate solutions are geometry independent and all the influence of the shape of the spreading element is concentrated in the outer solution of the problem and even though it is not exactly the case, with $\beta_m = 0$, the only geometry dependent member in Cox-Voinov law(2.44) is the constant c, which is influencing the result only logarithmically and thus is far less important, than the influence of outer solution.

With the above stated in mind, in the simplest case, one can obtain the dependence rivulet apparent contact angle on time directly from (2.45) with c defined same as it is in (2.53). Or, it is possible to use more elaborate solution of McHale [11], derived directly for the stripe (part of the cylinder) geometry. Both ways, however, raise same two questions:

1. How to express the profile shape not as function of the spreading object volume but through the liquid volumetric flow rate?

2. As the solution of finding the free surface shape of symmetrical shape spreading in time is of a form $h(t,y)$, how to transform it to the wanted form $h(x,y)$. In brief, how should be the transformation $x \rightarrow t(x)$ defined?

Note: Usage of the McHale's *et al.* [11] equation raises yet another question, how to express the ratio of rivulet volume to its length, Ω/L, using its volumetric flow rate, Q and longitudinal coordinate of the current cut through it, x.

Answer to the first question can be found from models used to simulate the rivulet with pinned contact lines. If the plate would be divided in N infinitesimally short cuts of length δx, one could picture the spreading rivulet as a series of short rectilinear ones with fixed three phase lines. Thus the models presented in section 2.2 (Steady rivulet) can

be used to specify the local rivulet interface profile shape for given Q and its local width, $\alpha(x)$ and contact angle,$\beta(x)$.

As for the second question, each of the spreading shape equations contents a members expressing the properties of microscopic material interactions, the microscopic contact angle,β_m, and the intermediate region length scale, l. McHale *et al.* [11] have proposed, that the point with distance l from the contact line is at height h_l over the surface.

However, the later is not the case of the studied situation as there is supposed film presence of a constant thickness on the whole substrate. The consequence of this is, that the height of the contact point over the solid surface is constant and is equal to the thickness of the precursor film. Without a loss of generality, one can assume the film thickness and the intermediate length scale, l to be the same (as it is depicted in Figure 2.1 on page 2).

The proposed transformation from time to spatial range uses assumption, that the precursor film covering the inclined plate is moving along it in the same way as any free film would. This is obviously only approximative as the intermediate region length scale is assumed to be small enough for the long range molecular forces to have some effects.

Nevertheless, with this simplification, one can define τ to be a point of the contact line at specified distance from the top of the plate, x, and define speed of its movement along the plate as the surface speed of free falling film of thickness l,

$$u_\tau = \frac{\rho g \sin\alpha}{2\mu} l^2. \tag{2.74}$$

From the above equation, one can easily obtain transformation of $x \to t(x)$ as

$$t = \frac{x}{u_\tau} = \frac{2\mu}{\rho g \sin\alpha l^2} x. \tag{2.75}$$

With introduction of constant ϖ, the obove equation can be rewritten in more brief form,

$$t = \varpi x, \qquad \varpi = \frac{2\mu}{\rho g \sin\alpha l^2}. \tag{2.76}$$

From equation (2.76), it can be stated, that the coordinate to time transformation is dependent only on the position of τ on the plate.

The aim of the derivation is to obtain a relation for β as function of time and then to transform it to function of the plate length coordinate, x, using the transformation (2.76). The following will be reduced to using the intermediate solution obtained for case of two dimensional droplet. However, this solution should be, for well defined l, universal.

Equation (2.45), for the rivulet, $\beta_m = 0$ and $c = 1/2e^2$ becomes

$$\beta(t)^3 = 9\frac{\mathrm{d}a(t)}{\mathrm{d}t}\frac{\mu}{\gamma}\ln\left(\frac{a(t)}{2e^2 l}\right), \tag{2.77}$$

which is one first order ODE for two unknowns functions, $\beta(t)$ and $a(t)$. Nevertheless, for the case of neglected gravity effects on the interface shape, one can express β or a from (2.29) proposed by Duffy and Moffat in [7].

The reason to use equation (2.29) and not some more elaborate relation is that both β and a can be expressed explicitly from it and one can substitute for them directly in equation (2.77). As β appears directly into transformation (2.76), it is more useful to express a as function of β from (2.29) (generalized for the case of non-vertical plate [7]) and to simplify for the case of flat rivulet,

$$a = \left(\frac{105\mu Q}{4\rho g \sin\alpha \tan^3\beta}\right)^{\frac{1}{4}} \approx \eta\frac{1}{\beta^{3/4}}, \qquad \eta = \left(\frac{105\mu Q}{4\rho g \sin\alpha}\right)^{1/4}. \tag{2.78}$$

Substituting from (2.78) to (2.77), one arrives at

$$\beta(t)^3 = -\frac{27}{4}\frac{\eta\mu}{\gamma}\frac{1}{\beta(t)^{7/4}}\frac{\mathrm{d}\beta(t)}{\mathrm{d}t}\ln\left(\frac{\eta}{2e^2 l\beta(t)^{3/4}}\right), \tag{2.79}$$

which can by simplified by lumping all the constant terms in two constants,

$$A = \frac{27}{4}\frac{\eta\mu}{\gamma}, \qquad B = \frac{\eta}{2e^2 l}, \tag{2.80}$$

to

$$\beta^{19/4} = -A\frac{\mathrm{d}\beta}{\mathrm{d}t}\ln\left(\frac{B}{\beta^{3/4}}\right), \qquad \beta = \beta(t). \tag{2.81}$$

Solving the equation (2.81) yields an implicit relation for $\beta(t)$,

$$t - \frac{4}{15}\frac{A}{\beta^{15/4}}\left[\ln\left(\frac{B}{\beta^{3/4}}\right) - \frac{1}{5}\right] + c = 0. \tag{2.82}$$

The integration constant, c is then specified by initial condition, $\beta(0) = \beta_I$. Inserting the initial condition into (2.82), solving for c and then resubstituting the result back into (2.82), one obtains the dependence of β on time for the rivulet geometry and for known β_I,

$$t - \frac{4}{15}\frac{A}{\beta^{15/4}}\left[\ln\left(\frac{B}{\beta^{3/4}}\right) - \frac{1}{5}\right] + \beta_I^{5/4} + \frac{4}{15}\frac{A}{\beta_I^{15/4}}\left[\ln\left(\frac{B}{\beta_I^{3/4}}\right) - \frac{1}{5}\right] = 0. \tag{2.83}$$

Notes on the equation (2.83)

1. It is an implicit relation which defines evolution of the liquid contact angle in time for the case of a spreading rivulet of volumetric flow rate Q.

2. Neglecting the logarithmic terms and solving (2.83), one finds, that contact angle is decreasing approximately with $t^{4/15}$, which is in agreement with McHale's solution of the problem for the geometry of horizontally placed stripes of silicon oil (consult with equation (2.54)), where the found power factor was the one of 2/7.

Substituting for t from (2.76) into (2.83) and rearranging the terms, one finds the final relation for the dependence of the contact angle on the plate longitudinal coordinate, x:

$$x - \frac{\bar{A}}{\beta^{15/4}}\left[\ln\left(\frac{B}{\beta^{3/4}}\right) - \frac{1}{5}\right] + \beta_I^{5/4} + \frac{\bar{A}}{\beta_I^{15/4}}\left[\ln\left(\frac{B}{\beta_I^{3/4}}\right) - \frac{1}{5}\right] = 0, \qquad \bar{A} = \frac{4}{15}\frac{A}{\varpi} \tag{2.84}$$

Notes on the equation (2.84)

1. The approximative dependence of β on x is of the same kind as its dependence on time (with power factor of 4/15), which is obvious, as the transformation is linear.

2. For reasonably low flow rates, $Q \approx 10^{-6}\,\mathrm{m^3\,s^{-1}}$, $\bar{A}$ is very small number, as it contains second power of small intermediate length scale, l. Otherwise, it can be explained as it is multiplied with the speed of τ on the plate, which is very small.

3. The obtained profiles will be all of the shape of circle segments, even though it is not the case of the rivulets influenced by the gravity.

4. The problem of finding the shape of the rivulet's interface was reduced to specifying the right intermediate region length scale, l, which defines the resulting spreading speed (in dependence on time) as well as the transformation from time to spatial coordinates.

In the following text, the calculation method to calculate the interfacial area of a spreading rivulet based on the approximation of the rivulet by N static rivulets with constant width and length δx is presented. The width of i-th subrivulet is determined by its contact angle, $\beta_i(x)$, specified from equations (2.84) and (2.78). Its profile shape is then given by equation (2.27).

Calculation method:
For subrivulet placed at coordinate $i\delta x, i = 1,2,\ldots,N, \delta x = L/N$ from the plate top do:

1. Solve equation (2.84) and obtain β_i.
2. Substitute for the β_i in equation (2.78) and get the current rivulet half width, a_i.
3. Obtain the current profile length by substituting for a and $beta_i$ in equation (2.72) and obtain current subrivuleth profile arc length, ς_i^f.

After each subrivulets arc length are obtained, numerically evaluate the integral (2.70) to obtain the simulated interfacial area size.

3. Experiments

Experiments presented in this work were carried out at Institut für Thermische Verfahrenstechnik, Umwelt- und Naturstoffverfahrenstechnik of TU Bergakademie Freiberg during summer 2012.

3.1 Experimental set up description

3.1.1 Measuring technique

Optical experimental set up to measure the rivulet width was first used by Towell and Rothfeld [6]. They used simple glass plate with graph paper taped to its bottom side to measure the distances. However current measurement techniques for study of the liquid free surface are more advanced and mainly based on gaining images of the measured surface and evaluating them through some image processing software [14,51,52].

The goal of the experiments was to obtain the rivulet flow and geometry data from an optical measuring technique based on the light induced fluorescence (LIF).

Light or laser (based on the light source type) induced fluorescence is technique that involves the excitation of a target by a radiation of specified type followed by the detection of the subsequent emission of radiation from the target [53].

Chosen radiation source for the carried out experiments was visible violet light. With a fluorescent dye dissolved in a measured liquid flow, one is, through a procedure of converting the emitted radiation (which is for the presented case visible light) intensities to the local film heights, capable of quantitatively investigating the liquid surface properties [54,55].

The use of high speed camera as the emitted light detector promises the possibility of future measurement of the fluid velocity fields.

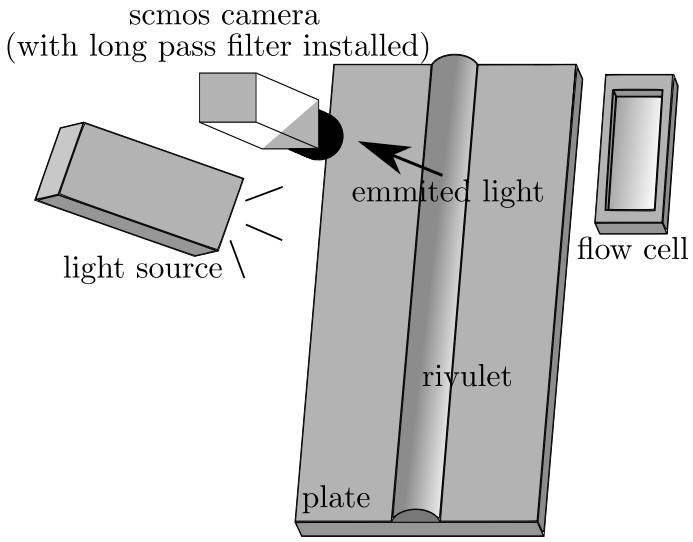

Figure 3.1: Scheme of used experimental set up.

Experimental installation used at TU Bergakademie Freiberg was inspired mainly by the ones presented by Hagemeier *et al.* in [51] and by Alekseenko *et al.* in [52]. Schematic of the used experimental set up is in Figure 3.1. It is formed by an inclined plate made of steel of surface roughness approximately 36 μm, flow cell allowing conversion of emitted light intensity into local film thicknesses, sCMOS camera [56] with a long pass filter installed and by a light source.

Output of the measurement are gray scale digital photographies of the inclined plate with measured rivulet and of the flow cell. There is linear increase of the film thickness along the flow cell, which is used as the calibration scope for conversion of measured emitted light intensities into the local film thicknesses into the rivulet.

3.1.2 Carried out experiments

Main goal of the experiments was to obtain a set of data which could be used to deduce and verify a model for calculation of the size of (g)–(l) interfacial area, S_{g-l}, from some input parameters. Based on the literature (i.e. [6,7,15]), following parameters were identified as the ones with the highest impact on the rivulet's S_{g-l}: $\alpha, \gamma, \mu, \rho, Q$.

To obtain a representative dataset, four types of liquid with different properties were used. Table 3.1 contains a list of properties of each liquid as well as marker used for LIF.

Table 3.1: Used liquids properties at $T = 298.15$ K

Liquid[1]	ρ $[\mathrm{kg\,m^{-3}}]$	γ $[\mathrm{mN\,m^{-1}}]$	μ [mPa s]	Marker
DC 05	920	17.57	5.073	Coumarin 152a
DC 10	940	17.89	10.419	Coumarin 152a
Water	998	55.18	1.178	Fluorescein
Tenzids	998	29.36	1.114	Fluorescein

Images of rivulets of each liquid type were taken at various liquid mass flow rates, $Q \in \langle 0.2, 13 \rangle\,\mathrm{g\,s^{-1}}$, for four different plate inclination angles, $\alpha = \{45\,^\circ, 52\,^\circ, 60\,^\circ, 75\,^\circ\}$.

Experimental condition were set such as the plate stayed wetted during all the experiments. The process was kept isotherm, at temperature $\theta = 25\,^\circ\mathrm{C}$.

3.1.3 Process scheme

The scheme of the experimental setup is shown in Figures 3.2 and 3.3 on page 26. In the first one of them, there is a sketch of liquid circulation in the whole apparatus, whilst in the second, there is demonstrated the front view of the inclined plate with the measured rivulet itself.

The measured liquid circulating in the measurement apparatus. It is stored in the main liquid reservoir, (Liquid reservoir I on the Figure 3.2). From there it is driven by the pump through rotameter and heat exchanger, fixing the liquid temperature at 25 °C, to the flow cell and to the secondary liquid reservoir (Liquid reservoir II). Next, liquid is freely falling from the liquid inlet onto the inclined plate, as it is shown on Figure 3.3. At the bottom side of the plate liquid overflows down to the sunk collector and is returned back to the main liquid reservoir.

[1] DC 05 and DC 10 are distributor's (Sigma-Aldrich) names for silicon oils with dynamic viscosities approximately 5, respectively 10, mPa s. Tenzids is a working name for water with surface tension lowered by surfactants

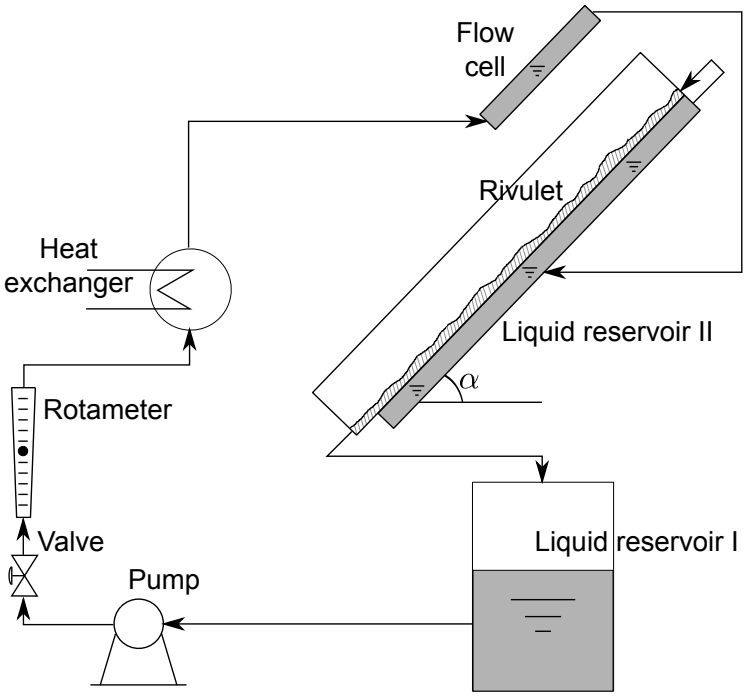

Figure 3.2: Liquid circulation scheme.

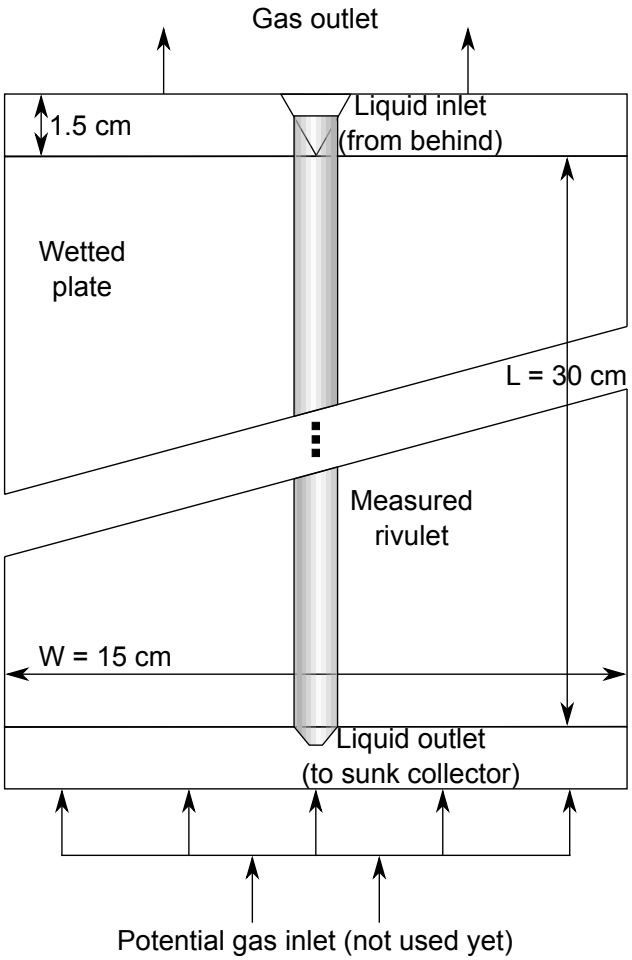

Figure 3.3: Front view of the measurement cell - inclined plate.

Volumetric flow rate of the circulating liquid is measured by a rotameter and set approximately by changing pump frequency and finely adjusted by valve in front of the rotameter.

The flow cell is placed on the same construction element as the plate and their inclination angles are therefore altered simultaneously.

Even though it was not used yet, the experimental apparatus is prepared also for the measurement of the rivulet behavior under shear stress induced by a counter-current gas flow. Diagram of the possible gas flow through the cell with inclined plate is shown in the Figure 3.3. The most uniform gas distribution possible is ensured by diversification of the gas inlet into at first two, then into five equivalent slots.

3.1.4 Experimental set up options and problems

At the current state of the experimental set up, it is possible to carry out experiments with the rivulet flown on the inclined plate with or without counter-current gas flow. The plate inclination angle, α is limited to be between $\sim 45\,^\circ$ and $\sim 75\,^\circ$.

With slight modifications, it should be possible to:

1. Measure the properties of falling film. This should be doable through change of the liquid distributor – replacing the triangular one by a simple overfall coverring the whole plate width.

2. Measure the rivulet properties for plate inclination angle, $\alpha > 90\,^\circ$. For this, the camera would have to be placed not above, but underneath the inclined plate, the plexiglas protecting the measurement cell from the dust and keeping the gas flow inside the measurement cell would have to be removed and the system of the liquid recollection system would have to be altered. No measurements with gas flow would have been possible either. Similar experimental set up can be found in [52] (for the case of the rivulet on tube, though).

3. Measure the properties of the rivulet on textured plate. For this, the smooth plate would have to be replaced by a textured one. Nevertheless, for such a measurements, there was a different experimental set up constructed in Freiberg.

The experimental apparatus however has also some minor flaws, namely:

1. Lower limit of α is caused by the placement of the camera, which is standing on a tripod in front of measurement device. The stand is not high enough to allow the camera lens axis to be perpendicular to the plate, which is necessary for the measurement.

2. Higher limit of α is due to the fact, that for $\alpha \geq\sim 75\,^\circ$, the liquid is falling from the plate onto the gas distributor.

3. During the measurement, especially with higher liquid flow rates, sometimes there is a gas bubble going through the device. Imperfections on the flow cell cover glass then cause a formation of very small bubbles on its underside. Still the formation of these can be reduced by introduction gas release into the liquid flow circuit. Furthermore, the analysis of influence of these bubbles on the experimental results was effectuated and no strong impact was proven.

3.1.5 Measurement procedure

Measurements were carried out for four different types of liquid (as listed in Table 3.1) differing mainly by their surface tensions and viscosities. Each liquids was measured separately and the apparatus were at first dried out and then rinsed by the consecutively used liquid before each measurement.

Experimental treatment of each liquid was divided in four parts by different plate inclination angle used. In each part, the liquid volumetric flow rate was slowly increased and rivulet was photographed.

Because of the background light noise (as the light source and emitted radiation wavelengths appertained to the visible light), all the experiments were conducted in a darkened room.

The procedure of measurements for one plate inclination angle for one liquid can be described as follows:

1. Set up the plate inclination angle and the positions of camera and light source.
2. Flood the experimental cell with measured liquid to wash out any droplets remaining on the plate or on the cover glass and to rewett it.
3. Reduce the liquid flow rate to minimum and wait for the cell depletion. Thus the straightness of the rivulet is ensured.
4. Set roughly set up the liquid volumetric flow rate via the pump frequency.
5. For a short period of time, sharply increase the liquid flow rate to ensure existence of precursor film all around the rivulet.
6. Adjust the liquid flow rate to desired value using the valve before rotameter.
7. Wait for the rivulet shape to become steady and take the picture of an experiment.
8. If it is the first measurement for newly set plate inclination angle, evaluate it immediately using the data evaluation program (see 4) to ensure that all was installed correctly. If the correct arrangement is verified, repeat the points 5. and 6. at least four times for each measured liquid flow rate.
9. Reflood the experimental cell with each change of the liquid flow rate.
10. Measure at least ten different liquid flow rates for each liquid and plate inclination angle.

3.2 Measured quantities

There are several rivulet characteristics obtained from the measured data. Their list and brief description is given in the following text. For the principles of processing of the experimental photographies, identifying the rivulet and flow cell on them and converting the emitted light intensities into local film thicknesses, consult the corresponding algorithms descriptions in the Appendix D, Data evaluation program documentation.

3.2.1 Gas-liquid interface shape evolution along the plate

The local rivulet transversal profile shape is saved at specified distances from the top of the plate. It serves for calculation of other rivulet properties as well as for the control of the derived model. For example, it is using these profiles, it is possible to investigate the assumption of nearly flat surface of the rivulet.

How are these profiles obtained is explained in section D.3.2 (CutRiv). In essence, it can be said, that they are mean values of obtained local rivulet heights taken at small x-span near each made horizontal cut.

3.2.2 Size of the gas-liquid interfacial area

The size of gas-liquid iterfacial area, S_{g-l}, is the main output of the measurements. Its evaluation from experimental photos is described in section D.3.2 (RivSurf).

The dependency of S_{g-l} on the liquid flow rate (of chosen type) is obtained for each liquid and plate inclination angle. These data are then fitted using model defined in 2.5.2.

3.2.3 Local width and height

At the same distances as the profile shapes are measured also the rivulet local width and height.

Scheme of their measurements is in the Figure D.10 on page 91. The local rivulet width is the distance between its two edges in the studied transversal cut and its height is the highest point of such a cut.

These values can be used to validate the obtained models for simulating the rivulet gas-liquid interface evolution along the plate. Also, their ratio, $\varepsilon = h_0/2a$, with the meaning of symbols as stated in chapter 2 (Theory), can be used to investigate validity of assumptions used during the model derivation. Namely for the defendability of use of the lubrication approximation and neglecting the effects of gravity on the interface shape.

3.2.4 Local mean speed and Reynolds numbers

Local mean liquid speed is calculated by dividing the liquid volumetric flow rate by the surface under the current, i-th, profile,

$$\langle u_E \rangle_i = \frac{Q}{\int_{-a_i}^{a_i} h_i(y)\mathrm{d}y} \tag{3.1}$$

Through this mean speed are defined two liquid Reynolds numbers differing by the used characteristic length. The first used characteristic length is the rivulet local width, $2a$. The second one is the liquid capillary length defined as $l_c = \sqrt{\gamma/\rho g \cos\alpha}$. The resulting relations are

$$\mathrm{Re}_a^i = \frac{\rho \langle u_E \rangle_i 2a}{\mu} \qquad \text{and} \qquad \mathrm{Re}_{l_c}^i = \frac{\rho \langle u_E \rangle_i l_c}{\mu}. \tag{3.2}$$

These values can be used to study the assumption of laminar flow of the liquid. From the character of the flow along the plate, it is obvious, that the Reynolds number defined through the capillary length, Re_{l_c} is better description of the actual situation than Re_a, but as the later one is, because of the small ratio of l_c to $2a$ for the studied rivulets significantly higher, one can easily take it as the safe boundary pointing towards the flow character.

Note: As for the integral rivulet flow number, one can assume the mean liquid speed along the plate to be of the same order of magnitude as the one of a free falling film, ζ, as defined by equation (2.63) in 2.4.2 and the rivulet heigh to be smaller than its capillary length. Substituting l_c for h_{0i} in (2.63) and using the result for the Reynolds number calculation, one obtains the higher estimate for the actual rivulet integral Reynolds number

$$\mathrm{Re}_{max} = \frac{\rho \zeta_{l_c} l_c}{\mu} = \frac{1}{3\mu^2}\sqrt{\frac{\rho\gamma^3 \tan^3\alpha}{g\cos\alpha}}. \tag{3.3}$$

Still, Re defined by the above relation is the highest possible value that can be gained by the liquid flowing down the plate inclined by an angle α to the horizontal and it is independent of an actual liquid flow rate.

3.2.5 Local contact angles

Johnson *et al.* [54,55] proposed and Hagemeier *et al.* [51] refined a method of measuring the liquid-solid apparent (dynamic) contact angle, β, using the light induced fluorescence.

It is based on knowing the local film thicknesses and the distance between two pixels on the plate in the direction transversal to the rivulet flow. With an assumption of $\beta < \pi/2$, it is possible to calculate it numerically from the measured profile using equation

$$\tan \beta^i = \max_{y \in \langle -a,a \rangle} \left| \frac{\partial h(x_i,y)}{\partial y} \right|, \tag{3.4}$$

with y being the plate transversal coordinate, x_i specified distance of the i-th cut from the top of the plate and β^i the dynamic contact angle at such a distance. The scheme of axis notation is in Figure 2.1 on page 2.

With this method, the apparent contact angles from the both left and right side of the rivulet, β_L^i and β_R^i, respectively, were measured in each taken horizontal cut. This way, the dependence of contact angles on the distance from the top of the plate was obtained.

Such data were used to evaluate the assumption of small contact angles made as well as the one of narrow rivulet flowing down an ideal surface. For the later case, the measured contact angles would have been the same from both sides of the rivulet.

4. Data evaluation program description

As the experimental apparatus was based on an optical technique which outputs were photographies of the experimental and flow cells such as the ones shown in Figure 4.1, development of some technique to evaluate the obtained data was necessary.

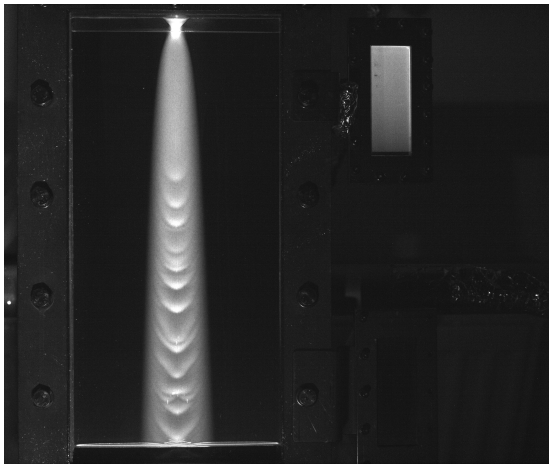

(a) Silicon oil DC 5

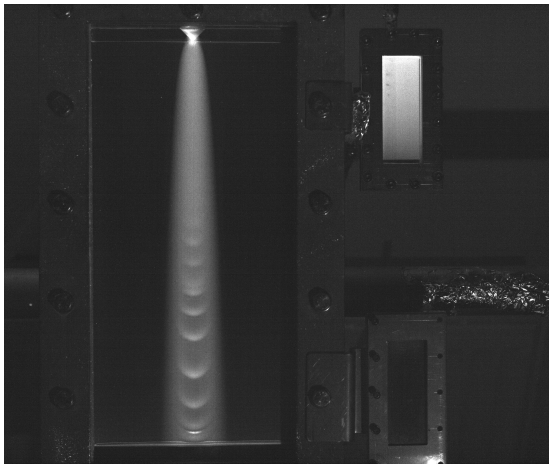

(b) Silicon oil DC 10

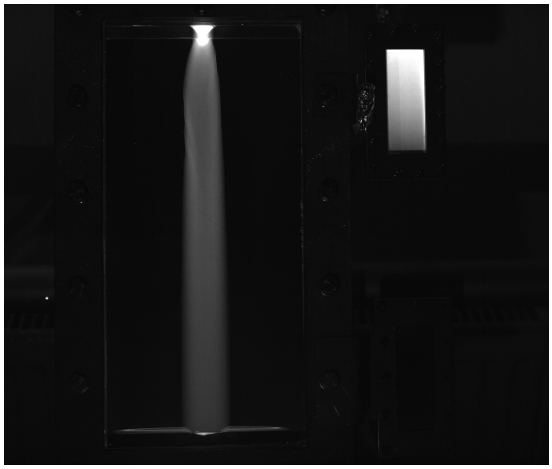

(c) Tenzids

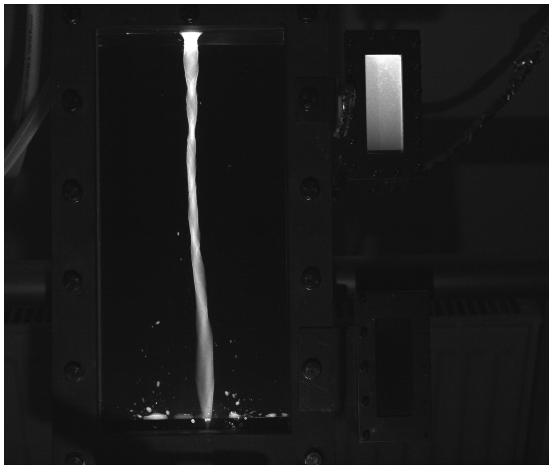

(d) Water

Figure 4.1: Examples of outputs of the experiment for different liquids. The plate is located at the center of the images, flow cell is in their upper right corner. Brightness of the images was enhanced for easier readability to human eyes.

To achieve that goal, a MATLAB program permitting in situ experiment processing

was written. The program source codes as well as its documentation and user manual [57] are published under MIT license [58] on GitHub [59] and they are also present on the DVD distributed with this work.

The software can:

1. Locate the inclined plate and flow cell on each experimental image.
2. Convert emitted light intensities (grayscale values) on the plate into distances.
3. Distinguish the rivulet from background noises.
4. Calculate the wanted quantities as they are described in 3.2.
5. Export the results into text files loadable in various spreadsheet programs (Microsoft Excel, LibreOffice Calc...).
6. Plot and compare the results of different experiments.
7. Evaluate the influence of various data processing parameters on the obtained results.

The program was developed with its usability even by not-a-programmer in mind and it can be divided into four main parts:

1. Preprocessing, loading and preparation of the experimental data.
   - Selected images are loaded from the source directory.
   - Background image is subtracted from images to be processed.
2. Image processing, locating plate and flow cell onto images.
   - Coordinates of the plate and flow cell edges are proposed to the user.
   - User verifies them and saves them into the program runtime environment.
3. Processing, calculation of rivulet's monitored properties.
   - Grayscale values are converted into local film thicknesses.
   - Rivulet is distinguished from the background noise.
   - Size of rivulet's (g)–(l) interfacial area and its other characteristics are calculated.
   - Study of different processing parameters on the results can be made.
4. Postprocessing and data visualization.
   - Previously calculated data are organized into tables and made plotable.
   - Calculated data can be fitted by the model presented in 2.5.2.

In the following text, there are presented the three most essential algorithms of the application. For more thorough description of it, see Appendix D or [57].

The presented algorithms are consecutively, the flow and measurement cells location algorithms, both part of the image processing part of the program and the rivulet distinction algorithm, which is used to cut off the rivulet from background noises and to calculate some of its most important properties.

4.1 Flow cell finding algorithm

The flow cell finding algorithm is, as it is obvious from its name, used for the flow cell location on the experimental photographies. It is a part of `findEdges.m` function, described in D.2.

As the flow cell is on the experimental images well visible (consult Figure 4.1), its location algorithms does not have to be very complicated. As the flow cell is always placed in right part of the image and it is the most rectangular (and with well prepared experimental apparatus also the most distinctive) element there, this knowledge can be used to simplify a search for it.

The algorithm itself is based on the contrast enhancement of the right part of experimental image, its conversion from grayscale to black and white with rather high threshold (brightness level under which the pixel is considered to be black), location of the various present elements boundaries and on choosing the most rectangular one between them.

The scheme of this algorithm is in Figure D.5 on page 78. The thorough description of it is presented in D.2.1, in Description of the flow cell finding algorithm.

4.2 Plate finding algorithm

As it is obvious from the Figure 4.1, borders of the inclined plate with the rivulet itself are much lest distinct than other elements present on the experimental images. Because of this, the plate finding algorithm needs an approximate position of the plate on which it is able to suppress the unsearched for image parts.

The plate localization itself is based on the Hough transform [60], a mathematical procedure used to distinguish straight lines on bitmap images.

After the straight lines are found on the examined part of the image, they are filtered based in their properties, such as their verticality or horizontality and relative distance from the approximately specified area edges. After this filtering, the remaining lines are divided in four groups based on their adjacency to one of the plate edges and from their location is estimated the precise position of the inclined plate borders.

The scheme of this algorithm is in Figure D.6 on page 79. The thorough description of it is presented in D.2.1, in Description of the plate finding algorithm.

Note: Both the flow cell and plate finding procedures are executed for each of the experimental images separately. With around 40 different images made with unchanged experimental set up, this usually provides large enough dataset to eliminate the algorithms fails using statistical methods as it is described in D.2.2 on page 81. Still even though it is not the case, user can always specify the poorly specified searched elements positions.

4.3 Rivulet distinction and interfacial area size calculation

With the plate edges distinguished and the emitted light intensities converted into local film heights on the plate, it is necessary to cut of the rivulet itself from any background noise possible.

To achieve this, two different algorithms were proposed. The first one is exploiting the fact, that outside the rivulet should in every transversal cut through the rivulet, denoted by i, apply the condition

$$\forall y \notin \langle -a_i, a_i \rangle, \quad \frac{\partial h(x_i, y)}{\partial (y)} = h_i'(y) = 0. \tag{4.1}$$

This algorithm is in the code and in Appendix D referred to as `'complex'`. However, as the emitted light intensity difference between two neighboring „noise“ pixel tends not to vary smoothly, this algorithm is not very reliable.

Second algorithm is based on the estimation of the background noise brightness level from the 25 % quantile of the brightness levels measured in each cut and on adding some relatively small value to it. Then the first values lower than the sum of 25 % quantile and such threshold encountered while moving to both left and right from the brightest (highest) point in the i-th cut are saves as the left and right rivulet edges. The scheme of this idea is in Figure D.10 on page 91. This referred to as `'simple'`. And it was proven to be quite robust. Still, its downside is the fact, that there is always part of the rivulet left out when evaluating its properties.

Both algorithms are described in detail in D.3.2 on page 89.

As each of the horizontal lines of the image of the plate has to be examined to find the rivulet edges, in the same program execution loop, there is also the addition of this i-th transversal cut the the whole rivulet interfacial area size calculated.

Because the distance between two neigboring pixels on the experimental image is very small (of order of magnitude $10^{-4}m$), no elaborate method had to be used for the interfacial area calculation. The profile shape between two pixels in rivulet transversal direction was approximated by straight line of length calculated from the Pythagorean theorem

$$\delta l_{ij} = \sqrt{(\delta y_{ij})^2 + (\delta h_{ij})^2}, \tag{4.2}$$

where δy_{ij} is the distance between points y_j and y_{j+1} in i-th transversal cut, δh_{ij} is their height difference and δl_{ij} the approximative distance between them.

With above defined δl_{ij}, size of the rivulet interfacial area is calculated from the data as

$$S^E_{g-l} = \delta x \sum_{i=1}^{N_C-1} \sum_{j=j\left(a^i_L\right)}^{j\left(a^i_R\right)} \delta l_{ij}, \tag{4.3}$$

with δx standing for the distance between two transversal cuts (or between two pixels in the vertical direction of the image), N_C being the total number of horizontal lines between upper and lower edges of the plate and $j\left(a^i_L\right)$ and $j\left(a^i_R\right)$ being index of the left and right edges of the rivulet in the i-th cut.

5. Results and Discussion

Following section is divided in two consecutive parts. In the first one are shown and commented the data obtained from experiments. Then, in the second part, the experimental data are compared to the theoretical results.

5.1 Experimental results

In the following text will be presented results obtained by performing experiments described in chapter 3. For each plate inclination angle were measured at least ten different liquid flow rates, when the measurement for one flow rate consisted of taking at least four different pictures of the rivulet under independent conditions.

At first, the description of measured rivulets interface shape is given. Next the measured sizes of gas-liquid interfacial area sizes in dependence on liquid type and volumetric flow rate are described. Then, the assumptions made in 2.5 are examined against the experimental results.

Only part of commented plots is placed in the following section. The rest of them is present in Appendix E which begins on page 105.

5.1.1 Experimental study of the gas-liquid interface shape

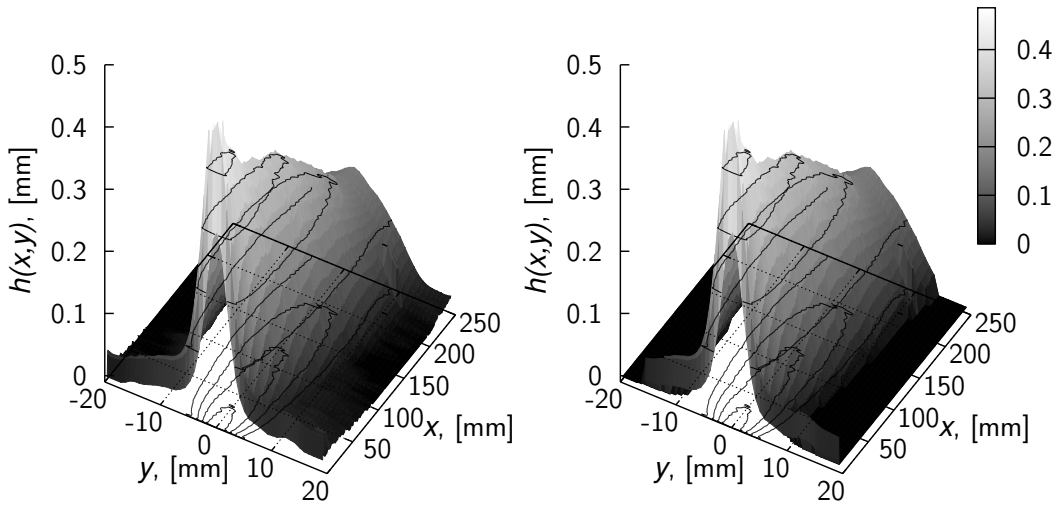

Figure 5.1: Comparison of measured rivulet surfaces before (left) and after processing, DC 10 oil, $\alpha = 75\,°$, $Q = 0.18 \cdot 10^{-6} m^3\, s^{-1}$

As the experiments were based on an optical method yielding primarily local film thicknesses at discrete points on the measured, inclined plate, the descriptive study of rivulet gas-liquid interface shape was performed.

Example of measured interface shape as function of plate dimensional coordinates, $h^E(x,y)$, is depicted in Figure 5.1 on page 35. On the left side of the presented image, direct result of conversion of the emitted light intensities into local film thicknesses is shown. On the right side, the product of cutting out the rivulet from background noise is presented. On both images, h^E are plotted as complete surfaces with added contours.

From the direct comparison of left and right side of Figure 5.1, it can be established that almost all the neglected surface does not belong to the rivulet. Consequence of this is that the cut off part of the rivulet does not have any substantial effect on the measured gas-liquid interfacial area size, S^E_{g-l}.

Also, one can make some general notes on the $g-l$ interface shape. At first, it is well visible, that the liquid is spreading along the plate – the width of the depicted rivulet is increasing along the plate while its height is decreasing.

However, the liquid flow rate of the rivulet in Figure 5.1 is very low and on top of that, it is a silicon oil, for which the observed wetting properties were much better than for the water.

Increasing the liquid flow rate caused the appearance of laminar waves on top of the rivulet. Examples of such behavior can be seen in Figure 4.1 on page 31, especially for the cases of DC 05 and DC 10 silicon oils. This topic was, for the case of free film, described for example by Moran, Inumaru and Kawaji in [23]. As the waving instabilities of formed rivulets were ignored in the scope of this thesis, the reader will have to settle for the explanation, that for wide enough rivulets (which corresponds to high liquid flow rates), one can expect the gravity to flatten the center part of the rivulet and to induce a formation of a region which is behaving in same way as the free falling films. For details, reader is reffered to previously mentioned literature on wavy films or to study of the problem by Weiland and Davis [50].

As for the influence of liquid wetting properties on rivulet shape, for the water, which has on steel bad wetting properties, the formation of precursor film on the plate could not be assured during the experiments. The reason of this was, that the film broke up almost instantly after flooding the cell or after the liquid flow rate increase (for details on these parts of experimental procedure, see measurement procedure description in subsection 3.1.5). In the absence of precursor film, the rivulet contact lines were pinned[1] by the imperfections of the steel plate surface almost immediately after insertion of the liquid on the plate. Thus, the rivulet spreading became more or less random. Besides, the meandering instabilities of formed rivulet as described for example in [61] were encountered.

In Figure 5.2 on page 37, there are depicted the transversal cuts through the rivulet made at each five centimeters from the top of the plate. The shown result was obtained for DC 05 oil, plate inclination angle $\alpha = 60\,^\circ$ and for the relatively small flow rate, $Q = 0.24 \cdot 10^{-6}\,\mathrm{m^3\,s^{-1}}$. For higher flow rates and silicon oils, the above described waving occurs on the rivulet.

The lines in Figure 5.2 are representing the actual measured profile (as the distance between two neighboring pixels in y direction of the image was of order of $10^{-4}\,\mathrm{m}$). Each tenth point is highlighted by the symbol to distinguish between different cuts. Only the cut out part of the rivulet is shown, the distance between the lowest point of the shown profile and the line $y = 0$ illustrates the size of neglected part of the rivulet.

The axis in Figure 5.2 are not in equal ratio. The order of magnitude of the rivulet height is of $10^{-4}\,\mathrm{m}$ whilst its width is of $10^{-2}\,\mathrm{m}$. As the result, the rivulet is much flatter than it would appear from the presented image. For better notion of the rivulet height to

[1] For details of contact line pinning, see [8] or [5].

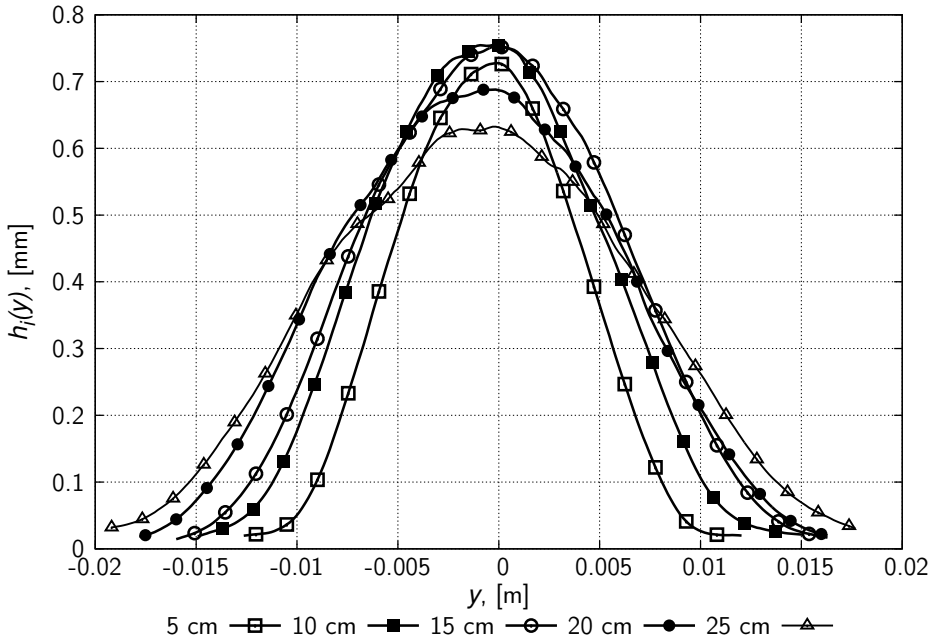

Figure 5.2: Measured profile shapes along the plate for silicon oil DC 05, $\alpha = 60\,^\circ$ and $Q = 0.24 \cdot 10^{-6}\,\mathrm{m^3\,s^{-1}}$.

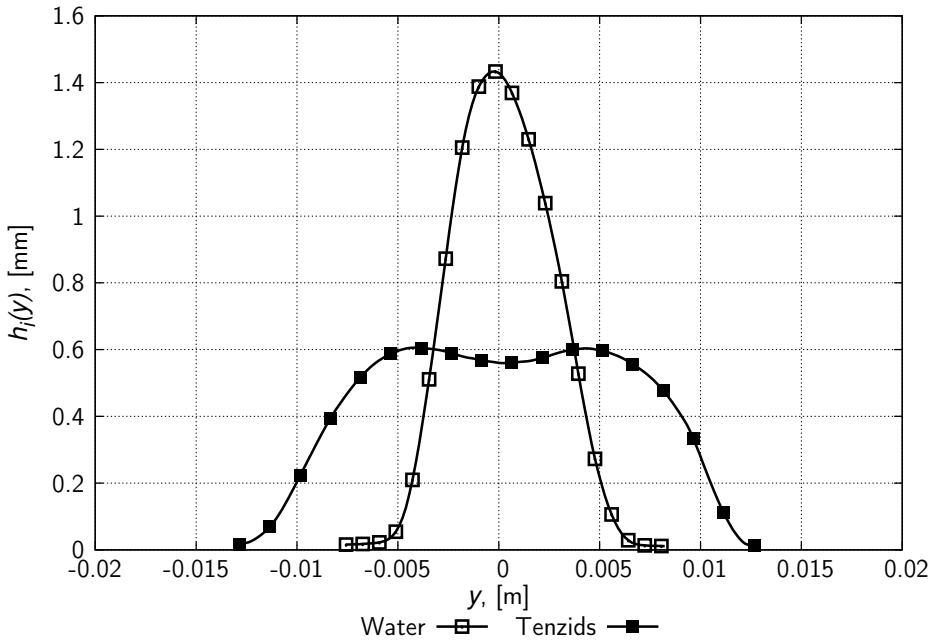

Figure 5.3: Comparison of profile shapes of water and tenzids at 15 cm from the plate top for $Q = 5.77 \cdot 10^{-6}$ and $\alpha = 45\,^\circ$.

width ratio, consult subsection 5.1.4, especially the Figure 5.12 on page 45.

Also, from the Figure 5.2, it is obvious, that the decrease of rivulet height is not as sharp as it would suggest the corresponfing increase of width. As the reason of this behavior, one could point out only fluctuations in the liquid velocity in the x-axis direction, u, which would appear to decrease as the liquid is flowing down the plate. However, if one compares the profiles for silicon oils and the ones for water and water with added surfactants (in the following often referred to as „tenzids“) (see Figure E.1 in Appendix E), it can be stated, that for liquids with lower viscosities this does not happen and the liquid velocity rests approximately constant along the plate.

The comparison between rivulet profile shapes for two liquids differing mainly by their surface tension is shown in Figure 5.3. The displayed liquid types are the water and water with added surfactants (tenzids). The cut in the middle of the plate was chosen for the comparison, as both profiles are well developed.

From the comparison, one can establish that the surface tension coefficient is crucial for the gas-liquid interface shape. However, the height profile for water with surfactants has two local maximums and is sunken in the middle. This points to strong effects of gravity on its shape, but even with that taken into account, the theory and numerical simulations would suggest the presence of only 1 height maximum, at the rivulet centerline [7,62]. This can be taken as reminder of the fact, that even now, there is very little known on the subject of influence of surfactants on the spreading properties of the liquids [5,20]. Furthermore, it is well visible, that ratio of two liquids capillary lengths can be used to estimate their ratio rivulet heights at centerline,

$$\frac{l_c^1}{l_c^2} \sim \frac{h_0^1}{h_0^2}. \tag{5.1}$$

5.1.2 Measured sizes of the gas-liquid interfacial area

A dependence of measured rivulet interfacial area size, S_{g-l}^E on the liquid volumetric flow rate was obtained for each combination of the liquid type and plate inclination angle.

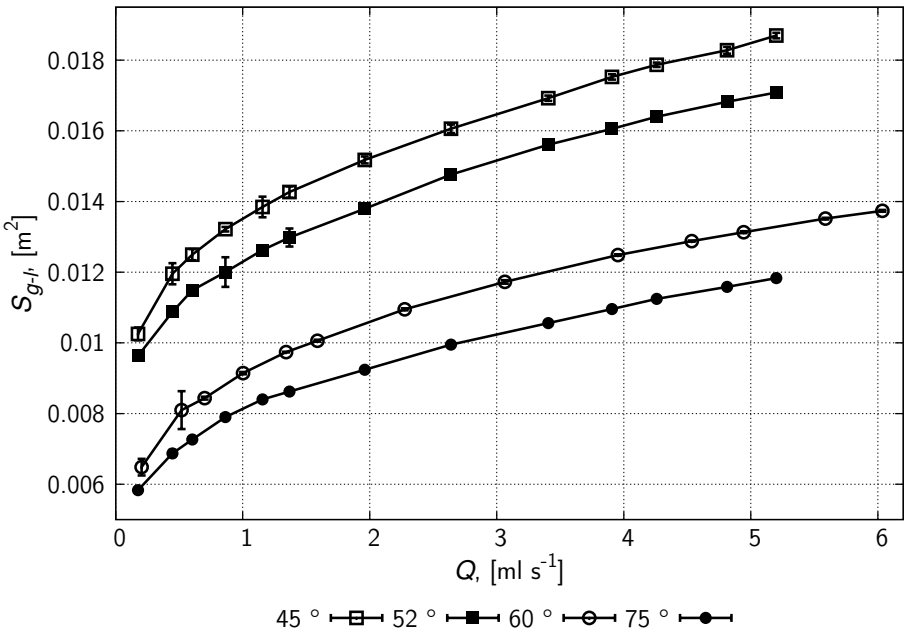

Figure 5.4: Measured S_{g-l}, DC 10 oil, influence of the plate inclination angle. Mean values with errorbars are depicted.

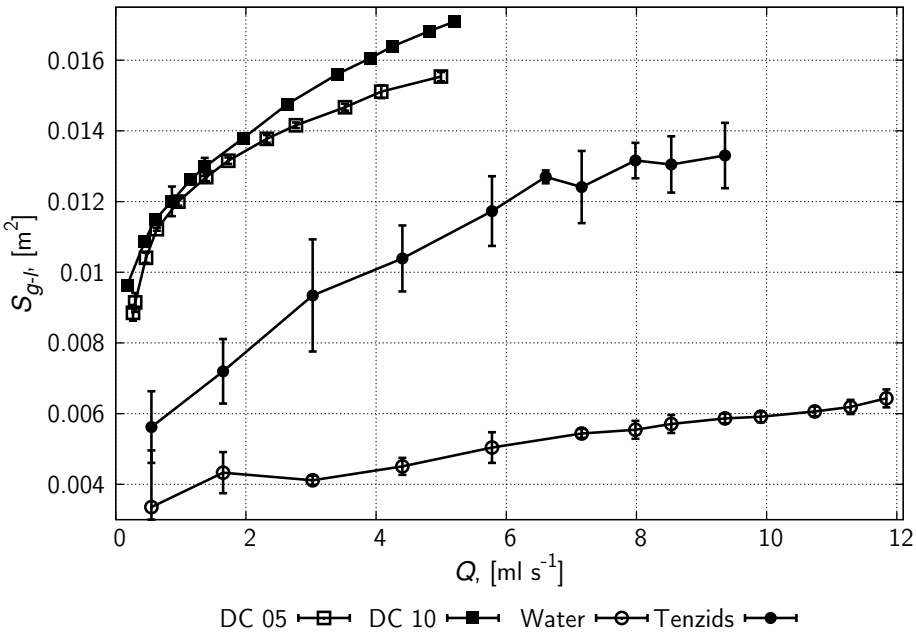

Figure 5.5: Measured S_{g-l}, $\alpha = 52\,^\circ$, different liquids. Mean values with errorbars are depicted.

Note: All the lines shown in figures in Experimental results section of the text are generated only as connections of experimental points and have no theoretical meaning.

Example of experimental measurement results for one liquid type, DC 10, and four plate inclination angle is shown in Figure 5.4. In the Figure 5.5, there is similar situation depicted, nonetheless, this time with only one plate inclination angle, $\alpha = 52\,^\circ$, and all four measured liquids.

From the measured dependencies, one can conclude the following:

1. S^E_{g-l} is inversely proportional to plate inclination angle.
2. S^E_{g-l} is proportional to liquid flow rate
3. S^E_{g-l} is inversely proportional to the surface tension.
4. S^E_{g-l} is almost the same for silicon oils DC 05 and DC 10 which viscosities differ approximately by factor of two. Thus it is probable, that the effect of viscosity on the S_{g-l} is not crucial.
5. Density of used liquids is to similar one to each other to recognize its influence on S_{g-l}.

Comparing the measured results with theoretical relations derived in subsection 2.5.2 (Interfacial area size of rivulet with moving contact lines) one can predict the low effects of viscosity on the results, as it influences the resulting $\beta(x)$ only with power of 1/4 (hidden in constant $\bar{A}$ in equation (2.84)) and logarithmically. On the other hand, the influence of surface tension on the resulting contact angle, β, dependence on x rests of the form $1/\gamma$. Thus its higher influence on the rivulet interfacial surface area size can be anticipated.

As for the effects of plate inclination angle, α, in the relation (2.84), all the effects of gravity on the interfacial profile shape were neglected. However, it is still influencing the resulting spreading of rivulet and hence its interfacial area size by the transformation of

$t \to x(t)$ as defined by (2.76). Other effect of it was introduced by generalizing the relation (2.29) to its form for an inclined plate, (2.78). Both of these influences are pointing towards the same result being that S^E_{g-l} should decrease with increase of $\sin\alpha$.

The effect of liquid flow rate increase is obvious as the interfacial surface size is increasing with higher amount of liquid flowing undernieth it.

Furthermore, as no distinctive discontinuity of measured S^E_{g-l} was observed with appearance of the laminar waves on the film (they were noticed for the silicon oils with flow rates higher than $\approx 3 \cdot 10^{-6}\,\mathrm{m^3\,s^{-1}}$), it can be deduced, that their effect on the interfacial area size should not be substantial.

5.1.3 Measured contact angles

The measure of apparent contact angles and their evolution along the rivulet was done mainly to test the derived model and made assumptions. As the contact angles were measured simultaneously from both sides of the rivulet, one could study not only their dependence on the plate length coordinate but also the contact angle hysteresis.

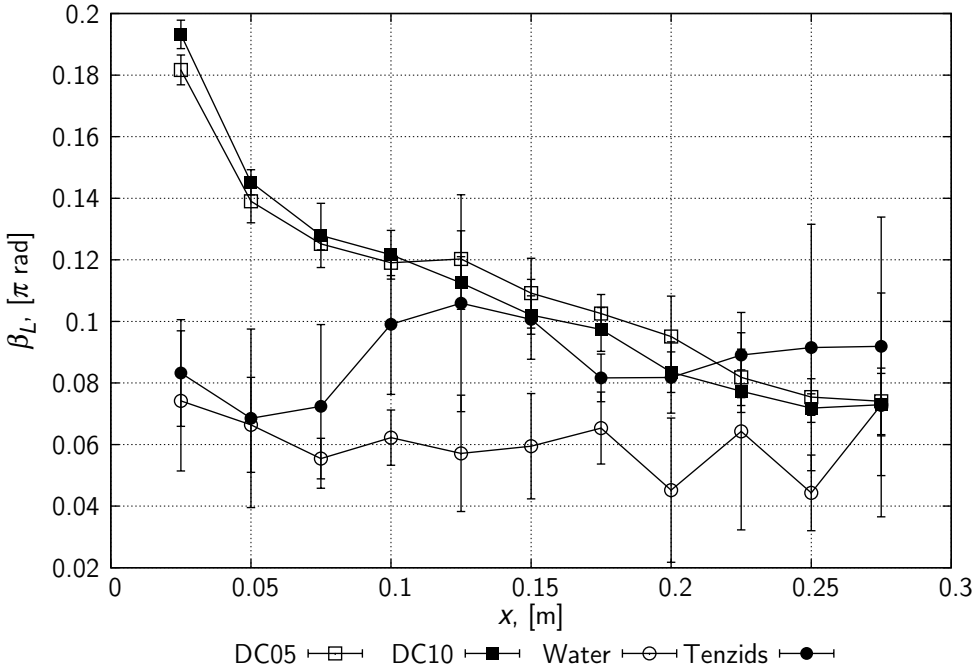

Figure 5.6: Comparison of measured apparent contact angles measured from the left side of the rivulet for different liquids, $Q \sim 0.56 \cdot 10^{-6}\,\mathrm{m^3\,s^{-1}}$, $\alpha = 45\,^\circ$.

In the first of presented results, Figure 5.6, the measured contact angles for one (small) liquid volumetric flow rate, $Q \approx 0.56 \cdot 10^{-6}\,\mathrm{m^3\,s^{-1}}$, and plate inclination angle $\alpha = 45\,^\circ$ are compared.

For such a low liquid flow rate, there were observed no waves on rivulet that could influence the measured contact angles. Besides, for this flow rate, one can safely assume the laminar flow of the liquid along the plate (for details see 5.1.5).

In case of both silicon oils, the strong trend of the contact angle decrease can be observed. However, for the water and water with added surfactants, the evolutions of contact angles along the plate seem rather arbitrary. For the water, the contact line could be assumed as pinned to the imperfections of steel plate (for example due to its roughness) making the rivulet width as well as its contact angle approximately constant (compare this Figure with Figures 4.1 (d) and E.3). Water with the surface tension lowered by surfactants is clearly spreading over the plate, although there could not be established any

trend for its measured apparent contact angles. This lack of connection between the tenzid rivulet spreading and its contact angles is yet another proof of unresolved problematics of surfactants effects on liquid spreading.

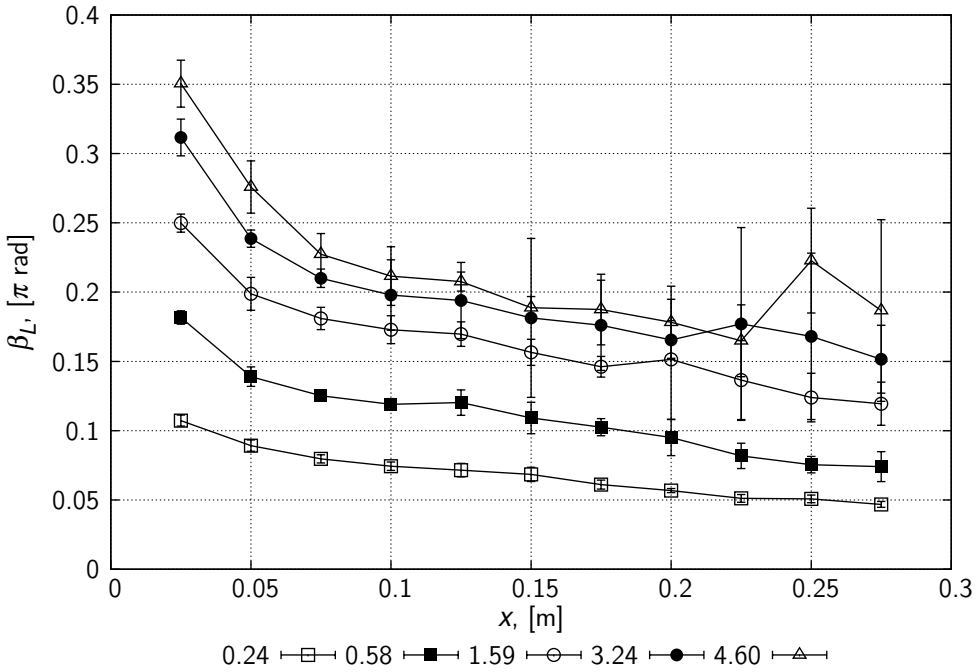

Figure 5.7: Measured values of apparent contact angle from the left side of the rivulet for different Q along the plate. DC 05 oil, $\alpha = 45\,^\circ$. Mean values with errorbars are depicted. Liqud flow rates in $Q \cdot 10^{-7}\,\mathrm{m^3\,s^{-1}}$ are specified in graph legend.

In Figure 5.7 are presented measured dynamic contact angles along the plate for one of the silicon oils, DC 05, at plate inclination angle $\alpha = 45$ and for different liquid flow rates. The contact angles are increasing with increase of Q, yet the trends are remaining the same.

The higher initial contact angles, β_I^E (and the resulting stronger dependence of β^E on the plate longitudinal coordinate) can be attributed to the fact, that the maximal initial rivulet width, a_I, is effectively limited by the size of the liquid inlet on the experimental apparatus (see the Figure 3.3). This limitation is also the main reason, that the initial rivulet contact angle was not used as the initial condition of the equation (2.82) directly, but was calculated from this maximal initial rivulet width (for details, see 5.2.1).

Another noticeable aspect of the Figure 5.7 is the influence of the waves forming on the rivulet on the measured contact angles as it can be visible especially for the case of $Q = 4.60 \cdot 10^{-6}\,\mathrm{m^3\,s^{-1}}$. Such behavior can be assigned to the two different causes.

The first one would be, that the formed wave is in some manner influencing the contact line movement. The second reason for such effect would be the imperfection of chosen contact angle measuring technique. The contact angle is evaluated from the slope of the most steep tangent to the interface profile. Hence with a sharp wave formation, β^E could be evaluated inadequately.

In the Figure 5.8 on page 42, the measured contact angles from left and right side of the rivulet, β_L^E, β_R^E are compared for different liquids and flow rates. One plate inclination angle, $\alpha = 45\,^\circ$, is used for all the depicted data.

As the behavior of DC 05 silicon oil is almost the same as the one of DC 10 and as the behavior of tenzids is quite random, these two liquids were omitted from comparison.

Even though the β_L^E and β_R^E were quite different for the case of DC 10 silicon oil and

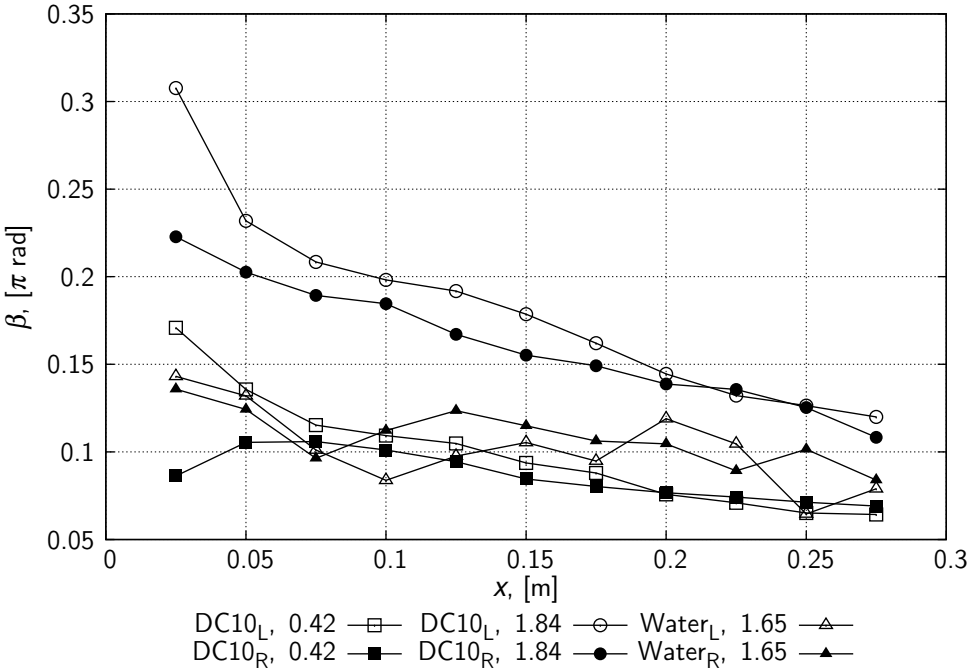

Figure 5.8: Comparison of apparent contact angles measured from the left and right side of the rivulet for different liquids and flow rates. Liquid type and volumetric flow rate in $Q \cdot 10^{-6}\,\mathrm{m^3\,s^{-1}}$ are specified in plot legend. Plate inclination angle is the same for all the data, $\alpha = 45\,^\circ$

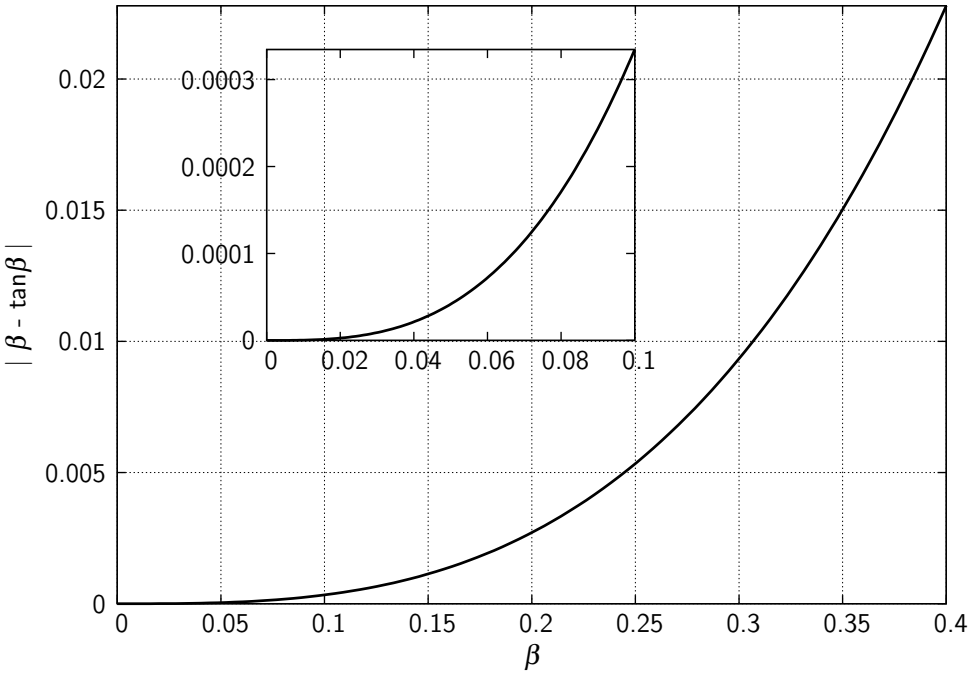

Figure 5.9: Study of absolute error introduced into calculation by assumption $\tan\beta \approx \beta$

low Q, the trend was (mainly in the lower part of the plate) the same and the measured values converged one to another. For higher flow rate, the difference between these two angles was even less important. This observation is pointing towards the deduction, that the measured silicon oil rivulets can be, in general, taken as symmetric, hence laying on the precursor film surpressing the steel surface imperfections.

The case of water is, however, completely different. As it is well visible from the discussed Figure 5.8, both the contact angles are remaining roughly constant with some arbitrary jumps along the plate. This is suggesting, that the contact line is mainly fixed and the plate can not be taken as completely wetted.

The last note about measured apparent contact angles is about their absolute values. In the theoretical part of the work, the assumption of small rivulet contact angles was made multiple times, resulting in simplification $\tan\beta \approx \beta$. This simplification was used for example in derivation of equation (2.84).

The measured contact angles, β^E, were all in range of $\langle \sim 0.03, \sim 0.4 \rangle$. The study of absolute error introduced into calculation by the above mentioned simplification is in the Figure 5.9 on page 42. In the main part of the plot, there is evolution of absolute error along the whole range of obtained β^E. In the enhanced part, there is the same thing for $\beta^E \in \langle 0{,}0.1 \rangle$, which was the case for small liquid flow rates.

The maximal error caused by small angles approximation was of order of magnitude 10^{-2}. However, for small Q, it was substantially smaller.

5.1.4 Measured widths, heights and their ratio

Another tracked quantities were the rivulet dimensions along the plate. Namely its width, $2a = a_L^E + a_R^E$, and its height at centerline, h_0^E. The notation of the rivulet width was altered to heighten the fact, that real rivulets were not exactly symmetric, so the additions to their width, $2a$, from the left and right side were different.

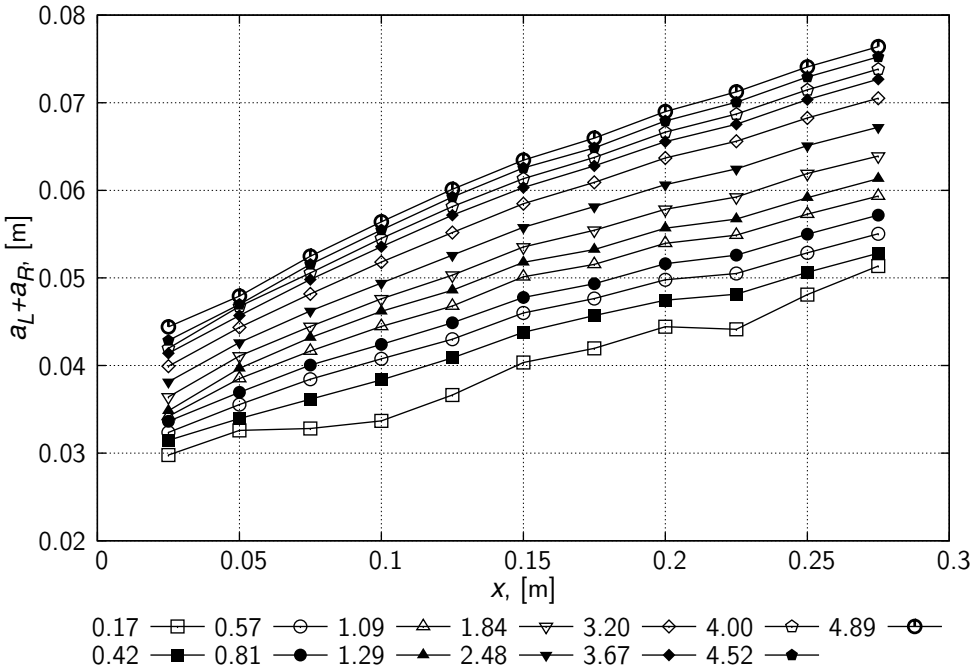

Figure 5.10: Mean values of measured rivulet widths along the plate for silicon oil DC 10, $\alpha = 45\,^\circ$. Liqud flow rates in $Q \cdot 10^{-6}\,\mathrm{m^3\,s^{-1}}$ are specified in graph legend.

In Figure 5.10 are shown the measured rivulets width for the DC 10 silicon oil and plate inclination angle, $\alpha = 45\,^\circ$. The increase of measured rivulet widths for increasing Q is

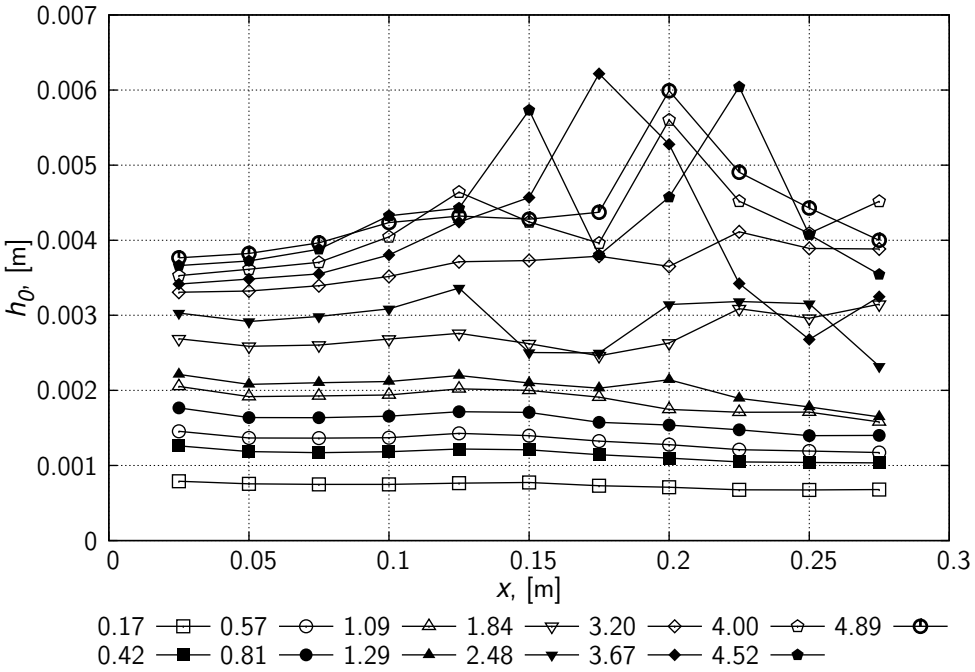

Figure 5.11: Mean values of measured rivulet heights along the plate for silicon oil DC 10, $\alpha = 45\,^\circ$. Liquid flow rates in $Q \cdot 10^{-6}\,\mathrm{m^3\,s^{-1}}$ are specified in graph legend.

understandable. The increase of $a_L^E + a_R^E$ along the plate longitudinal coordinate, x, is due to the rivulet spreading. Comparing the Figure 5.10 to the E.3 in Appendix E, one finds, that no assumptions on water on steel spreading based on the experimental results can be made. Comparison of behavior of different liquids can be done by putting in contrast the Figures 5.10 on page 43 and Figures E.2, E.3, and E.4 in Appendix E.

In Figure 5.11 are shown the measured rivulets heights at centerline, h_0^E for the same liquid and plate inclination as in Figure 5.10 (DC 10 oil, $\alpha = 45\,^\circ$). For lower Q, the slight decrease of the rivulet height along the plate can be noticed. For $Q \geq 1.84 \cdot 10^{-6}\,\mathrm{m^3\,s^{-1}}$, especially in lower parts of the plate, one can see the effects of laminar waves on the rivulet height.

As it is visible from Figures E.5, E.6, and E.7 in Appendix E, both silicon oils are behaving in almost the same way with only difference being that due to its lower viscosity, the laminar waves are appearing sooner on DC 05 than on DC 10.

As for the water and tenzids, the first named one is, for low Q, practically not spreading at all and its height therefor remains constant. For higher flow rates, the meandering instabilities appear and the evolution of h_0^E along the plate becomes arbitrary.

From comparing the Figures E.6 and E.7 on page 108, it can be viewed, that the addition of the surface tension lowering agent to the water has substantial effect on its behavior. For higher Q, the liquid height decreases sharply from its initial values forced by the liquid inlet geometry (see 5.2.1) and than the liquid spreading slows down to the point, that it almost stops.

The last plot presented in this section, Figure 5.12, and the Figure E.8 on page 109 serve to examine the assumption of small height to width ratio, ε, of the rivulet made in derivation of the equation (2.84). For silicon oils and tenzids, ε^E is decreasing along the plate, as the liquid is spreading over it. In case of the water, its behavior is unpredictable as both water rivulet height and width are behaving mostly randomly due to the measurement technique imperfections (the existence of thin film over the whole plate could not be ensured).

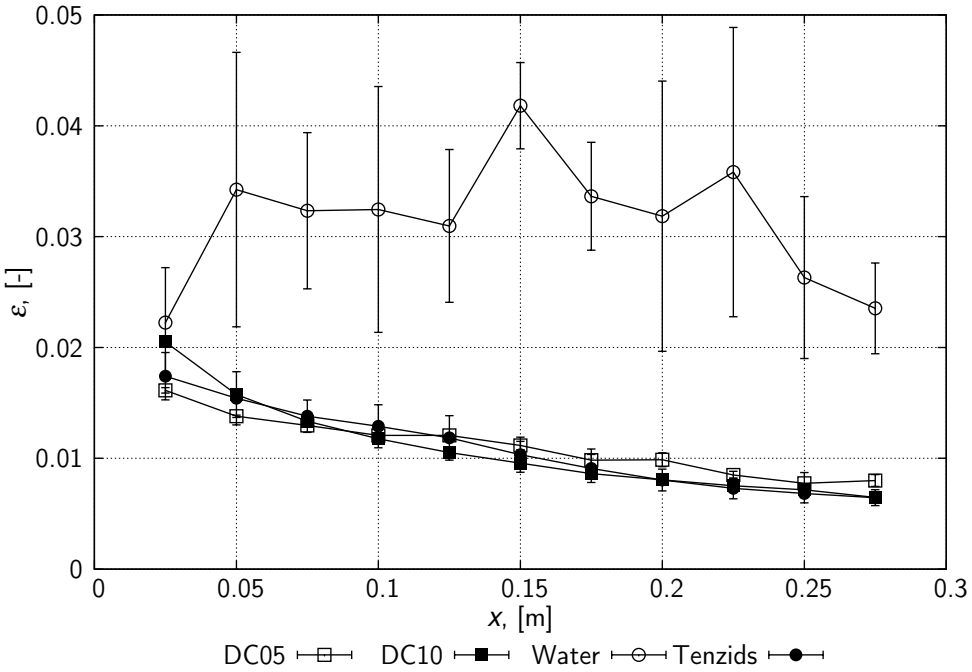

Figure 5.12: Rivulet centerline height to width ratio for different liquids. $\alpha = 60\,^\circ$, $Q \sim 0.56 \cdot 10^{-7}\,\mathrm{m^3\,s^{-1}}$.

In the Figure E.8 is depicted the ε^E for the case of DC 10 oil spreading over the plate inclined by $\alpha = 45\,^\circ$ to the horizontal with different Q. From this Figure, it can be seen, that the ε^H is increasing with increase of Q. This can be added to the effects of the liquid inlet on the spreading of the examined rivulets.

5.1.5 Measured Reynolds numbers

Throughout the theoretical part of the presented thesis, the laminar flow of liquid was assumed. To examine the validity of this hypothesis, the liquid Reynolds numbers were calculated from the measured quantities at different positions from the plate top.

Two different characteristic lengths were used for these calculations, as it is described in subsection 3.2.3 on page 29. Based on the liquid behavior, it was concluded, that the capillary length, l_c, is better length scale for such calculations than the rivulet width, $2a$, as the maximal x-direction velocity of the liquid will be of the same order of magnitude as the maximal velocity in free falling film of the thickness h_0^E.

Hence, as the h_0 in the rivulet will be always smaller than its l_c, but they are of the same order of magnitude, it is more suitable as the characteristic length for the Reynolds number calculations, than $2a$, which is to l_c in approximate relation

$$2a \approx \frac{l_c}{\varepsilon}. \tag{5.2}$$

Also, witch l_c being the justified length scale for the Reynolds number calculation, one can predict as well its highest possible value based on the approach explained in subsection 3.2.3.

The above described situation is shown in Figure 5.13 on page 46, where the Reynolds numbers calculated with l_c and $2a$ as the characteristic lengths are compared for the case of DC 10 silicon oil, $Q = 0.57\ \cdot 10^{-6}\,\mathrm{m^3\,s^{-1}}$ and $\alpha = 60\,^\circ$. The dash-dotted line represents the value of maximal Reynolds number of DC 10 oil rivulet flowing down the plate inclined by $\alpha = 60\,^\circ$ to horizontal as defined by the equation (3.3).

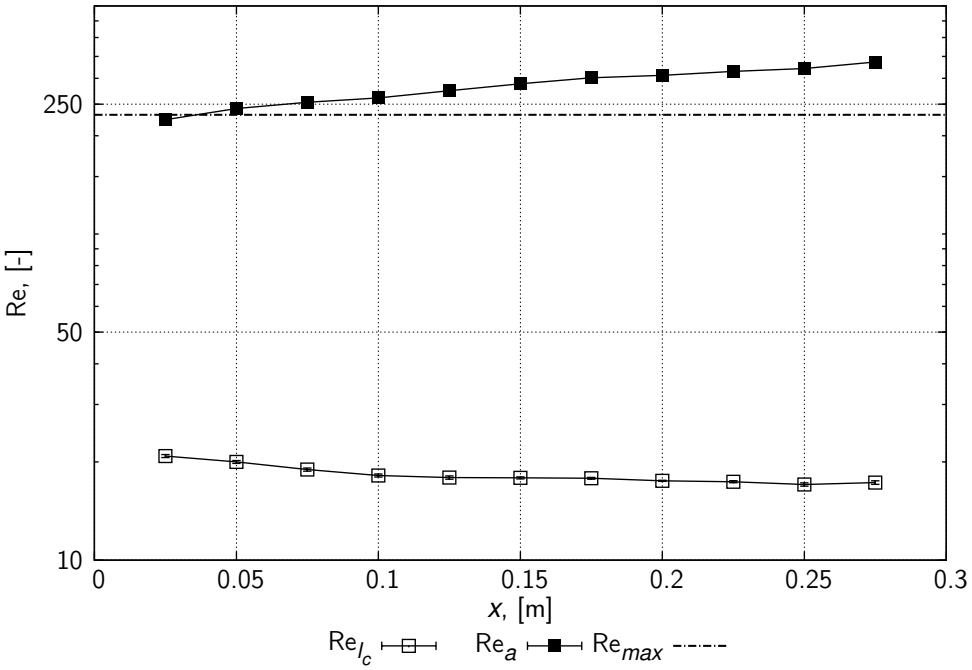

Figure 5.13: Comparison of Re_{max}, Re_{l_c} and Re_a for DC 10 oil, $\alpha = 60\,^\circ$ and $Q = 0.57 \cdot 10^{-6}\,\mathrm{m^3\,s^{-1}}$.

In the Table 5.1, there are calculated Re_{max} for different liquids and plate inclination angles. As the usual estimates of Reynolds number for transition between laminar and turbulent flows is in case of free falling film $\mathrm{Re} \approx 1000$ [63], the laminar flow can be assumed without any problems for the DC 10 silicon oil and for most of the measurements with DC 05 oil. The water and water with added surfactant could potentially exhibit a turbulent flow behavior, still, the values calculated from the equation (3.3) are especially for the higher plate inclination angles strongly overestimated, as the capillary length diverges with vanishing effects of gravity. The dependence of Re_{max} on the plate inclination angle is shown in Figure E.9 in Appendix E. Clearly, the capillary length cannot be used as the characteristic length for the film flow down the vertical plate or anywhere near such situation. Nevertheless, it still remains good estimate for $\alpha \leq\sim 60\,^\circ$.

Table 5.1: Re_{max} for different fluids and plate inclination angles

α	DC 05	DC 10	Water	Tenzids
$45\,^\circ$	347.4	85.53	$3.735 \cdot 10^4$	$1.621 \cdot 10^4$
$52\,^\circ$	539.1	132.7	$5.796 \cdot 10^5$	$2.515 \cdot 10^4$
$60\,^\circ$	941.7	231.9	$10.12 \cdot 10^5$	$4.394 \cdot 10^4$
$75\,^\circ$	4140	1019	$44.51 \cdot 10^5$	$19.32 \cdot 10^4$

In Figure 5.14 on page 47, Re_{l_c} calculated from measured mean liquid velocities, $\langle u_E \rangle$, for relatively high liquid flow rates are shown. The plate inclination angle was for all the depicted measurements $\alpha = 60\,^\circ$. It is visible, that the lowest obtained Re_{l_c} corresponds to the DC 10 oil, which is understandable as both its capillary number and measured $\langle u_E \rangle$ are relatively low due to DC 10 high viscosity.

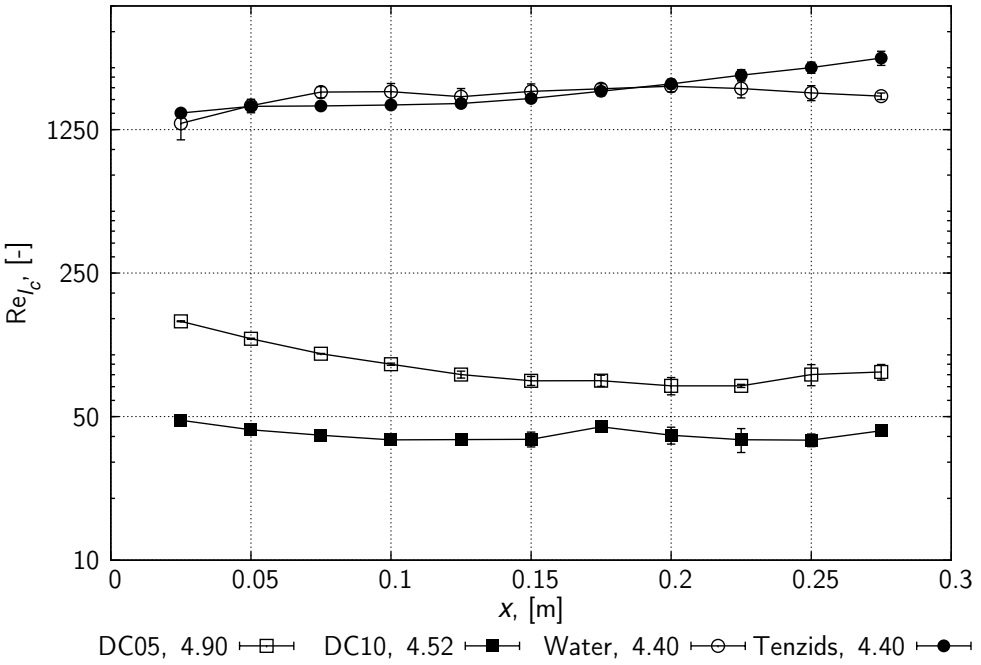

Figure 5.14: Reynolds numbers calculated from $\langle u_{exp} \rangle_i$ and l_c for different liquids and $\alpha = 60\,^\circ$. Liquid types and flow rates in $Q \cdot 10^{-6}\,\mathrm{m^3\,s^{-1}}$ are specified in graph legend.

5.1.6 Summary of experimental results

The obtained experimental results can be summarized in a following few points. In the parenthesis is mentioned the part of the text, where details on each proposed statement can be found.

1. The difference between real and measured S^E_{g-l} is not substantial (5.1.1).

2. Proposing any S_{g-l} calculation method for liquid with added surfactants agent is not defendable, as the effects of them on the liquid spreading are fundamental and not yet very well understood ([5,8,20],5.1.1, 5.1.3).

3. The effects of liquid properties, plate inclination angle and liquid volumetric flow rates on S^E_{g-l} would suggest at least qualitative agreement with the model derived in subsection 2.5.2. However, this is more thoroughly tested in 5.2 (5.1.2).

4. Measured values of apparent contact angles, β^E, would suggest, that the assumption of $\tan\beta \approx \beta$ is defendable in a scope of the carried out experiments (5.1.3).

5. Obtained rivulet height to width ratios, ε^E, support the simplification of wide and flat rivulet as it has been used in theoretical part of the work at least for the case of silicon oils and tenzids (5.1.4).

6. The conditions of completely wetted plate were not achieved during the experiments with water. Dry areas on the plate caused the pinning of the water rivulet contact lines and made the results more close to the ones obtained for example by Towell and Rothfeld [6] or Duffy and Moffat [7] for the case of rivulet with fixed contact lines (5.1.3, 5.1.4).

7. The assumption of laminar flow is easilly defendable for the case of silicon oils. As for the water, both distilled and with added surfactants, it would have to been put under more thorough testing (5.1.5).

To conclude, one can state, that the model derived in subsection 2.5.2 should be able to describe at most the cases of low flow rates for silicon oils. At higher Q or with the other two types of used liquids, the simplifying assumptions made to derive it could not have been defended.

5.2 Theoretical results and their comparison and fitting to measured values

In this part of the text, the results obtained from use of the model derived in subsection 2.5.2 will be presented and compared to the experimental values. The comparison is divided in two parts. First one describes the case of silicon oils for which the experimental conditions were kept in accordance with assumptions made during the model derivation. Then, the situation of water, both with and without added surfactants is studied.

Before the comparison, there is placed derivation of the most suitable initial condition for the equation (2.84). The problem of this initial condition was not studied in theoretical part of the work, because it is not a general property of the derived model, but a specific feature of the studied system induced by the experimental set up construction.

5.2.1 Initial condition for the equation (2.84)

To obtain the best agreement between the theory and experimental data, it is crucial to supply the equation describing the evolution of apparent contact angle, β, along the plate, (2.84) (to be found in subsection 2.5.2, on page 22), with the right initial condition.

The problem of finding this condition is induced by the liquid inlet on the experimental apparatus (see Figure 3.3 on page 26). This inlet has limited cross sectional area which, for higher flow rates, forces it to behave as a spring, not letting the liquid fall onto the plate freely, but giving it an initial height far higher than it should be. Such behavior can be observed the best on Figure E.7 in Appendix E.

The consequence of this is, that the apparent contact angle on the top of the plate is very hard to guess from its behavior on the rest of the plate. On the other hand, the maximal initial width of the rivulet is limited by the geometry of the liquid inlet and is easily calculable

$$a_{I,max} = \frac{1}{2}\sqrt{3} \cdot 10^{-2}\,\mathrm{m}, \tag{5.3}$$

as the liquid source is an equilateral triangle of height 1.5 cm.

Substituting from the equation (5.3) into (2.78) and solving for β, one finds lower estimate for initial condition for equation (2.84) in form dependent on the liquid flow rate and the plate inclination angle,

$$\beta_I \approx \left(\frac{105}{4} \frac{\mu Q}{\rho g \sin\alpha a_{I,max}^4} \right)^{1/3} \tag{5.4}$$

Unfortunately, as the liquid source is of a form of a triangle, the lowest possible initial width would be $a_{I,min} = 0\,\mathrm{m}$, causing the contact angle to diverge. Due to this, the initial condition for β will be calculated from (5.4).

5.2.2 The case of silicon oils

For the case of silicon oils and the initial condition specified by (5.4), there rests only one parameter to be fitted in the equation (2.84) and it is l, the intermediate region length scale and member representing all the solid-liquid microscopic interactions. As the study of such forces is outside of the scope of this thesis, l was kept as an adjustable parameter and

its exact values were searched for by fitting the dependencies of S_{g-l} on Q to experimental data.

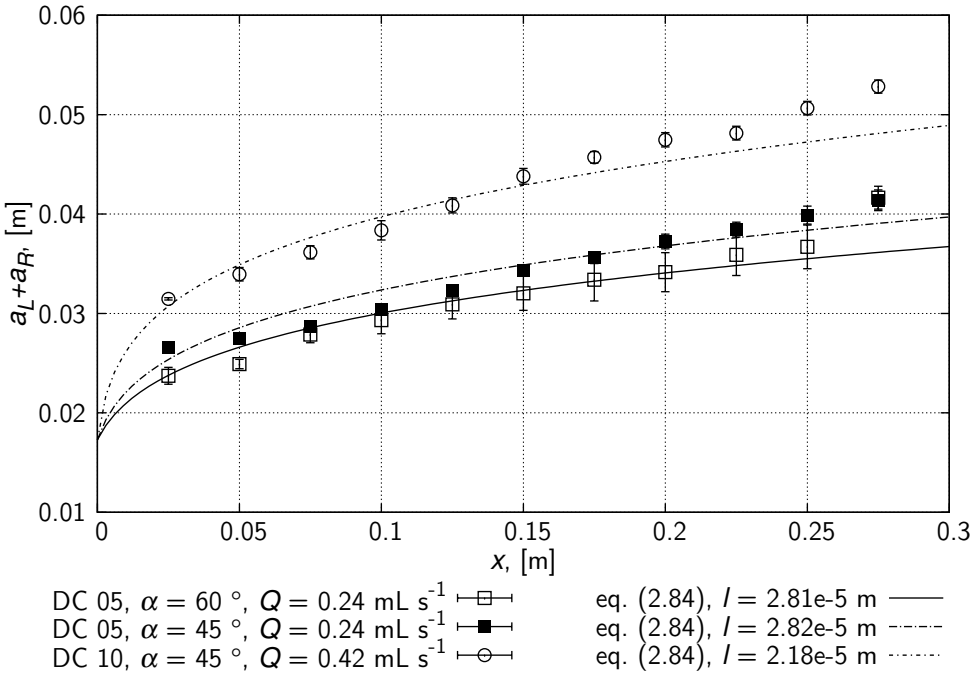

Figure 5.15: Comparison of measured and calculated rivulet widths, $2a$, for both silicon oils and different plate inclination angles

In Figure 5.15, there are compared the predicted dependencies of the rivulet width on the plate length coordinate with the experimental data. The intermediate length scale (or the precursor film thickness), l, was proven to be approximately constant for both silicon oils and independent of the plate inclination angle. For DC 05 oil, $l \approx 2.8 \cdot 10^{-5}\,\mathrm{m}$ and for DC 10, $l \approx 2.2 \cdot 10^{-5}\,\mathrm{m}$.

Another thing to notice would be the remarkably good agreement between the obtained values of l and the experimental method resolution as described in section 4.3 on page 33 and in section D.3.2 on page 89. Optimal threshold values for the `'simple'` algorithm, which are based on the real film thickness, are for all the measurements $\sim 3 \cdot 10^{-5}\,\mathrm{m}$. This is not only of the same order of magnitude as found l, but also of approximately the same absolute value. Thus, the value of threshold used for the experimental data evaluation is good initial guess for fitting l.

The comparison of the size of gas-liquid interfacial area calculated for different values of l and to the experimental data is displayed in Figure 5.16 on page 50. The depicted situation is for DC 05 oil and plate inclination angle $\alpha = 60\,°$.

Finally, in Figure 5.17 on page 50, there is a comparison of theoretical and experimental values of the apparent contact angle, β, evolution along the plate. The case of DC 05 silicon oil flowing down the plate inclined by $\alpha = 45\,°$ to horizontal, with $Q = 4.90 \cdot 10^{-6}\,\mathrm{m^3\,s^{-1}}$ is studied.

From the graphics, it is visible, that the derived model successfully predicts a qualitative behavior of the contact angles. However, the quantitative agreement is not as good.

The profile calculated by the method proposed in 2.5.2 is compared to the measured one in Figure F.1 in Appendix F. The case of DC 10 oil for the plate inclination angle, $\alpha = 50\,°$and volumetric flow rate of liquid, $Q = 0.42 \cdot 10^{-6}\,\mathrm{m^3 s^{-1}}$ is displayed. The profile obtained from theory shows quantitatively the same behavior as the measured one, however, the widening of the theoretical rivulet is much faster than the one observed from

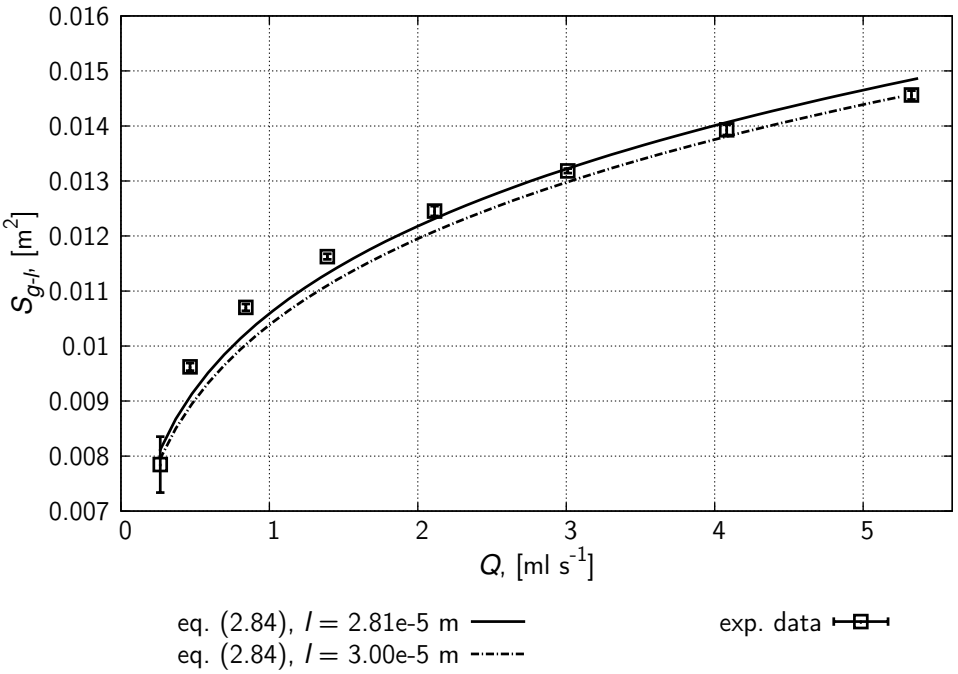

Figure 5.16: Comparison of predicted and measured values of S_{g-l} for fitted l and l equal to threshold of experimental data evaluation procedure. DC 05 oil, $\alpha = 60\,^\circ$

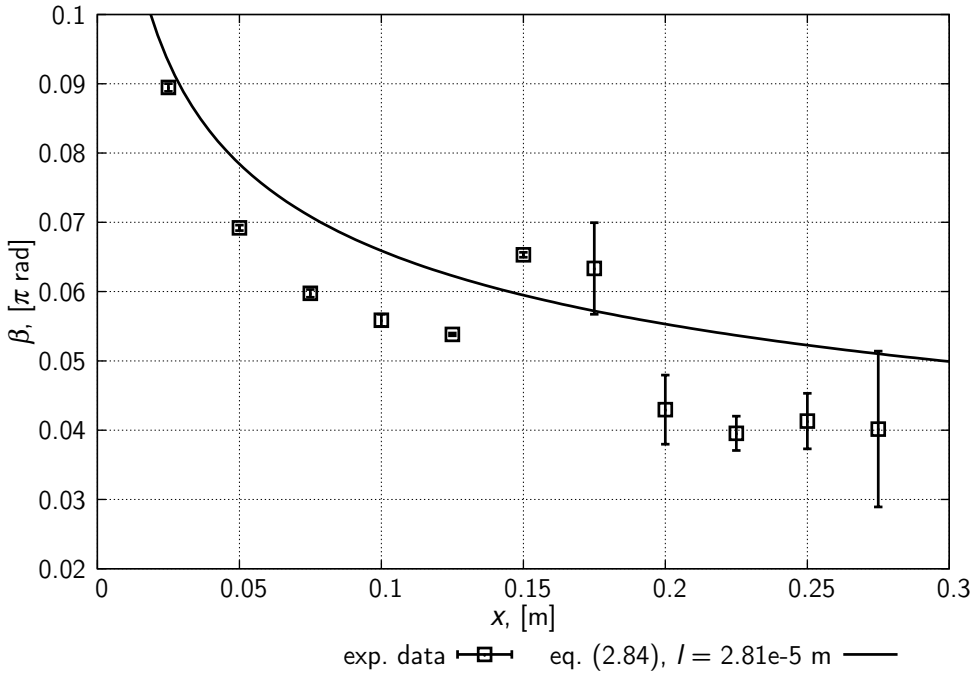

Figure 5.17: Comparison of predicted and measured values of apparent contact angle, β. DC 05 oil, $\alpha = 45\,^\circ$, $Q = 4.90 \cdot 10^{-6}\,\mathrm{m^3\,s^{-1}}$

experiments.

For higher flow rates, even the qualitative agreement between the theory and practice was lost due to appearance of laminar waves on the rivulet. However, as the rivulet width is higher than its height by approximately two orders of magnitude, the waves cannot have any substantial effect on the size of gas-liquid interfacial area. Hence, the proposed model is usable even for calculation of the S_{g-l} of waving rivulet. This can be seen also from Figure 5.16, where the line obtained from proposed calculation method approximates the experimental values throughout the range of measured Q despite the fact, that the waves are present on the rivulet for all $Q \geq\sim 2 \cdot 10^{-6}\,\mathrm{m^3\,s^{-1}}$.

5.2.3 The case of water

As it was already concluded from study of experimental results, the derived model is not directly applicable onto the spreading of water both with and without addition of surfactants. The reasons of this can be found in 5.1.6 (Summary of experimental results). Briefly, they are mainly the strong dewetting behavior of distilled water on steel and the generally unpredictable effects of surfactants on the liquids wetting properties.

The above stated resulted in addition of yet another adjustable constant to the model proposed in subsection 2.5.2. The resulting fitting equation was then

$$S_{g-l} = \Phi S_{g-l}(l,...), \tag{5.5}$$

with Φ and l as fitted parameters.

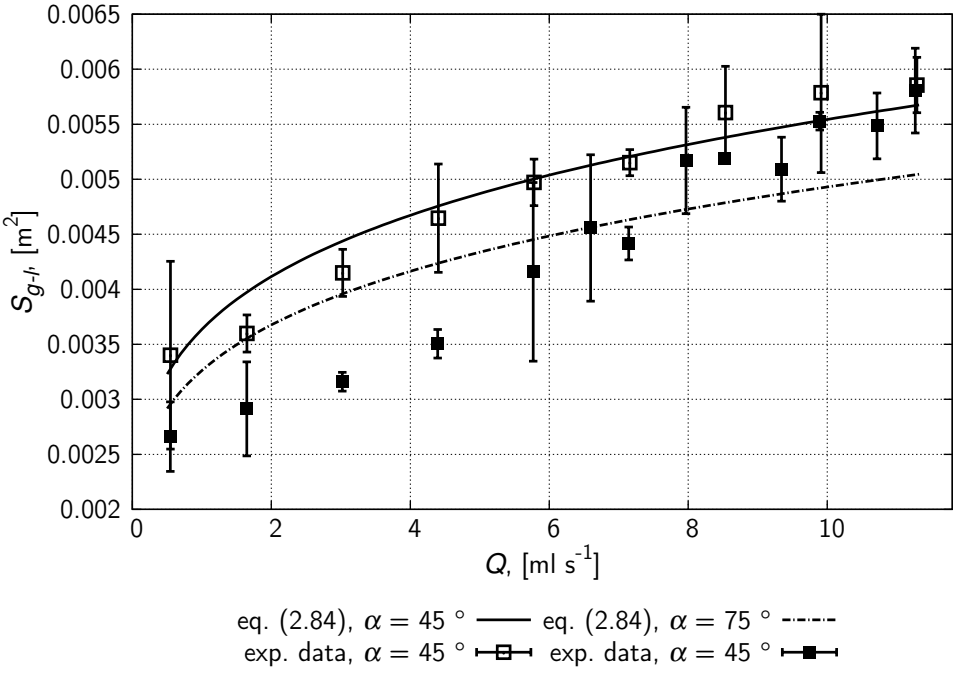

Figure 5.18: Comparison of predicted and measured values of S_{g-l} for water, for different plate inclination angles. The fitted parameters were in both cases, $l = 4.3 \cdot 10^{-5}\,\mathrm{m}$, $\Phi = 0.389$

The problem with equation above is that nothing can be said about the values of Φ. However, for the case of distilled water, this constant remained the same throughout the fitting for all four plate inclination angles and thus appeared to be the function only of the liquid wetting properties.

On the other hand, as it is clearly visible from the Figure 5.18, where the predicted and measured S_{g-l} are compared for the case of distilled water and varying plate inclination

angle, the increase of α causes the decrease of the effects of gravity onto the rivulet, making the behavior of water more and more unpredictable, as the above described effects of meandering and contact line pinning occurre with higher intensity.

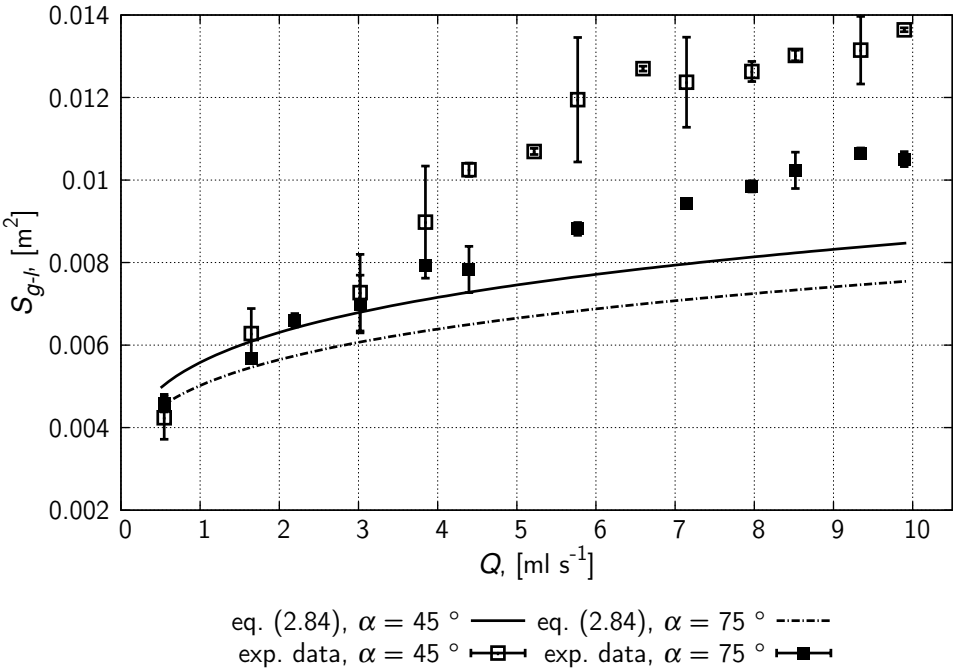

Figure 5.19: Comparison of predicted and measured values of S_{g-l} for tenzids, for different plate inclination angles. The fitted parameters were in both cases, $l = 3.3 \cdot 10^{-5}$ m, $\Phi = 0.624$

Furthermore, as it is visible from the Figure 5.19, which is showing the comparison of calculated and measured values of S_{g-l} for tenzids, even two adjustable constants are not enough for the derived model to fit the data obtained from measuring tensids proving the derived calculation method unusable for such applications.

6. Conclusions

In the presented thesis, a thorough analysis of the rivulet flow spreading down an inclined plate was completed. Accomplished work can be divided in three main parts.The first and second of these parts were connected to an experimental analysis of studied problem, the third one to its theoretical description.

Series of optical measurements of the rivulet flow was carried out at the TU Bergakademie Freiberg and a MATLAB program allowing, among other, quick and in situ evaluation of experiments was designed, written, tested and documented.

To gain a representative dataset for experimental study of the problematics, four different liquids were measured, each of them for various flow rates and plate inclination angles. Each measurement was repeated several times to exclude the possibility of errors.

Along with the experimental work, an extensive literature study was conducted by the author with an aim to gain general awareness of the current state of the understanding of the problematics of liquid spreading dynamics.

The obtained knowledge was then applied to propose a number of simplifications to the studied problem and to construct a mathematical model of the steady rivulet spreading along an inclined plate.

All the made assumptions were carefully tested against the experimental results and the borders of validity of derived relations were determined.

Next, the theoretical results were, within the previously defined limits, compared to the experimental data giving an excellent verification to the theory and proving the derived method applicable for calculation of the size of rivulet gas-liquid interfacial area (S_{g-l}) for the case of completely wetted inclined plate and conventional liquid.

For such a situation, the presented models were capable not only to describe the dependence of the S_{g-l} on the plate inclination angle and liquid volumetric flow rates, but they also could have been used for prediction of the rivulet width and contact angle evolution along the plate. The first one named quantitatively while the second at least qualitatively.

Furthermore, the proposed model of S_{g-l} calculation was shown to be, with some limitations, applicable also for the case of spreading of liquid on partially wetted plate (which was the case of distilled water measurements). However, the effects of surfactants on the liquid spreading properties were shown to be far outside the scope of applicability of proposed model.

The conducted analysis of the derived gas-liquid interfacial size calculation method suggest its wide usability for extrapolation based on the experimental results.

7. List of symbols

a ..... half-width of the rivulet, [m]
A,B ..... constants defined in (2.80), [s,−]
$\bar{A}$ ..... constant A modified as described in (2.84), [m]
c,C ..... universal, unspecified constant, [−]
D ..... dissipation energy, [J]
D ..... substantial derivative, [−]
e ..... Euler's constant, [−]
E ..... surface energy, [J]
F ..... implicitly defined surface, [−]
$\mathbf{F}$ ..... vector of accelerations corresponding to body forces, [$\mathrm{m\,s^{-2}}$]
g ..... gravitational acceleration, [$\mathrm{m\,s^{-2}}$]
h ..... height, [m]
H ..... general problem height scale, [m]
J_W ..... integration constant as defined in (2.55), [−]
K ..... Gaussian curvature, [$\mathrm{m^2}$]
l ..... intermediate region length scale, [m]
L ..... general problem length scale, total rivulet length, [m]
$\dot{m}$ ..... mass flow rate, [$\mathrm{kg\,s^{-1}}$]
$\mathbf{n}$ ..... outer unit normal vector, [−]
N ..... number of infinitesimal cuts made along the rivulet, [−]
p ..... pressure, [Pa]
Q ..... volumetric flow rate, [$\mathrm{m^3\,s^{-1}}$]
Q ..... curvature tensor, [−]
r ..... radial coordinate, [m]
$\mathbf{r}$ ..... Monge parametrization of a surface, [−]
R ..... droplet radius, [m]
S ..... surface, [$\mathrm{m^2}$]
t ..... time coordinate, [s]
T ..... thermodynamic temperature, [K]
$\mathbf{u}$ ..... liquid velocity vector, [$\mathrm{m\,s^{-1}}$]
u, v, w ..... liquid velocity in x, y and z directions, [$\mathrm{m\,s^{-1}}$]
U, V, W ..... general liquid velocity scales, [$\mathrm{m\,s^{-1}}$]
x,y,z ..... coordinate system, [m]

Greek letters

α ..... plate inclination angle, [°]
β ..... contact angle at the three phase contact line, [°]
γ ..... surface tension, [$\mathrm{N\,m^{-1}}$]
Γ ..... norm of implicitly defined surface gradient, [−]
δ, Δ ..... small difference, [−]

ϵ ..... rate of viscous dissipation per unit volume, [kg s^{-1} m^{-3}]
ε ..... rivulet height at centerline to width ratio, [−]
ζ ..... mean free falling film velocity, [m s^{-1}]
η ..... constant defined in the equation (2.78), [m]
θ ..... temperature, [°C]
ϑ .... ratio of the rivulet height at centerline and standard deviation of the profile shape function, [−]
κ ..... surface mean curvature, [m]
λ ..... Navier slip length, [m]
Λ ..... adjustable parameter in (2.68)
μ ..... dynamic viscosity, [Pa s]
ξ ..... dimensionless rivulet height, [−]
Ξ ..... liquid spreading coefficient, [−]
π ..... ratio of a circle circumference to its diameter, [−]
ϖ ..... coefficient of transformation from time to spatial coordinate, [m^{-1} s]
ρ ..... density, [kg m^{-3}]
ϱ ..... mean curvature radius, [m^{-1}]
σ ..... interface profile shape standard deviation, [m]
Σ ..... general surface representation, [−]
ς ..... arc length, [m]
τ ..... contact point for 2D interface, [−]
Υ ..... dimensionless constant, [−]
ϕ ..... dissipative pressure, [Pa]
Φ ..... multiplicative constant in (5.5), [−]
Ψ ..... dimensionless film height, [−]
Ω ..... volume, [m^3]

Dimensionless numbers and important constants

capillary length ..... , [m]

$$l_c = \sqrt{\frac{\gamma}{\rho g \cos\alpha}}$$

viscous length scale ..... , [m]

$$l_v = \frac{\mu^2}{\rho\gamma}$$

Bond number as defined by Duffy and Moffat in [7] ..... , [−]

$$\mathrm{Bo} = \frac{a}{l_c}$$

Bond number as defined by Shetty and Cerro in [9],

$$\overline{\mathrm{Bo}} = \frac{27}{6\pi}\frac{\cos\alpha}{\sin^2\alpha}\frac{\mu^2 Q^2}{g\gamma h_{0i}^6}$$

capillary number ..... , [−]

$$\mathrm{Ca} = \dot{R}\frac{\mu}{\gamma}$$

capillary number, as defined by Shetty and Cerro in [9] ..... , [–]

$$\overline{\mathrm{Ca}} = \zeta \frac{\mu}{\gamma}$$

Reynolds numbers, general, defined rivulet width and capillary length ..... , [–]

$$\mathrm{Re} = \frac{\rho u H}{\mu}, \qquad \mathrm{Re}_a = \frac{\rho u 2a}{\mu}, \qquad \mathrm{Re}_{l_c} = \frac{\rho u l_c}{\mu}$$

maximal height-defined Reynolds number of the rivulet ..... , [–]

$$\mathrm{Re}_{max} = \frac{1}{3\mu^2}\sqrt{\frac{\rho\gamma^3 \tan^3\alpha}{g\cos\alpha}}$$

Subscripts and superscripts

0 ..... at $y = 0$, rivulet centerline
$0I$ ..... at $x = 0, y = 0$
a ..... connected to the rivulet half width
A ..... atmospheric
c ..... capillary
D ..... dynamic solution member in profile shape
E ..... obtained from the experiment
eq ..... at the thermodynamic equilibrium
f ..... describing the fixed contact line problem
$g-l, s-l, s-g$ ..... gas – liquid, solid – liquid, solid – gas interface
h ..... connected to film height
i ..... discrete cut, transversal to the plate
I ..... initial value, at $x = 0$
ie ..... outside of the thermodynamic equilibrium
in ..... appertaining to the inner (microscopic) problem length scale
j ..... discrete cut, longitudinal to the plate
l ..... connected to the intermediate region length scale
L ..... on the left side of the rivulet
l_c ..... connected to the capillary length
m ..... concerning the microscopic region
max ..... maximal value
out ..... appertaining to the outer (macroscopic) problem length scale
p ..... connected to pressure
R ..... on to the right side of the rivulet
S ..... static solution member in profile shape
t,r,x,y,z ..... partial derivative with respect to noted coordinate
τ ..... concerning the contact point for 2D interface

8. Bibliography

[1] Kister, H. Z.; et al. *Distillation Design*, 1st ed.; McGraw-Hill: USA, 1992.

[2] Bornhutter, K.; Mersmann, A. Mass Transfer in Packed Columns: The Cylinder Model. *Chem. Eng. Technol.* **1993**, *16*, 46–57.

[3] Cooke, J. J. Gu, S. Armstrong, L. M. Luo, K. H. Gas-liquid flow on smooth and textured inclined planes, *World Ac. of Sc., Eng. and Tech.* **2012**, *68*, 1712–1719.

[4] Ataki, A. Kolb, P. Bühlman, U. Bart, H. J. Wetting performance and pressure drop of structured packing: CFD and experiment, *I. Chem. E. – symposium series*, **2006**, *152*, 534–543.

[5] Bonn, D. Eggers, J. Indekeu, J. Meunier, J. Rolley, E. Wetting and Spreading. *Rev. Mod. Phys.* **2009**, *81*, 739–805.

[6] Towell, G. D. Rothfeld, L. B. Hydrodynamics of rivulet flow, *AIChE J.*, **1966**, *9*, 972–980.

[7] Duffy, B. R. Moffat, H. K. Flow of a viscous trickle on a slowly varying incline, *Chem. Eng. J.*, **1995**, *60*, 141–146.

[8] de Gennes, P. G. Wetting: statics and dynamics. *Rev. Mod. Phys.* **1985**, *57* (3), 827–863.

[9] Shetty, S. A. Cerro, R. L. Spreading of Liquid Point Sources over Inclined Solid Surfaces, *Ind. Eng. Chem . Res.*, **1995**, *34*, 4078–4086.

[10] Davis, S. H. Moving contact lines and rivulet instabilities. Part 1. The static rivulet, *J. Fluid. Mech.* **1980**, *98*, 225–242.

[11] McHale, G. Newton, M. I. Rowan, S. M. Banerjee, M. The spreading of small viscous stripes of oil. *J. Phys. D: Appl. Phys.* **1995**, *28*, 1925–1929.

[12] Davis, S. H. Contact line problem in fluid mechanics, *Trans ASME J. Appl. Mech.*, **1983**, *50*, 977–982.

[13] Safran, S. A. Curvature elasticity of thin films, *Adv. in. Phys.* **1999**, *48* (4), 395–448.

[14] Ataki, A. Wetting of Structured Packing Elements - CFD and Experiment. Dissertation, Technischen Universität Kaiserslautern, 2006.

[15] Fedotkin, I. M. Melnichuk, G. A. Koval, F. F. Klimkin E. V. Hydrodynamics of rivulet flow on a vertical surface, *Inzhenerno-Fizicheskli Zhurnal*, **1984**, *1*, 14–20.

[16] Carlos, P. A. Gratton, J. Navier–Stokes solutions for parallel flow in rivulets on an inclined plane, *J. Fluid Mech.*, **2004**, *507*, 367–397.

[17] Nawrocki, P. A. Chuang, K. T. Hysteresis in stable rivulet flows, *Chem. Eng. Comm.*, **1995**, *132*, 239–255.

[18] Zhilin, L. Ming-Chih, L. Guowei, H. Hongkai, Z. An augmented method for free boundary problems with moving contact lines, *Comp. and Fl.*, **2010**, *39*, 1033–1040.

[19] Renardy, M. Renardy, Y. Li, J. Numerical simulation of moving contact line problems using a Volume-of-fluid method. *J. Comp. Phys.* **2001**, *171*, 243–263.

[20] Lai, M.-C. Tseng, Y.-H. Huang, H. Numerical simulation of moving contact lines with surfactant with immersed boundary method. *Commun. Comput. Phys.* **2010**, *8* (4), 735–757.

[21] Afkhami, S. Zaleski, S. Bussman, M. A mesh-dependent model for applying dynamic contact angles to VOF simulations. *J. Comp. Phys.* **2009**, *228*, 5370–5389.

[22] 0'Brien, S. B. G. Schwartz, L. W. *Encyclopedia of Surface and Colloid Science*, Theory and Modeling of Thin Film Flows, 1st ed.; Marcel Dekker, Inc: New York, 2002.

[23] Moran, K. Inumaru, J.Kawaji, M. Instantaneous hydrodynamics of a laminar wavy liquid film, *Int. J. of Multiphase Flow*, **1999**, *28*, 731–755.

[24] von Karman, T. Biot, M. A. *Mathematic Methods in Science and Engineering*, 1st ed.; McGraw-Hill: New York , 1940.

[25] Bentwich, M. Glasser, D. Kern, J. Williams, D. Analysis of Rectilinear Rivulet Flow, *Al. Che. J.* **1976**, *22* (4), 772–779.

[26] Huh, C. Scriven, L. E. Hydrodynamic model of steady movement of a solid/liquid/fluid contact line. *J. Col. Int. Sci.* **1971**, *35* (11), 85–101.

[27] Smith, M. J. Variational Derivation of Young's Law and Laplace's Capillary Equation, *The Am. J. of Phys.* **1970**, *30* (9), 1153–1160.

[28] Chen, J. D. Experiments on a spreading drop and its contact angle on a solid, *J. Colloid Interface Sci.* **1998**, *120* (1), 60–72.

[29] Voinov, O. V. Hydrodynamics of wetting, *Fl. Dyn.* **1976**, *11*, 714–721.

[30] Tanner, L. H. The spreading of silicone oil drops on horizontal surfaces. *J. Phys. D: Appl. Phys.* **1979**, *12*, 1473–1486.

[31] Hocking, L. M. A moving fluid interface on a rough surface, *J. FLuid Mech.* **1976**, *76*, 801–817.

[32] Landau, L. D. Lifshitz, E. M. *Fluid Mechanics*, 3rd ed.;Pergamon: Oxford, 1966.

[33] Hervet, H. de Gennes, P.-G. The dynamics of wetting: Precursor films in the wetting of "dry" solids, *C. R. Acad. Sci., Ser. II: Mech., Phys., Chim., Sci. Terre Univers* **299**, 499–512.

[34] Eres, M. H. Schwartz, L. W. Roy, R. V. Fingering phenomena for driven coating films, *Phys. FLuids* **2000**, *12*, 1278–1295.

[35] Thompsom, P. A. Troian, S. M. A general boundary condition for liquid flow at solid surfaces, *Nature (London)* **1997**, *389*, 360–362.

[36] Weidner, D. E. Schwartz, L. W. Contact-line motion of shear-thinning liquids, *Phys. Fluids* **1994**, *6*, 3535–3538.

[37] Wayner, P. C. Spreading of a liquid film with a finite contact angle by the evaporation/condensation process, *Langmuir* **1993**, *9*, 294–299.

[38] Seppecher, P. Moving contact lines in the Cahn-Hilliard theory, *Int. J. Eng. Sci* **1996**, *34*, 977–984.

[39] Boudaoud, A. Non-Newtonian thin films with normal stresses: dynamics and spreading, *Eur. Phys. J. E* **2007**, *22*, 107–113.

[40] Oron, A. Davis, S. H. Bankoff, S. G. Long.scale evolution of thin liquid films. *Rev. Mod. Phys.* **1997**, *69*, 931–980.

[41] Bertozzi, A. The mathematics of moving contact lines in thin films, *Not. of the AMS* **1998**, *17*, 689–697.

[42] Snoeijer, J. H. Andreotti, B. Moving Contact Lines: Scales, Regimes and Dynamical Transitions, *Annu. Rev. Fl. Mech.* **2013**, *45*, 269–292.

[43] Snoeijer, J. H. Free surface flows with large slopes: Beyond lubrication theory, *Phys. Fluids* **2006**, *18*, 021701-1–021701-4.

[44] Cox, R. G. The dynamics of spreading of liquids on solid surface. Part 1. Viscous Flow, *J. Fluid. Mech.* **1986**, *168*, 169–194.

[45] Lauga, E.; Brenner, M. P.; Stone, H. A. Microfluidics: The No-Slip Boundary Condition. In *Handbook of Experimental Fluid Dynamics*; Foss, J., Tropea, C., Yarin, A., Eds.; Springer: New-York, 2005.

[46] Benilov, E. S. On The Stability of Shallow Rivulets. *J. Fluid Mech.* **2009**, *636*, 455–474.

[47] Diez, J. A. González, A. G. Stability of a finite-length rivulet under partial wetting conditions, *J. of Phys: Conf. Ser.* **2009**, *166*, 1–12.

[48] Diez, J. A. Gonzáles, A. G. Kondic, L. On the breakup of fluid rivulets, *Phys. of Fl.* **2009**, *21* (8), 082105-1–082105-15.

[49] Sullivan, J. M. Paterson, C. Wilson, S. K. Duffy, B. R. A thin rivulet or ridge subject to a uniform transverse shear stress at its free surface due to an external airflow, *OCCAM Reports* **2012**, *53*, 1–30.

[50] Weiland, R. H. Davis, S. H. Moving contact lines and rivulet instabilities. Part 2. Long waves on flat rivulets, *J. Fluid. Mech.* **1981**, *107*, 260–281.

[51] Hagemeier, T. Hartmann, M. Kühle, M. Thévenin, D. Zähringer, K. Experimental characterization of thin films, droplets and rivulets using LED fluorescence, *Exp. in Fluids*, **2011**, *52*, 361–374.

[52] Alekseenko, V. S. Aleksey B. V. Kharlamov, S. M. Markovich, D. M. In *Frequency susceptibility of rivulets flowing down vertical plate*, 4th Int Symp on Applications of Laser Techniques to Fluid Mechanics; , Ed.; 2008.

[53] Zare, R. N. My life with LIF: A personal Account of developing Laser-Induced Fluorescence, *Annu. Rev. Anal. Chem.* **2012**, *5*, 1–14.

[54] Johnson, M. F. G. Schluter, R. A. Bankof, S. G. Fluorescent imaging system for global measurement of liquid film thickness and dynamic contact angle in free surface flows, *Rev. Sci. Instrum.* **1997**, *68* (11), 4097–4102.

[55] Johnson, M. F. G. Schluter, R. A. Miksis, M. J. Bankof, S. G. Experimental study of rivulet formation on an inclined plate by fluorescent imaging, *J. Fluid Mech.* **1999**, *394*, 339–354.

[56] Coates, C.; Fowler, B.; Holst, G. Scientific CMOS Technology A High-Performance Imaging Breakthrough, 2009. sCMOS Whitepaper. http://www.scmos.com/files/high/scmos_white_paper_8mb.pdf (accessed May 06, 2013).

[57] Isoz, M. *RivuletExpDataProcessing Program Documentation*, 0.9th ed.; Freiberg, 2012.

[58] Open Source Initiative MIT Licence, 2013. Opensource.org. http://opensource.org/licenses/MIT (accessed May 07, 2013).

[59] Isoz, M. RivuletDataProcessing, 2013. GitHub. https://github.com/MartinIsoz/RivuletDataProcessing (accessed May 07, 2013).

[60] Duda, R. O. Hart, P. E. Use of the Hough Transformation to Detect Lines and Curves in Pictures. *Comm. ACM* **1971**, *15*, 11–15.

[61] Birnir, B. Mertens, K. Putkaradze, V. Vorobieff P. Morphology of a stream flowing down an inclined plane. Part 2. Meandering, *J. Fluid Mech.*, **2008**, *607*, 401–411.

[62] Reznik, S. N. Yarin, A. L. Spreading of an axisymmetric viscous drop due to gravity and capillarity on a dry horizontal wall. *Int. J. Multiph. Fl.* **2002**, *28*, 1437–1457.

[63] Moran, K. L. M. Experimental study of laminar liquid films falling on an inclined plate. Master Thesis, University of Toronto, 1997.

[64] Shifrin, T. *DIFFERENTIAL GEOMETRY: A First Course in Curves and Surfaces*, Prelim. ed.; University of Georgia: Tbilisi, 2010.

[65] Safran, S. A. *Statistical Thermodynamics of Surfaces, Interfaces, and Membranes*, Reading; Massachusetts: Addison-Wesley , 1994.

[66] Quéré, D. Rough ideas on wetting, *Physica A* **2002**, *313*, 32–46.

[67] Mathworks, Inc. MATLAB Documentation. http://www.mathworks.com/help/ (accessed Nov 21, 2012).

[68] Serra, J. *Image Analysis and Mathematical Morphology*, 1st ed.; Academic Press: New York, 1982.

[69] Hosking, J. R. M. Moments or L Moments? An Example Comparing Two Measures of Distributional Shape, *The American Statistician* **1992**, *46* (3), 186–189.

A. Surface curvature

Because of the wide usage of the terms in the presented work, the mean and Gaussian curvature of a mathematically infinitely thin surface are defined in the following text. The presented is based on the article by Safran [13], and textbook by Shifrin [64] but rather simplified.

Note: Because of the nature of described problems, all the following definitions are limited to $\mathbf{R^3}$.

A.1 Surfaces

The surface can be described either by its parametric form, $x = f(u,v)$,$y = g(u,v)$ and $z = h(u,v)$, which determine the vector $\mathbf{r}(u,v)$, describing the position of the points on the studied surface. Or by an implicit equation, $F(x,y,z) = 0$.

From the obvious reasons (see Figure 2.1), in the following text, all will be limited to the case of so called *Monge parametrization*, defined as follows:

$$\mathbf{r} = (u,v,h(u,v)) = (x,y,h(x,y)) \tag{A.1}$$

There is a need to define two tangent vectors on the studied surface,

$$r_u = \frac{\partial \mathbf{r}}{\partial u} \qquad r_v = \frac{\partial \mathbf{r}}{\partial v} \tag{A.2}$$

Please note, that there are no other conditions posed on these vectors other, that they have to be tangent to the surface and linearly independent. These vectors define the tangent plane to the surface given by equation:

$$\mathbf{r} \cdot \mathbf{n} = 0, \tag{A.3}$$

where $\mathbf{n}$ is the outer unit normal to the tangent plane at (u,v),

$$\mathbf{n} = \frac{\mathbf{r}_u \times \mathbf{r}_v}{|\mathbf{r}_u \times \mathbf{r}_v|}. \tag{A.4}$$

As for the implicitly defined surface, $F(x,y,z)$, it gives Monge representation $F(x,y,z) = z - h(x,y) = 0$. The normal then can be obtained by realizing that on the surface, $F(x,y,z)$ is constant and its derivative is equal a zero. Thus $\mathrm{d}F = \mathrm{d}\mathbf{r} \cdot \nabla F = 0$ with $\mathrm{d}r$ as a vector connecting two unspecified points of the surface. Since for smooth surface, d is tangent to a certain direction in the surface, and ∇F is orthogonal to this tangent. The normal vector is thus parallel to ∇F evaluated on the surface. Hence, the unit normal can be defined as:

$$\mathbf{n} = \frac{\nabla F}{|\nabla F|} \tag{A.5}$$

The curvature of the curve on a surface can be derived, similarly to the one of linear object, from the implicit form of its definition, $F(x,y,z) = 0$ by considering the change

in normal vector, n defined in (A.5) during the movement along the surface. Thus if one moves along the surface by distance d$\mathbf{r}$, $\mathbf{n}$ changes by an amount:

$$\mathrm{d}\mathbf{n} = \mathrm{d}\mathbf{n} \cdot \mathbf{Q}, \tag{A.6}$$

where $\mathbf{Q}$ is tensor with elements (in Cartesian coordinates) given by differentiation of the equation (A.5). Hence:

$$Q_{ij} = \frac{1}{\Gamma}\left(F_{ij} - \frac{F_i \Gamma_j}{\Gamma}\right), \tag{A.7}$$

with $\Gamma = |\nabla F|$, $F_i = \partial F/\partial r_i$ and $\Gamma_i = \partial|\nabla F|/\partial r_i$, where $\mathbf{r} = (x,y,z)$.

Then, from equation (A.6) one obtains an expression for curvature along a given curvilinear direction direction that is proportional to the trace of the tensor $\mathbf{Q}$. Thus, the curvature is associated with the change in the normal as one moves along the surface. Since both the normal and the direction along the surface are vectors, the curvature is, in general, a tensor quantity.

A.2 Curvature tensor invariants

Since the invariants do not change with rotation of the coordinate system, it is useful to describe the curvature tensor (Γ) by its invariants. In three dimensions, $\mathbf{Q}$ is 3×3 matrix. It is obvious from equation (A.7) that $\det \mathbf{Q}$ and hence one of its eigenvalues are equal a zero. The remaining two eigenvalues are two principal curvatures of the surface and for any F they can be obtained by explicit calculation from equation (A.7). The corresponding eigenvectors are known as the principal directions of the surface and along them, the curvature tensor is diagonal.

Tensor $\mathbf{Q}$ has (in three dimensions) under similarity transformations three invariants, its trace, the sum of its principal minors and its determinant (proof can be found for example in [65]). The mean curvature, κ, is defined as one half of the trace of the curvature tensor and has dimension of inverse length. The other invariant of $\mathbf{Q}$ is its sum of principal minors. It has dimension of inverse length squared and is usually named as Gaussian curvature, K.

Expression for the mean curvature is found from equation (A.7):

$$\kappa = \frac{1}{2\Gamma^3}\left[F_{xx}(F_y^2 + F_z^2) - 2F_x F_y F_{xy} + \mathrm{Perm}\right], \tag{A.8}$$

where Perm stands for other permutations of (x,y,z) ((z,x,y) and (y,z,x)).

Gaussian curvature is then given by following equation:

$$K = \frac{1}{2\Gamma^4}\left[F_{xx}F_{yy}F_z^2 - F_{xy}^2 F_z^2 + 2F_{xz}F_x(F_y F_{yz} - F_z F_{yy}) + \mathrm{Perm}\right]. \tag{A.9}$$

With Γ defined with euclidean norm as

$$\Gamma = |\nabla F| = \sqrt{F_x^2 + F_y^2 + F_z^2} \tag{A.10}$$

and with use of Monge representation of the surface, equations (A.8) and (A.9) can be substantially simplified and one obtains:

$$\kappa = \frac{(1 + h_x^2)h_{yy} + (1 + h_y^2)h_{xx} - 2h_x h_y h_{xy}}{2(1 + h_x^2 + h_y^2)^{\frac{3}{2}}} \tag{A.11}$$

$$K = \frac{h_{xx}h_{yy} - h_{xy}^2}{(1 + h_x^2 + h_y^2)^{\frac{3}{2}}} \tag{A.12}$$

With the assumption of nearly flat surface, $h_x \ll 1$ and $h_y \ll 1$, one can further simplify the above relations and finally obtain:

$$\kappa = \frac{h_{yy} + h_{xx}}{2} = \frac{1}{2}\nabla^2 h(x,y) \tag{A.13}$$

$$K = h_{xx}h_{yy} - h_{xy}^2 \tag{A.14}$$

The definition of mean surface curvature is crucial for the thin film calculations, because the capillary pressure in the liquid can be defined as $p_c = \gamma\kappa$ and then used in the boundary conditions for the system of Navier-Stokes equations (consult subsection 2.2.1).

B. Young equation derivation

There are two main approaches to derivation of the Young equation, the first one is rather straightforward logical reflexion and the other is minimization of the energy functional on three phase line.

The first idea (which was actually used by Young [66]) is based on an presumption, that contact angle is a local property, not influenced by the droplet size and that it is fixed near the contact line. At this line, all the three surface tensions are acting to reduce corresponding surface area and simple balance of these three forces yields the equation (2.30).

The second approach takes into account the whole drop, but with an assumption that it is flat enough for gravity to be neglected, hence the drop forms a spherical cap onto the underlying surface. With droplet surface energy written as:

$$E = \Sigma_{lg}\gamma_{lg} + \Sigma_{sl}\gamma_{sl} + (\Sigma_s - \Sigma_{sl})\,\gamma_{sv}, \tag{B.1}$$

where Σ_{ij} is the surface area between phases i and j and Σ_s is the total surface of the solid, and using the assumption above, one can easily obtain simple relations for Σ_{lg} and Σ_{sl}.

After substituting them into (B.1) and minimizing E, one, again, obtains equation (2.30).

C. Derivation of the thin film governing equation

With usage of some simplifications, usually known as the lubrication approximation, one can convert a set of Navier-Stokes equations for the problem of thin falling film to a single, fourth order partial differential equation with only one independent variable being the film height as function of time and spatial coordinates. In the following text, the thin film governing equation will be derived at first for one-dimensional problem (which is the usual case for a free falling film and the spreading droplet) and then, the derivation will be widened for the three dimensional problem.

For simplifying the notation, a horizontal solid substrate will be assumed in the following text. Modification of the resulting equations for the case on an inclined substrate is, as it will be clear from the derivation, straightforward.

For clarity of the writing, the list of general assumptions is given before proceeding to the derivation itself:

1. Incompressible Newtonian liquid with constant viscosity and surface tension coefficient.
2. Only acting body force is the gravity.
3. No shear at the gas-liquid interface.

C.1 One dimensional case

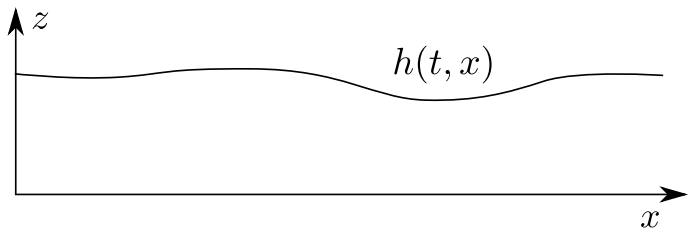

Figure C.1: One dimensional free surface problem

In the Figure C.1, there is a schematic drawing of a one dimensional case of a free surface interface problem. The axis notation is kept to be consistent with the one stated in Figure 2.1 on page 2.

Navier-Stokes equations, as written in equation (2.1) can be, for the case above, rewritten in the following form:

$$\rho(u_t + uu_x + wu_z) = -p_x + \mu\,(u_{xx} + u_{zz}) \tag{C.1}$$

$$\rho(w_t + uw_x + ww_z) = -p_z + \mu\,(w_{xx} + w_{zz}) + g, \tag{C.2}$$

where the indexes indicates the corresponding partial derivatives and u and w are the velocities in directions x and z, respectively.

This system can be non-dimensionalized with the following:

$$\bar{x} = \frac{x}{L}, \quad \bar{z} = \frac{z}{\varepsilon L}, \quad \bar{u} = \frac{u}{U}, \quad \bar{v} = \frac{v}{\varepsilon U}, \quad \bar{p} = \frac{\varepsilon^2 L}{\mu U^2} p, \tag{C.3}$$

with $\varepsilon = H/L$, H and L being the film height and length scale.

Using the non-dimensionalization (C.3), the equations (C.1) and (C.2) can be rewritten as:

$$\begin{aligned} \frac{U^2}{L}\left(\bar{u}_t + \bar{u}\bar{u}_x + \bar{w}\bar{u}_z\right) &= \frac{\mu U}{\varepsilon^2 \rho L^2}\left(-\bar{p}_x + \varepsilon^2 \bar{u}_{xx} + \bar{u}_{zz}\right) && \text{(C.4)} \\ \varepsilon\frac{U^2}{L}\left(\bar{w}_t + \bar{u}\bar{w}_x + \bar{w}\bar{w}_z\right) &= \frac{\mu U}{\varepsilon^3 \rho L^2}\left(-\bar{p}_z + \varepsilon^4 \bar{w}_{xx} + \varepsilon^2 \bar{w}_{zz}\right) + g, && \text{(C.5)} \end{aligned}$$

After defining the Reynolds number for the film flow, $\mathrm{Re} = \rho L U/\mu$, one can substitute Re into the equations above and obtain:

$$\begin{aligned} \varepsilon^2 \mathrm{Re}\left(\bar{u}_t + \bar{u}\bar{u}_x + \bar{w}\bar{u}_z\right) &= -\bar{p}_x + \varepsilon^2 \bar{u}_{xx} + \bar{u}_{zz} && \text{(C.6)} \\ \varepsilon^4 \mathrm{Re}\left(\bar{w}_t + \bar{u}\bar{w}_x + \bar{w}\bar{w}_z\right) &= -\bar{p}_z + \varepsilon^4 \bar{w}_{xx} + \varepsilon^2 \bar{w}_{zz} + g, && \text{(C.7)} \end{aligned}$$

When using the lubrication approximation, one assumes $\varepsilon \ll 1$, as the film is taken to be thin and also $\varepsilon^2 \mathrm{Re} \ll 1$, because the flow is expected to be laminar.

Note: From assumption of the thin film, it very often follows the neglecting of gravity effects. However, in these calculation, the gravity is kept because to make its effects obvious for later use of equations on the inclined plate.

With the assumptions made, after reintroduction of dimensional variables, the equations (C.6) and (C.7) simplify to:

$$\begin{aligned} p_x &= \mu u_{zz} && \text{(C.8)} \\ p_z &= \rho g && \text{(C.9)} \end{aligned}$$

These equation can be partially solved subject to the following boundary conditions:

1. No slip at the substrate,
$$u(0) = w(0) = 0. \tag{C.10}$$

2. No shear at the free surface,
$$u_z(h) = 0. \tag{C.11}$$

3. At the free surface, there is a pressure jump due to surface tension forces,
$$p(h) = p_a - \gamma\kappa, \tag{C.12}$$
With κ being the mean surface curvature as defined in Appendix A.

4. Kinetic equation is satisfied for the free surface. Expressing the free surface using the Monge parametrization (see Appendix A), $F(x,t) = h(x,t) - z = 0$, validity of this relation poses following condition on the free surface:
$$\frac{\mathrm{D}F}{\mathrm{D}t} = 0 \Leftrightarrow h_t + uh_x = w \tag{C.13}$$

5. Continuity equation. As the liquid is supposed to be incompressible, it reduces to $u_x + w_z = 0$. This can be rewritten in a more useful form,

$$w(h) - w(0) = w(h) = -\int_0^h u_x \mathrm{d}z \tag{C.14}$$

To obtain a single PDE from equations (C.6) and (C.7), one has to at first integrate the later,

$$\int_z^h p_z \mathrm{d}z = \int_z^h \rho g \mathrm{d}z \tag{C.15}$$

$$p(h) - p(z) = \rho g(h - z). \tag{C.16}$$

After solving the equation (C.16) for $p(z)$ and substituting for $p(h)$ from the condition (C.12), the following relation for the pressure field in a film is obtained:

$$p(z) = p_a + \rho g(z - h) - \gamma\kappa. \tag{C.17}$$

Then, substituting it into (C.8) yields:

$$p_x = -\rho g h_x + \gamma\kappa_x = \mu u_{zz} \tag{C.18}$$

As p_x does not depend on z, one can integrate once again and get,

$$\int_z^h p_x \mathrm{d}z = \mu \int_z^h u_{zz} \mathrm{d}z \tag{C.19}$$

$$p_x h - p_x z = \mu \left(u_z(h) - u_z(x)\right), \tag{C.20}$$

which, after substitution from the boundary condition (C.11) and yet one more integration with respect to z leads to:

$$p_x hz - p_x \frac{z^2}{2} = -\mu \int_0^z u_z \mathrm{d}z = -\mu \left(u(z) - u(0)\right) = -\mu u(z), \tag{C.21}$$

where the value of $u(0) = 0$ was obtained from the no-slip boundary condition, (C.10). Note, that the parabolic velocity profile was obtained for $u(z)$.

Once the velocity profile is obtained, it can be introduced to the combination of the last two unused boundary conditions, (C.13) and (C.14),

$$h_t + u h_x = -\int_0^h u_x \mathrm{d}z \tag{C.22}$$

to obtain the resulting PDE.

Just to summarize, the velocity profile v and its derivation with respect to the film longitudinal coordinate, y are:

$$u(z) = \frac{1}{\mu}\left(p_x \frac{z^2}{2} - p_x hz\right) \tag{C.23}$$

$$u_x(z) = \frac{1}{\mu}\left(p_{xx} \frac{z^2}{2} - p_{xx} hz - p_x h_x z\right) \tag{C.24}$$

Substituting these two relations in (C.22) yields:

$$h_t + \frac{1}{\mu}\left(p_x \frac{z^2}{2} - p_x hz\right) h_x = -\int_0^h \frac{1}{\mu}\left(p_{xx} \frac{z^2}{2} - p_{xx} hz - p_x h_x z\right) \mathrm{d}z. \tag{C.25}$$

After integration and simplification, one obtains

$$h_t - \frac{1}{3\mu}\frac{\partial}{\partial x}\left(p_x h^3\right) \tag{C.26}$$

and then finally, after substituting for the pressure field:

$$h_t - \frac{1}{3\mu}\frac{\partial}{\partial x}\left[h^3\left(\rho g h_x - \gamma\kappa_x\right)\right] = 0. \tag{C.27}$$

The equation (C.27) can be further simplified using following additional assumptions:

1. The surface is nearly flat.
2. The gravity can be neglected.

The result is then

$$h_t - \frac{\gamma}{3\mu}\frac{\partial}{\partial x}\left(h^3 h_{xxx}\right) = 0 \tag{C.28}$$

and this is the equation from which the relation (2.42) in subsection 2.3.4(Spreading dynamics of a drop) was derived.

C.2 Three dimensional case

A thin film governing equation for the three dimensional case is a strict generalization of the equation (C.27). And also its derivation is very similar to the one noted above. From these reasons, it will be mentioned only very briefly.

In three dimensions and Cartesian coordinates, the Navier-Stokes equations become:

$$\begin{aligned}
\rho(u_t + uu_x + vu_y + wu_z) &= -p_x + \mu\left(u_{xx} + u_{yy} + u_{zz}\right) && \text{(C.29)}\\
\rho(v_t + uv_x + vv_y + wv_z) &= -p_y + \mu\left(v_{xx} + v_{yy} + v_{zz}\right) && \text{(C.30)}\\
\rho(w_t + uw_x + vw_y + ww_z) &= -p_z + \mu\left(w_{xx} + w_{yy} + w_{zz}\right) + g, && \text{(C.31)}
\end{aligned}$$

Then, the non-dimensionalization (C.3) has to be completed by $\bar{y} = y/H$ (assuming the film width is of the same order of magnitude as its length). After simplification and introduction of the Reynolds number as defined above, the set of non-dimensional and simplified equations is:

$$\begin{aligned}
\varepsilon^2\mathrm{Re}\left(\bar{u}_t + \bar{u}\bar{u}_x + \bar{v}\bar{u}_z + \bar{w}\bar{u}_z\right) &= -\bar{p}_x + \varepsilon^2\bar{u}_{xx} + \varepsilon^2\bar{u}_{yy} + \bar{u}_{zz} && \text{(C.32)}\\
\varepsilon^2\mathrm{Re}\left(\bar{u}_t + \bar{u}\bar{u}_x + \bar{v}\bar{v}_z + \bar{w}\bar{u}_z\right) &= -\bar{p}_y + \varepsilon^2\bar{v}_{xx} + \varepsilon^2\bar{v}_{yy} + \bar{v}_{zz} && \text{(C.33)}\\
\varepsilon^4\mathrm{Re}\left(\bar{w}_t + \bar{u}\bar{w}_x + \bar{v}\bar{w}_z + \bar{w}\bar{w}_z\right) &= -\bar{p}_z + \varepsilon^4\bar{w}_{xx} + \varepsilon^4\bar{w}_{yy} + \varepsilon^2\bar{w}_{zz} + g, && \text{(C.34)}
\end{aligned}$$

And with the same set of assumption made as in the previous section, the above equations can be simplified an written in a dimensional form:

$$\begin{aligned}
p_x &= \mu u_{zz} && \text{(C.35)}\\
p_y &= \mu v_{zz} && \text{(C.36)}\\
p_z &= \rho g && \text{(C.37)}
\end{aligned}$$

Note: Compare these equations to the equations (2.5),(2.3) and (2.4) in subsection 2.2.1. It is well visible from the comparison, how the effect of the gravity should be introduced into the equations. The difference in the y-wise member of the pressure field is due the the assumption of unidimensional flow made in 2.2.1.

The set of boundary conditions for the equations above is:

1. No slip at the substrate,
$$z = 0, \qquad u = v = w = 0. \tag{C.38}$$

2. No shear at the free surface,
$$z = h(x,y), \qquad u_z = v_z = 0. \tag{C.39}$$

3. At the free surface, there is a pressure jump due to surface tension forces,
$$z = h(x,y), \qquad p = p_a - \gamma\kappa, \tag{C.40}$$

4. Kinetic equation is satisfied for the free surface.
$$h_t + uh_x + vh_y = w \tag{C.41}$$

5. Continuity equation. As the liquid is supposed to be incompressible, it reduces to $u_x + v_y + w_z = 0$. This can be rewritten in a more useful form,
$$w(h) - w(0) = w(h) = -\int_0^h (u_x + v_y)\,\mathrm{d}z \tag{C.42}$$

The equations (C.35), (C.35) and (C.35) are treated almost the same way as (C.8) and (C.9). The obtained pressure field is the same as defined by equation (C.17). Substituting it into (C.35) and (C.36) one obtains:

$$p_x = -\rho g h_x + \gamma\kappa_x = \mu u_{zz} \tag{C.43}$$
$$p_y = -\rho g h_y + \gamma\kappa_y = \mu v_{zz} \tag{C.44}$$

As neither p_x nor p_y are the functions of z, it is possible to integrate both and ultimately obtain the parabolic velocity fields in the x and y direction respectively and write in complete analogy to (C.23) and (C.24):

$$u(z) = \frac{1}{\mu}\left(p_x\frac{z^2}{2} - p_x h z\right) \tag{C.45}$$
$$u_x(z) = \frac{1}{\mu}\left(p_{xx}\frac{z^2}{2} - p_{xx}hz - p_x h_x z\right) \tag{C.46}$$
$$v(z) = \frac{1}{\mu}\left(p_y\frac{z^2}{2} - p_y h z\right) \tag{C.47}$$
$$v_y(z) = \frac{1}{\mu}\left(p_{yy}\frac{z^2}{2} - p_{yy}hz - p_y h_y z\right) \tag{C.48}$$

Combining the boundary conditions (C.41) and (C.42) same way as it was done for the conditions (C.13) and (C.14), substituting from (C.45), (C.46), (C.47) and (C.48) to the resulting relation, after integration with respect to z and simplification one obtains in complete analogy to the previous case

$$h_t - \frac{1}{3\mu}\nabla\left[h^3\left(\rho g\nabla h - \gamma\nabla\kappa\right)\right] = 0, \tag{C.49}$$

which is single PDE, fourth order in spatial derivatives of h (because there is $\nabla^2 h$ hidden in the term κ).

However, the above derived equation is not usable for the description of the problem of free surface of a rivulet, because in the derivation, there were not introduced any mechanism to treat the divergence of the dissipation energy near the contact line, which is, as it was stated in subsection 2.3.3 (Huh and Scriven's paradox), directly caused by use of a no-slip boundary condition.

The ideas of evading this problem, as they are listed in Table 2.1, are mainly based on two principles. The first one is introduction of some small slip at the surface, for example the linear Navier slip,

$$z = 0, \qquad \mathbf{u} - \lambda \frac{\partial}{\partial z}\mathbf{u} = 0, \tag{C.50}$$

with λ being some small slip length (and usually a function of h). Usage of this eventually leads to modification of the equation (C.49) by addition of a new member. The modified equation is then

$$h_t - \frac{1}{3\mu}\nabla\left[\left(h^3 + 3\lambda h^2\right)\left(\rho g \nabla h - \gamma \nabla \kappa\right)\right] = 0. \tag{C.51}$$

Other approaches are usually based on some type of introduction of long range forces (i.e. Van der Waals forces) effects into the equation (C.49). Even though based on a completely different approach, it yields also to addition of another member to this equation (but it will influence the pressure term). Completely general form of equation (C.49) would be then:

$$h_t - \frac{1}{3\mu}\nabla\left[\left(h^3 + 3\lambda h^2\right)\left(\rho g \nabla h - \gamma \nabla \kappa - \nabla \phi\right)\right] = 0, \tag{C.52}$$

with ϕ being the h dependent addition to the pressure field by introduced long range forces.

D. Data evaluation program documentation

As it was stated before, the output of experiments are the photographies of the experimental apparatus. Examples of these images for used liquids are in the Figure 4.1 on page 31. The plate with the measured rivulet is in the left side of the images and the flow cell is in theirs upper right corner.

MATLAB program was developed to provide possibility of quick experimental data evaluation doable directly into the laboratory. The program source codes and its documentation are published under MIT license [58] on GitHub [59] and they are also present on the CD distributed with this work.

For better orientation in it, the program source codes are divided into various subprograms and GUI figures. The complete list of the files needed to run the application is given in the Table D.1.

Table D.1: List of files of RivuletExpDataProcessing program

Name of the file	Associated .fig file	Short description
RivuletExpDataProcessing.m	✓	Main program file
postProcPlotting.m	–	Post-processing tool
showProcData.m	✓	Shows data av. for postproc.
showOtherDataUITable.m	–	Filling uitable with data
findEdges.m	–	Elements edges finding
bestMethod.m	–	findEdges input optimization
changeIMPars.m	✓	findEdges input modification
controlFunction.m	–	findEdges output control
modifyFunction.m	–	findEdges output modification
rivuletProcessing.m	–	Data processing
changeRPPars.m	✓	rivuletProcessing input mod.
statusbar.m	–	Modifies main window status-bar
save_to_base.m	–	Saving all variables into the base workspace
distinguishable_colors.m	–	Generates RGB matrix for plots
fitIFA.m	✓	Measured data fitting
fluidDataFcn.m	–	Database of the fluids properties
normDistParsFit.m	✓	Fit of rivulet parameters based on [9]
treshInflStudy.m	✓	Study of the threshold influence on the results

The program functions can be divided into five main parts. The first one is the main program, `RivuletExpDataProcessing.m` which resolves the most basic data operations

and handles callings to other functions. The second part are the functions used for finding experimental plate and flow cell onto the images. This is provided by `findEdges.m` and its auxiliary functions. Third part of the application is the rivulet processing itself. The program outputs are calculated there, through function `rivuletProcessing.m`. Fourth is the calculated outputs visualization ensured by the `postProcPlotting.m` function. Into the fifth part of the program are then gathered the other, more standalone, functions, namely `treshInflStudy.m` allowing to study the image processing parameters inlfuence on the results and `fitIFA.m` which permits to fit experimental data using the model described into the 2.5.

The following text is divided, in accordance with the program parts as enumerated above, into five sections, each describing the most important algorithms and functions used in the matching application segment.

More detailed description of the used algorithms as well as the user manual are available in [57].

Note: The symbols in the following section do not correspond with the List of symbols on page 54. The reason of this ambiguity is better correspondace of presented program description with the previous its documentation and user manual [57].

D.1 RivuletExpDataProcessing.m

Function summary:

Name of the file	RivuletExpDataProcessing.m
Associated .fig file	✓
Short description	Main program file
Inputs	–
Outputs	datafiles, plots
Sub-functions	all other program parts

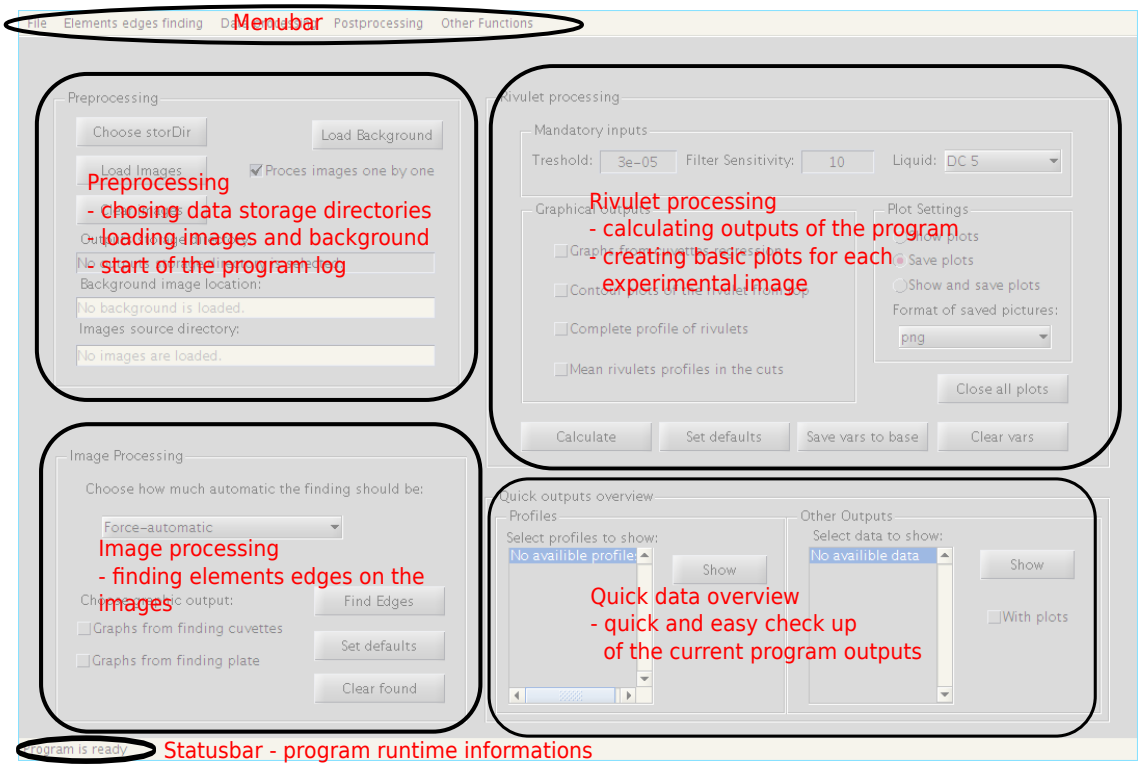

Figure D.1: Scheme of the main program window

`RivuletExpDataProcessing.m` is the main function of the program. It is linked with .fig file of the same name providing the main graphical user interface of the application. This function is used as the center of the code from where all other functions are called. All the program execution variables are stored in the workspace of this function.

On Figure D.2 on page 74 is shown the scheme of the main program execution. There are drown the main callable functions and the most important variables that are passed between them.

To understand the way that variables are passed from one function to another, it is necessary to mention some facts about the way that MATLAB is working with graphical user interfaces and objects. For controlling the graphical user interface, MATLAB is using so called `handles`. These work like pointers to certain objects. The main window created by application is `MainWindow`, so this window contains handles to all its `Children` (objects created inside this window or by the main program execution). `Handles` are generally structures of pointers to other objects and of user set data.

As it is mentioned above, all the program execution variables are stored into the main (`RivuletExpDataProcessing`) function workspace. So for the passing the data between

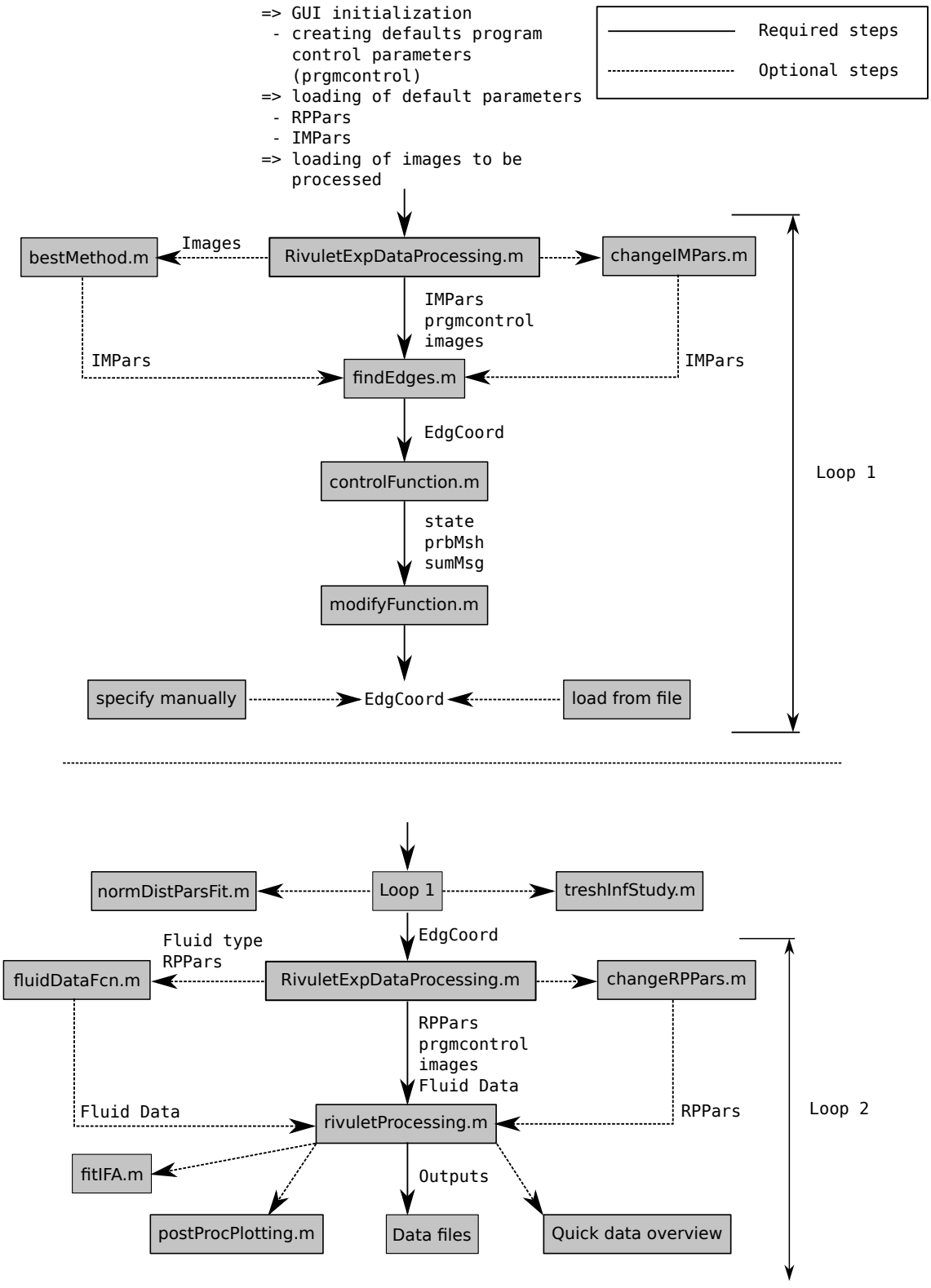

Figure D.2: Scheme of the main program execution process

the sub-functions, there were created two user defined fields into the `MainWindow ... handles`, one named `prgmcontrol` for the variables used for the program control (i.e. level of automaticity of the program...) and the second one named `metricdata` for data variables.

D.1.1 Description of the program

When the RivuletExpDataProcessing is launched, it forces the user to walk through the two main execution loops of the program (as they are shown in the Figure D.2).

In the first loop, user is at first asked to specify the folders where to save the outputs and from where to load the images to be processed. Then he is guided through the process of the plate and flow cell edges finding as it is shown on the upper part of the Figure D.2. However, this is skippable by loading these coordinates from presaved file or by entering the values manually.

After the plate and flow cell edges are specified, user can proceed to the second loop, the data evaluation part of the program. Output of the second loop are processed experimental data stored in text files into specified folder and into the `handles` of the program, to be used into post-processing.

Other possibility is, after the successful end of the first loop, to start one of the other functions, for example, `treshInflStudy.m`.

D.2 findEdges.m

Function summary:

Name of the file	findEdges.m
Associated .fig file	–
Short description	Finding coordinates of elements edges on images
Inputs	`handles`
Outputs	`EdgCoord` (matrix, number of images $\times 10$)
Subfunctions	`controlFunction`
	`modifyFunction`
	`changeIMPars`

Table D.2: Mandatory fields in `handles` when calling `findEdges`

Structure name	Mandatory fields
handles	MainWindow
	statusbar
	metricdata
	prgmcontrol
handles.metricdata	imNames
	daten or subsImDir
	IMProcPars
handles.prgmcontrol	DNTLoadIM
	autoEdges
	GR

In this section will be described the algorithm used for automatically finding the calibration flow cell and the plate in photos from experiments. In the main program, this

functionality was provided by custom written MATLAB function `findEdges`. This function takes as input all the `MainWindow handles`, but the only used fields are `MainWindow` for updating the status-bar during edges finding, `metricdata` and `prgmcontrol` for managing the program run. In the Table D.2 is complete list of fields that are needed in `handles` input of the `findEdges`.

The fields `MainWindow` and `statusbar` are necessary for handling and updating the status-bar in the main application window. Other fields are needed as data and program runtime specifications.

D.2.1 Description of the algorithm

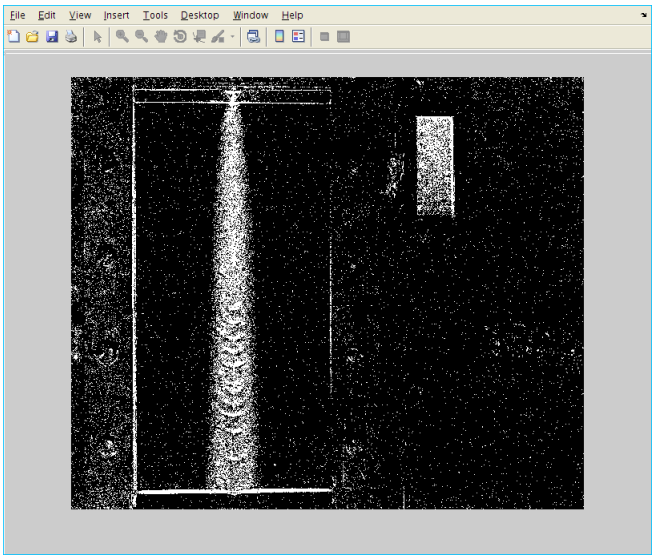

Figure D.3: Preprocessed experimental image, it is clear that flow cell and plate are of completely different graphic nature

The algorithm of `findEdges` is trying to specify position of two different objects on each experimental image. The first one is the calibration flow cell and the second is the actual plate with rivulet.

In each photograph, there are several distinct objects. Obviously, there are the two objects that the algorithm is trying to find, but there are also some unwanted elements (for example the rivulet itself, some parts of the experimental device...). As it is well visible from the Figure D.3 (preprocessed experimental image), flow cell and plate with the rivulet are of the completely different graphic nature. Because of this, their localization has to be based on different approaches, thus two algorithms had to be implemented.

Description of the flow cell finding algorithm

The flow cell is much more distinct than the plate, hence the algorithm for finding it is not very complicated (see the scheme on FigureD.5 on page 78).

1. For finding the cuvettes, the program is working with the right side of the picture (left side is dropped because of speed of the image processing and memory efficiency).
2. The contrasts for the picture are enhanced (see IMADJUST[1] and STRETCHLIM)
3. The image is converted into black and white (see IM2BW)

[1] In caps are written the names of MATLAB built-on functions, for further details on them, see [67]

4. The borders of different elements on the photo are found. (see BWBOUNDARIES)

5. Too big and too small elements are excluded (based on the length of the found boundary). This excludes the rivulet, most of the construction elements and noise at the image.

6. Between the remaining elements the flow cell has to be found. This task is completed using minimization of objective function containing sum of the following values:

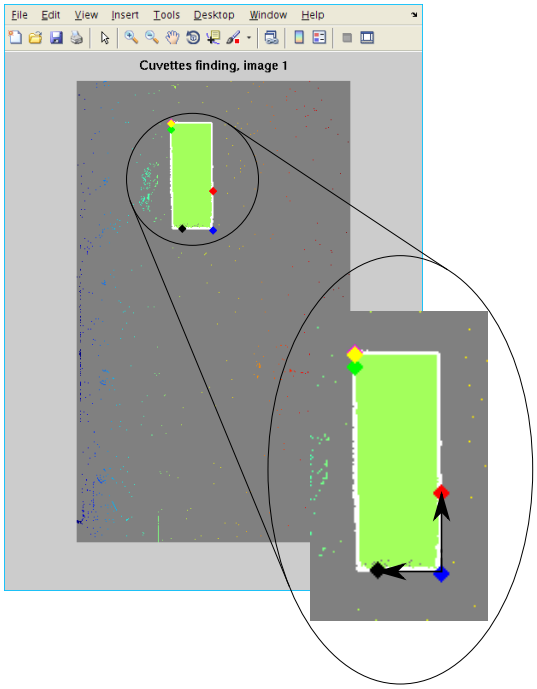

Figure D.4: Right side of the experimental image with found flow cell. In the magnified area is shown the idea between the sum of dot products.

- The first member of the objective function for each tested element is the relative difference between true and assumed rectangular areas which was calculated using following formula:

$$\Delta_r A = \frac{|\int_S dS - \max \Delta x \max \Delta y|}{\max \Delta x \max \Delta y}, \tag{D.1}$$

  where $\int_S dS$ is the actual tested elements area, $\max \Delta x \max \Delta y$ is the area of thought rectangle with sides defined as maximal differences in the x and y coordinates. For calculation of the additive member of the object function, absolute difference of area sizes had to be divided by the area of the thought rectangle.

- The second member is the sum of the dot products of direction vectors of sides. Scheme of the basic thought is in the Figure D.4. Main idea is that the tangent vectors defined in the clockwise and counterclockwise directions in the top left and bottom right corner of the tested element should be perpendicular to each other. The final used relation is the following:

$$DP = \sum_{i=1}^{2} \frac{\vec{u}_i}{\|\vec{u}_i\|} \cdot \frac{\vec{v}_i}{\|\vec{v}_i\|}, \tag{D.2}$$

where $\vec{u}_i, i = 1{,}2$ are the tangent vector defined in the clockwise direction in opposite corners and $\vec{v}_i, i = 1{,}2$ are the vectors defined in the counterclockwise direction.

- The value of objective function of the i-th tested element is then calculated as sum of the above defined members:

$$S_i = \Delta_r A_i + DP_i \tag{D.3}$$

It is obvious that both members of the objective function are penalizing the element for not being rectangular (with square taken as special case of rectangle), thus algorithm can malfunction in case that there is another distinct, roughly rectangular element on the image. However, the testing proved it to be very dependable.

7. Save the found coordinates into `EdgCoord` matrix.

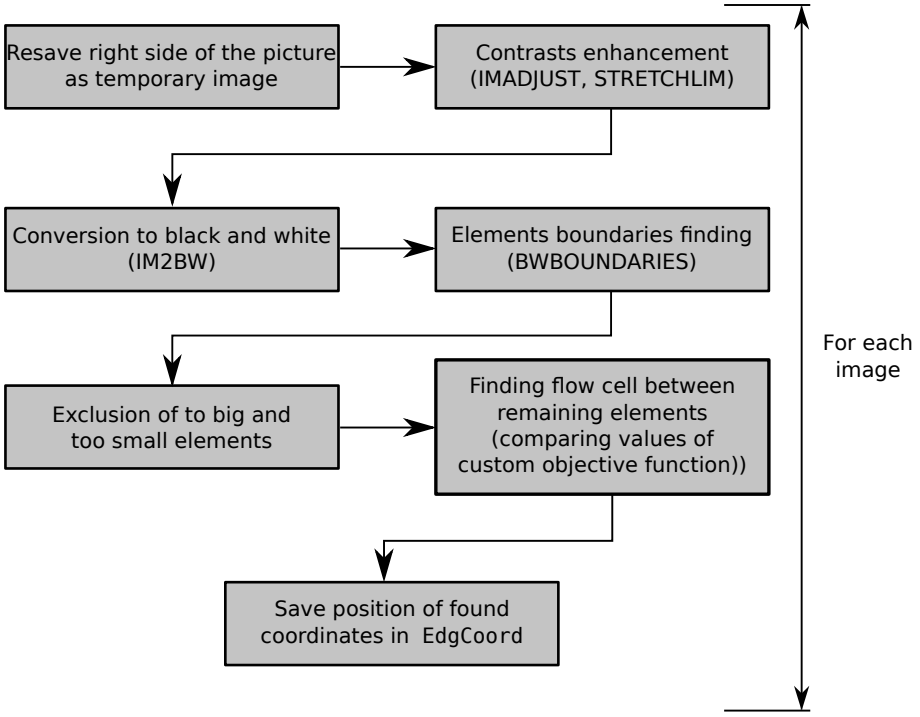

Figure D.5: Scheme of the flow cell finding algorithm

Description of the plate finding algorithm

The plate is much less distinctive than the calibration flow cell, so it has to be found using different approach. The general method is based on Hough transform [60], which is the image processing method used to find lines on specified image. This method is provided by MATLAB through built-in functions HOUGH, HOUGHPEAKS and HOUGHLINES. Scheme of the algorithm can be found in Figure D.6 on page 79. The text description is the following:

1. Ask user to provide approximate position of the plate (using GINPUT fucntion).
2. Cut of user-specified area from the original image and save it as temporary image.

[1]For each element, the algorithm is working only with 2 dot products - vectors in opposite corners.

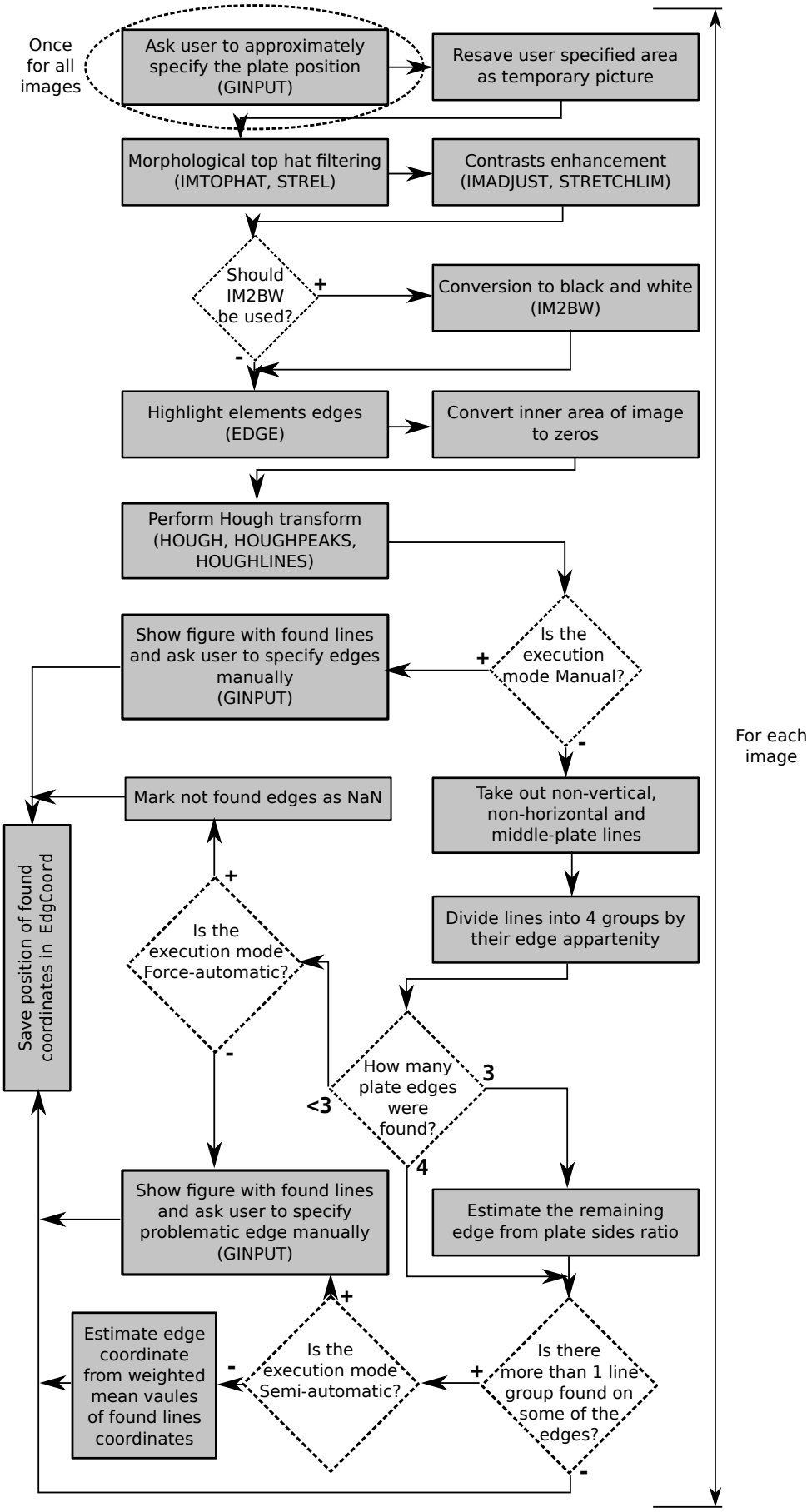

Figure D.6: Scheme of the plate finding algorithm

3. Use IMTOPHAT to perform morphological top hat filtering [68] to get rid of the background noise. This method uses morphological structuring element obtained by MATLAB function STREL.

4. Use MATLAB function IMADJUST with inner parameters `low_in, high_in`, specified by STRETCHLIM to enhance contrasts in the transformed temporary image.

5. Optional step: use MATLAB function IM2BW to convert image to black and white values (brings out the edges).

6. Use MATLAB function EDGE to find edges in obtained grayscale image. This also transforms the image to black and white colors. The default method used for EGES is `prewitt`.

7. Algorithm is not interested in finding lines specified by the rivulet itself, so the inner area of the black and white image is replaced by zeros (black).

8. Start the HOUGH transform with predefined parameters. This procedure consists of three commands HOUGH, HOUGHPEAKS and HOUGHLINES.

   (a) HOUGH command performs the standard Hough transform itself on the specified image. The outputs are `H,theta` and `rho`. `H` is the Hough transform matrix and `theta` and `rho` are the values over which HOUGH generates the Hough matrix, `H`.

   (b) HOUGHPEAKS command is used to find specified number of peaks in the Hough transform matrix. User can specify the number of peaks to be found (default value is largely overestimated 200) and the threshold at which the values of `H` are considered to be peaks. The output is `P`, the `numPeaks` $\times$ 2 matrix of row and column indexes of found peaks.

   (c) HOUGLINES takes the output of HOUGHPEAKS, `P` and outputs from HOUGH, `theta, rho` as well as the original image and extracts line segments from the input image based on the standard Hough transform. User can specify the size of gaps between lines that should be automatically filled and the minimal length of the line saved in the output variable. These parameters are in the code named `fG` and `mL`. Their default values are `fG = 35, mL = 25`, but can be changed from the GUI.

9. If the program is set to run manually (*Manual* mode), the figure with plotted lines is shown and user is asked to specify at least 3 edges manually. Otherwise (*Semi-automatic*, *Automatic* and *Force-automatic* mode) the program continues.

10. After the lines are extracted, the Hough transform output control follows. From the found lines are subtracted the ones that are not vertical/horizontal and the ones that are in the middle of user specified area.

11. The remaining lines are sorted into four groups base on the edge they are adjacent to.

12. In those groups, the lines are differentiated in accordance to their position on the plate (left – right, top – bottom). After this distinction, the output is controlled and the plate edges are estimated in dependence on the outcome of the previous code and level of automaticity specified by user.

    (a) There are found lines with very similar key[2] coordinate on each side of the plate $\Longrightarrow$ The key coordinates are saved as plate edges.

[2]The key coordinate is longitude for vertical lines and latitude for the horizontal ones.

(b) Lines with similar key coordinates are found only on 3 of 4 plate edges $\Longrightarrow$ The found 3 key coordinates are saved as plate edges and the position of the last edge position is estimated from the side ratio of the plate (length : width = 1 : 2).

(c) On 1 of the sides are found multiples different key coordinates. If the program is in the *Automatic* or *Force-automatic* mode, the weighted mean value of the lines on one edge is constructed and saved as edge position. Otherwise (*Semi-automatic* mode),the figure with found lines is shown and user is asked to specify the problematic edges manually.

(d) If there is less than 3 edges found and the mode of the program is *Semi-automatic* or *Automatic*, the figure with found edges is shown and user is asked to specify at least 3 edges manually. If the mode is set up to be *Force-automatic*, unspecified edges assigned `NaN` values.

13. The found edges are saved into output variable `EdgCoord`.

D.2.2 Subfunctions

The function `findEdges` has two main subfunctions for controlling and modifying its, matrix `EdgCoord`. First of these functions, `controlFunction` is used to find the outliers and `NaN` (not specified edges) in the `EdgCoord` matrix. The second function, `modifyFunction` serves to modify the values marked by `controlFunction` and to construct the final vector of elements edges coordinates, `EdgCoord`.

On top of these two functions, there is another subprogram associated with the finding of elements edges on the photographies from experiments, function `changeIMPars.m`, which is accessible from the RivuletExpDataProcessing program menu and provides a graphical user interface for changing the most important image processing parameters.

controlFunction.m

Function summary:

Name of the file	controlFunction.m
Associated .fig file	–
Short description	Finding outliers and `NaN` in `EdgCoord`
Inputs	`EdgCoord`, matrix (`nImages`×10)
Outputs	`state`
	`prbMsg`
	`sumMsg`

The output of the `findEdges` function can be burdened by some mistakes. Usually there are some outliers in the vaules caused by taking means of the found values and some `NaN` caused by plate finding algorithm failure (sometimes the edges of the plate are not very distinct from the noise on the images). The `controlFunction` is used to find these values. It is quite simple algorithm that walks through the columns of the `EdgCoord` matrix and processes the values for each column separately. The algorithm can be described as series of few simple steps.

Description of the algorithm

1. For every column there are found `NaN` values, their position is saved and they are removed from the column.

2. From the remaining values, it is calculated the standard deviation, σ.

3. For every column is calculated its kurtosis [69], Kurt. And from the kurtosis of a column is estimated coefficient, α, for identifying outliers in this column. The following relation is used:

$$\alpha = \frac{7}{\text{Kurt}} \tag{D.4}$$

   The curtosis of the normal distribution is equal to 3, so if the number 9 would be used, α obtained for a normal distribution would be 3, which is in accordance to practice. But the position of apparatus is not changing during the experiments, so the distribution of values should be closer to delta function then to normal distribution. Using the value 7 instead of 9 was shown to be providing the wanted narrowing of the values distribution type.

4. Every value in the column not satisfying condition $|x - \mu| \geq \alpha\sigma$, where μ is the mean value and σ is the standard deviation of the value stored in the current column is marked as outlier and its position is saved.

5. After checking every column of the matrix `EdgCoord`, the following output is created:

   - `state`, the vector where are saved numbers of outliers and NaN for each found device (flow cell and plate)
   - `prbMsg`, structure containing for each problematic value its position in `EdgCoord` matrix, number of the image where the problem occurred, type of the problem (`NaN` or outlier) and the device, where the problem was found.
   - `sumMsg`, structure with total number of found problem, with number of problems for each type and device and with user readable string summarizing all of the above.

modifyFunction.m

Function summary:	
Name of the file	modifyFunction.m
Associated .fig file	–
Short description	Modifying outliers and `NaN` in `EdgCoord`
Inputs	`EdgCoord`, matrix (`nImages`×10)
	`state`
	`prbMsg`
	`sumMsg`
Outputs	`EdgCoord`, vector (1×10)

The `rivuletProcessing` function is working with a vector of elements edges coordinates. So these coordinates are taken as invariant for all the images in one measurement. The `findEdges` function is providing a matrix of proposed elements edges coordinates. `controlFunction` is used to eliminate non-wanted values from this matrix and finally `modifyFunction` provides the final construction of the `EdgCoord` vector of found elements edges positions.

User can either take values proposed by algorithm (these are the mean values of found coordinates calculated without outliers and `NaN`s), he can directly modify the `EdgCoord` vector or by respecify outliers and `NaN`s graphically using GINPUT function.

Note: After this step, there must not be any `NaN` values in the `EdgeCoord` vector, otherwise all the functions depending on this vector will return an error.

The main idea of the algorithm is rather simple as it will be shown in following.

Description of the algorithm

1. Load output of the `controlFunction` and the `EdgCoord` matrix to be modified.
2. Propose a `EdgCoord` vector to user and let him modify it as he wants.
3. Replace `EdgCoord` matrix by vector of function outputs.

changeIMPars.m

Function summary:

Name of the file	changeIMPars.m
Associated .fig file	✓
Short description	Modification of image processing parameters
Inputs	`'onlyshow'`/`'nodata'`/`'imdata'`,`imDataCell`
Outputs	`IMProcPars`

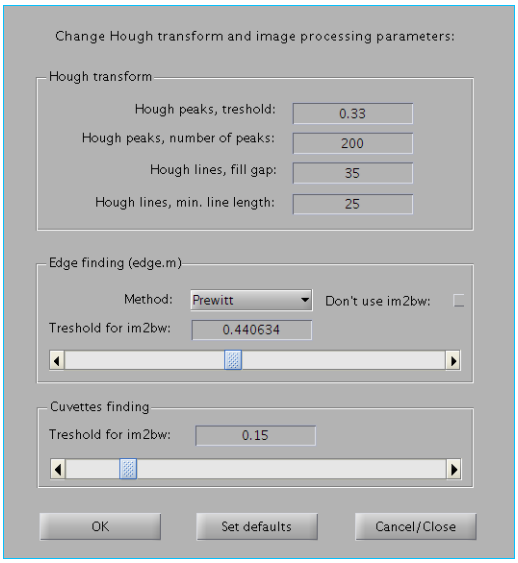

Figure D.7: GUI of the program for changing image processing parameters

Function for showing and modifying the values of image processing parameters. These parameters are used during the plate and flow cell coordinates finding as the inputs in HOUGH and IM2BW transforms and in EDGE function. There is a simple GUI created for this function where user can fill the wanted parameters into editable fields.

The function can be called with various options derived from the place from where it is called and from current state of the main program. For example, if this function is called with input parameter `'onlyshow'`, the OK pushbutton as well as the sliders are disabled and there is no output from the function. This call is used when user wants only to check current image processing values without changing them.

The GUI of this subprogram is shown in the Figure D.7.

D.3 rivuletProcessing.m

Function summary:	
Name of the file	rivuletProcessing.m
Associated .fig file	–
Short description	Processing the experimental data
Inputs	`handles`
Outputs	text files, `OUT`

Subfunctions	`rotameterCalib`
	`ImConv`
	`RivSurf`
	`CutRiv`
	`saveProf`
	`saveMatSliced`
	`saveCorrData`
	(all the subfunctions are in the main function code)

The `rivuletProcessing` function is the main data processing function of the RivuletExpDataProcessing application. Integration of this function into the main algorithm can be seen on the Figure D.2 on page 74. Function `rivuletProcessing` has only one input variable (`handles`), same as the function `findEdges`, but the required fields of the `handles` structure are different. Keeping all the inputs in one structured variable is good for quick and easy modifications of the functions input. However, the downside of this arrangement are requirements of the program on the computer memory (there is quite a lot of unused data passed into the called functions and all those data are, during the function execution, doubled into computer memory). Also this way of passing inputs to the function tends to be slower because of unnecessary data flows between the caller and called functions (time for preallocating memory for unused variables...). The list of the fields that have to be present into the `handles` structure when calling `rivuletProcessing` is in the Table D.3.

The fields `MainWindow` and `statusbar` are needed for handling and updating the status-bar in the main application window. The rest of the fields provides program data and runtime specifications.

The output of the function consists of two different parts, the data written directly in the chosen storage directory (`storDir`) and the function output variable, `OUT`. Complete list of outputs of the `rivuletProcessing` function is given in the Table D.4.

The other part of outputs are plots. User can specify from which parts of the algorithm he wants to create plots and what he wants to do with them (save them into files, show them on the screen or both).

D.3.1 Description of the algorithm

The main function, `rivuletProcessin` is constructed as caller of series of subfunctions. Only the input processing and some of the graphic outputs are treated in the body of the main function itself. The scheme of algorithm is in the Figure D.8 on page 86 and its written description can be specified by the following sequence:

1. Processing of the inputs
    - Extraction of the data and runtime parameters from handles
    - Preparation of the necessary program runtime variables

Table D.3: Mandatory fields in `handles` when calling `rivuletProcessing`

Structure name	Mandatory fields	Short description
handles	MainWindow	pointer to the main program window properties
	statusbar	pointer to the status-bar handles in main window
	metricdata	application data
	prgmcontrol	program runtime specifications
handles.metricdata	imNames	cell of the processed images names
	daten or subsImDir	images itselfs
	Treshold	threshold for rivulet distinction
	FSensitivity	noise removal parameter
	EdgCoord	location of the plate and calibration cell on images
	RivProcPars	experimental set up parameters
	fluidType	type of the used liquid
	fluidData	used liquids properties
	storDir	directory for storing results
	rootDir	program source codes location
handles.prgmcontrol	DNTLoadIM	
	GR	graphics export specifications
handles.prgmcontrol.GR	regr	parameters for `ImConv`
	contour	} type of graphs
	profcompl	} type of graphs
	profcut	} type of graphs
	regime	displaying the graphs
	format	format of exported images

Table D.4: Outputs of the `rivuletProcessing` function

subfolder of `storDir`	filenames	field in `OUT`	variable type
Correlation	IFAreaCorr.txt	IFACorr	`double`
	ARhoCorr.txt	ARhoCorr	`double`
Height	Height_00d.txt	RivHeight	`cell`
Speed	Speed_00d.txt	mSpeed	`cell`
Width	Width_00d.txt	RivWidth	`cell`
Others	ARhoL_00d.txt	ARhoL	`cell`
	epsHR_00d.txt	epsHR	`cell`
	locReA_00d.txt	locReA	`cell`
	locReW_00d.txt	locReW	`cell`
	thetaApL_00d.txt	thetaApL	`cell`
	thetaApR_00d.txt	thetaApR	`cell`
	00d → pump regime		
Profile	00d_00d.txt	Profiles	`cell`
	00d_00d → pump regime_measurement number		

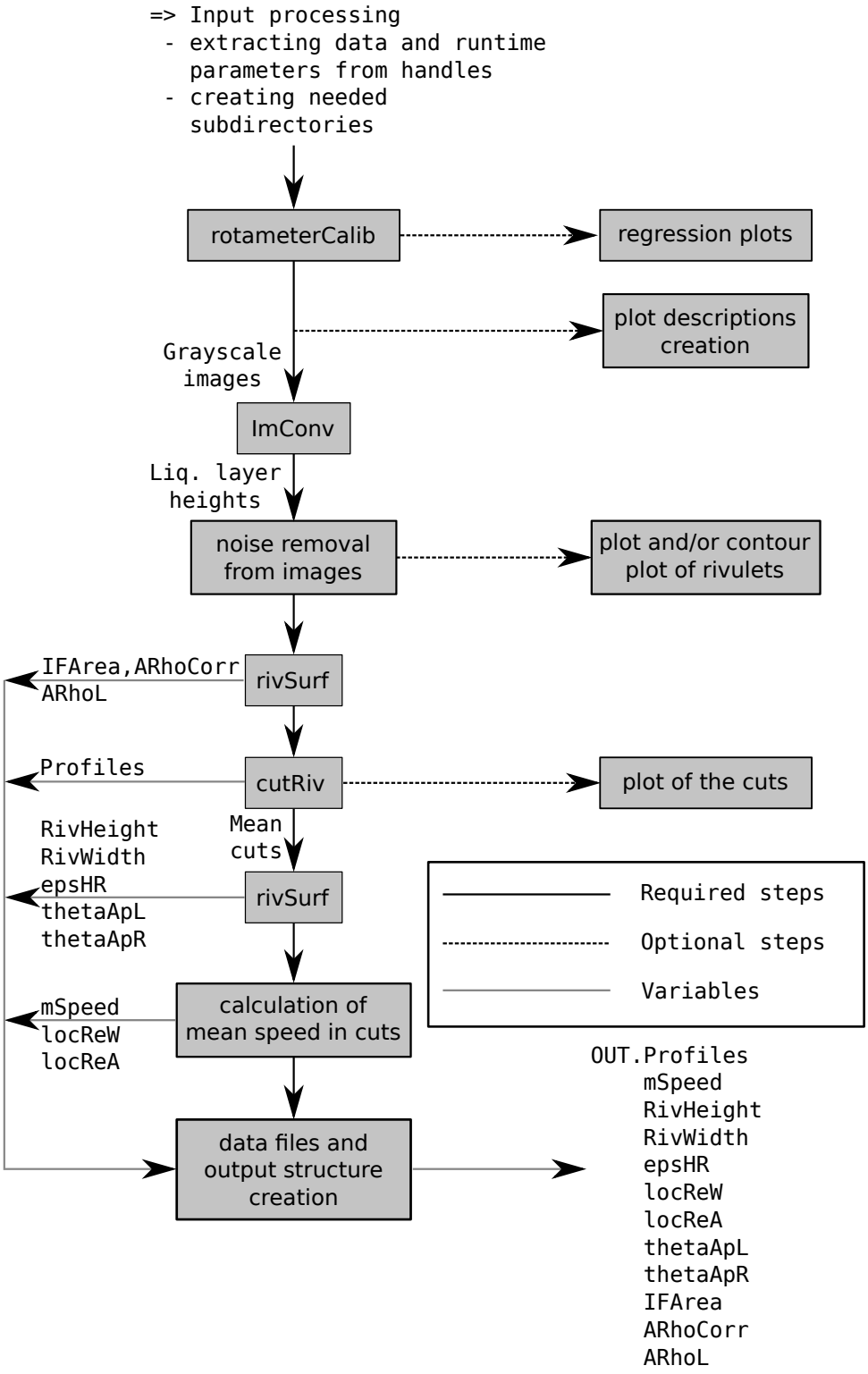

Figure D.8: Scheme of the `rivuletProcessing` function algorithm

2. Calibration of the rotameter (it is needed to convert values on the rotameter scale from water at 15 °C to the measured liquid at 25 °C). This is done by call to the `rotameterCalib` function.

3. Creation of the parameters for the plots description. On each exported plot, there is a description consisting of the following:

   - Liquid type
   - Liquid flow rate
   - Gas F-Factor (in $Pa^{0.5}$)
   - Rank of the image between the ones with the same liquid flow rate.

4. Conversion of the images from the grayscale values (emitted light intensities) into distance, done by the subfunction `ImConv`.

5. Removing noise from experimental images using MATLAB functions IMFILTER and FSPECIAL. Filter sensitivity is one of the functions inputs (`FSensitivity`, see Table D.3) and filter type is set as `'disk'`.

6. Optional: Creation of the plot of complete rivulet and/or contour plot – view of the rivulet from top.

7. Calculation of the interfacial area and interfacial area density of rivulets, done by call to function `RivSurf`. Threshold input parameter is used for distinguishing the rivulet from background noise on each image.

8. Creation of the specified number of transverse cuts along the rivulet and calculation of the mean profiles from the neighboring 50 transverse rows around each cut. Optionally program can plot these cuts separately for each rivulet. Done by call to function `cutRiv`.

9. Calculation of the rivulet width, height, its height to width ratio and apparent contact angles on its both sides for each cut. Done by calling function `rivSurf` once again with the different output parameters.

10. Calculation of mean speed of the liquid and local Reynolds numbers in each profile. The trapezoidal rule is used to obtain the rivulets cross section in each cut. The speed of liquid is determined with assumption of plug flow in the rivulet[3].

11. Saving results into the text files and output structure.

D.3.2 Subfunctions

All of the subfunctions of `rivuletProcessing` function are present in the code of this function. However, because the `rivuletProcessing` function is basically just a caller to its subfunctions, it is necessary to describe these subfunctions in great detail. However, there is one standalone subprogram very closely related to the `rivuletProcessing.m` function. It is `changeRPPars.m`, the graphical user interface callable from `RivuletExpDataProcessing.m` menus for changing the experimental set up parameters.

Note: Presence of the .m extension in the subfunction names states if it is in the separate source file or not. For details, see Table D.1.

[3]This assumption is not valid, but calculation of the liquid speed has only illustrational character

rotameterCalib

Function summary:	
Name of the file	rivuletProcessing.m
Associated .fig file	–
Short description	Conversion of set up vol. flow rates into dimensionless liq. flow rates and actual vol. flow rates
Inputs	`fileNames`
	`fluidData`
Outputs	`M`
	`V_Pumpe`

The rotameter on the experimental device is calibrated for the water at 15 °C. In this case, it shows volumetric flow rate of the water in L/h. However, the liquid type and temperature are. Because of this, it is necessary to calibrate the rotameter for different conditions.

Principle of the calibration: Mass of the liquid passed through the experimental apparatus during specified time interval (1 minute) is measured for different flow rates. Through this, the dependency $\dot{m}_l = \dot{m}_l(q)$, where $\dot{m}_l$ and q are the liquid mass and volumetric flow rates, is obtained and fitted using a polynomial regression. The obtained polynomial coefficients are one of the input arguments of the function `rotameterCalib`.

Description of the inputs: The function `rotameterCalib` has two input arguments. The first one, `fileNames`, contains names of the processed images in the form 00d_00d.tif, where 00d are representing numbers. Example of such a name could be 001_004.tif. First three digits contain information about volumetric flow rate shown at the rotameter scale during the experiment. The second three digits are the rank of the experiment between the ones with the same liquid flow rate.

Second input argument, `fluidData` is vector containing the different data needed for calculation of outputs and the coefficients of the polynomial obtained during the rotameter calibration.

Description of the outputs: The outputs are flow rate of the liquid in specified form (which has to be consistent through out the program and is currently fixed at mass flow rate in $\mathrm{g\,s^{-1}}$), `M` and its volumetric flow rate, `V_Pumpe`.

ImConv

This function is used to convert the grayscale values of the images from experiments into the metric thickness of the liquid layer on the plate.

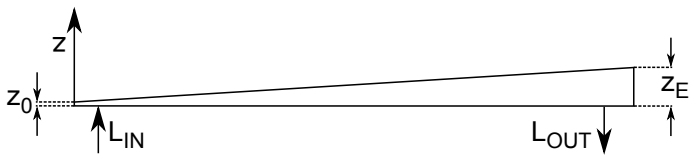

Figure D.9: Calibration flow cell used for conversion of grayscale values in the images in the film thickness

Function summary:

Name of the file	rivuletProcessing.m
Associated .fig file	–
Short description	Conversion of grayscale values into the distances

Inputs	`imData`
	`EdgCoord`
	`filmTh`
	`RegDegree`
	`GR`
	`GRregime`
	`GRformat`
	`txtPars`
	`storDir`
	`rootDir`
	`[imNumber]`

Outputs	`ImgConv`

On the experimental device is installed a flow cell with linear increase of the film thickness used to obtain the dependence of the film thickness on the grayscale values. Side projection of the flow cell with corresponding axes is shown in the Figure D.9.

Description of the algorithm:

1. Specify the position of the flow cell on the image using `EdgCoord` vector and calculate mean grayscale values for each row of the flow cell.
2. Create set of lineary increased values of the film thickness for flow cell. This is done using MATLAB LINSPACE function. As the limits for this function are used minimal and maximal film thicknesses in flow cell.
3. Obtain coefficients for the grayscale values to distances conversion using the polynomial regression. Independent variable are the greyscale values and the dependent is the obtained linear space.
4. Use calculated polynomial to convert the image.
5. Optional: plot the results.

RivSurf

Function `RivSurf` is used for calculation of the rivulet interfacial area, interfacial area density, its width, height, width to height ratio and the apparent contact angles and for specification of the borders of the rivulet in dependence of the input argument `Treshold`.

The code requires `YProfilPlatte` to be cell containing the profile data (heights of the liquid in mm for all the plate), `Treshold` to be scalar value representing the treshold for distinguishing between the rivulet and the background noise, in mm and `plateSize` to be vector containing plate width and length in m.

At the time, two different algorithms for determining edges of the rivulet are implemented. The first one, which is in the source code called `'complex'` is based on the presumption that outside the rivulet, each profile (transverse cut through the rivulet) should be constant. In case of using this algorithm, the input variable `Treshold` has the meaning specified by Equation (D.5).

Function summary:

Name of the file	rivuletProcessing.m
Associated .fig file	–
Short description	Calculation of the rivulet interfacial area, height and width
Inputs	`Treshold`
	`plateSize`
Outputs	`IFArea`
	`ARhoCorr`
	`ARhoL`
	`RivWidth`
	`RivHeight`
	`epsHR`
	`thetaApL`
	`thetaApR`
	`minLVec`
	`minRVec`
In/Out	`YProfilPlatte`

$$\left|\frac{dh(y)}{dy}\right| \leq \texttt{Treshold} \implies \left|\frac{dh(y)}{dy}\right| = 0, \tag{D.5}$$

where $h(y)$ is the current profile height as function of plate width coordinate, y. Upside of this algorithm is that in the ideal case, there should be no ignored part of the rivulet. However, its biggest disadvantage is that with higher liquid flow rate, the gravity causes flattening of the upper part of the profile and the algorithm crashes.

Other algorithm called `'simple'` is working with 25% quantile of profiles values, $h(y)$, (which is lower estimation of the „noise level“ on the images). In this case, `Treshold` is used as value added to the 25% quantile. The main advantage of this algorithm is its robustness (if the data are not extremely noisy, rivulet edges are used quite accurately). It downside however is that there always has to be some part of the rivulet ignored (yet, with rightfully adjusted threshold, the left out part of the rivulet can be reduced to approximately 5 % of its height).

Description of the `'complex'` algorithm: [4]

1. Find the dimensions of the plate in pixels and calculate the distance between two pixels in longitudinal and transverse direction (using input arguments `YProfilPlatte` and `plateSize`).

2. Smoothen the current rivulet (using function SMOOTH taking 30 neighbouring values).

3. For each row of the current `YProfilPlatte` cell do:

   (a) Find peaks (local maximum) of the row (transverse cut of the rivulet).

   (b) The peak nearest to the center of the plate is taken as current profile maximal height, $h_0(x)$. If there is more then 1 (2) peak with same distance from the plate center, take the higher one. Save it in the `RivHeight`.

   (c) Divide current row into two vectors (left and right from the center).

[4] For all the cells in `YProfilPlatte`

(d) Numerically derive each side of the rivulet (using function DIFF, this function uses simple fast-forward formula with error of order $O(h)$) to obtain 2 derivative vectors.

(e) Calculate absolute values of these vectors.

(f) In both vectors, locate values lower than `Treshold`. Save locations of these elements only if ten or more neighboring values satisfies the same condition.

(g) For the left side of the rivulet, take the last saved elements location as the rivulet edge. For the right side, take the first such location. Save these values as local rivulet edges.

(h) Save $\min |y(x_{\text{left}}), y(x_{\text{right}})|$ as local noise level.

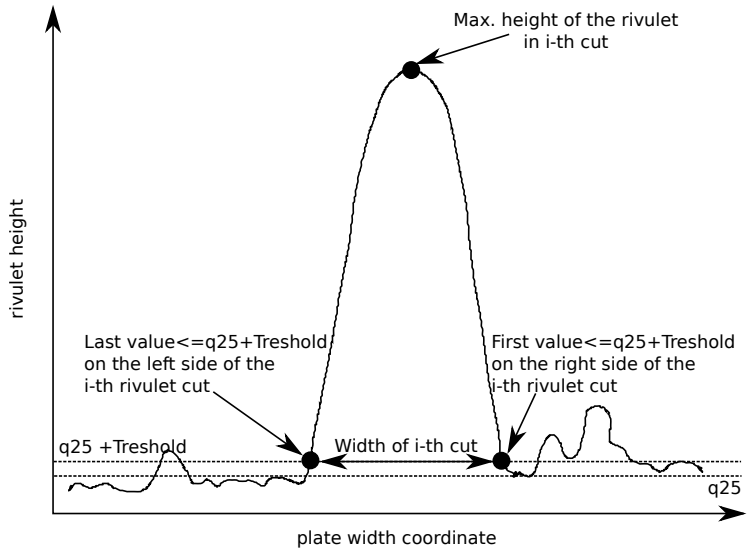

Figure D.10: Main elements identified by the `'simple'` algorithm

Description of the `'simple'` algorithm: [5]

1. Find the dimensions of the plate in pixels and calculate the distance between two pixels in longitudinal and transverse direction (using input arguments `YProfilPlatte` and `plateSize`).

2. Smoothen the current rivulet (using function SMOOTH taking 30 neighboring values).

3. Calculate 25% quantile, $\vec{q}_{25}$, for each column of the current `YProfilPlatte` cell (which is for each horizontal row of the image).

4. For each row of the current `YProfilPlatte` cell do:

   (a) Find peaks (local maximum) of the row (transverse cut of the rivulet).

   (b) The peak nearest to the center of the plate is taken as rivulet height. If there are more (2) peaks with same distance from the plate center, take the higher one. Save it in the `RivHeight`.

   (c) Divide current row into two vectors (left and right from the center).

[5] For all the cells in `YProfilPlatte`

(d) Find first value in the left side of the current profile (i) and last value in its right side that satisfies the condition: $y(x) \geq q^i_{25} + \texttt{Treshold}$. Save these values as local rivulet edges.

(e) Save value $q^i_{25} + \texttt{Treshold}$ as local noise level.

The basic principles of the `'simple'` algorithm are shown on the Figure D.10.

$$S^E_{(g)-(l)} = \delta x \sum_{(i)} \left(\sum_{(j)} \delta l_{ij} \right) \tag{D.6}$$

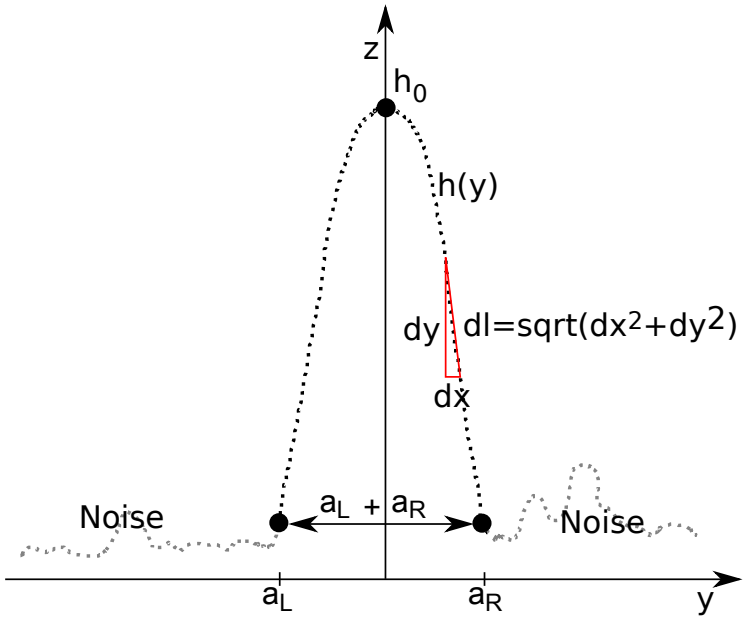

Figure D.11: Principle of the of the $(g) - (l)$ interfacial area size calculation

Rest of the algorithm:

1. If the number of taken profiles is lower than 100 (common case in evaluating cut rivulet), for each transverse cut do:

   (a) Calculate the derivation of left and right parts of the rivulet (using DIFF function).

   (b) Get 10 highest slopes for each vector of differences.

   (c) Use equation $\tan\beta \approx \max_y |h'(y)|$ for calculation of the local apparent contact angle. Calculate this angle for each side of the rivulet separately.

   (d) Save results in the `thetaApL` and `thetaApR` variables.

2. If the number of taken profiles is higher than 300 (usually when calculating interfacial area of the whole rivulet), smoothen found edges using 100 neighboring values.

3. Calculate width of the rivulet as difference between the right and left rivulet borders in pixels multiplied by distance between two pixels in horizontal direction. Save this value as `RivWidth`.

4. Calculate mean noise level from saved local ones.

5. Subtract mean noise level from current cell of `YProfilPlatte` and from `RivHeight` vector.

6. Calculate the rivulets height to width ratio and save it in the `epsHR` variable.

7. For each row of the current `YProfilPlatte` cell do:

   (a) Calculate length of the curve identified as the rivulet (between the previously found borders).

   (b) Calculate size of the area under the current profile.

   (c) Multiply length of the rivulet border and the area under it by distance between two pixels in longitudinal direction of the plate. This is an interfacial area of 1 transverse cut of the rivulet and the volume of liquid enclosed in it.

   (d) Divide this area by the volume and save it as local interfacial surface density in the `ARhoL` variable.

8. Sum all the transverse cuts interfacial areas to obtain interfacial area of the whole rivulet and save it in the `IFArea` variable. The main idea is presented in Equation (D.6) and in Figure D.11.

9. Divide the size of this area by sum of all the differential volumes to obtain the integral surface area density, save it in the `ARhoCorr` variable.

Note: The algorithm is called twice during the program execution. At first it is called for whole rivulet, to calculate the size of its interfacial area and the interfacial surface density. Then it is called for mean cuts of the rivulet, to calculate their width and height and apparent contact angles.

Note: At the time, to switch between `'complex'` and `'simple'` algorithm, the source code of the `RivSurf` function has to be modified. There is also commented section of the code that enables graphical control of found rivulet edges.

Note: Optimal value of `Treshold` seems to be approximately 10^{-3} for the `'complex'` algorithm and between $3 \cdot 10^{-5}$ and $5 \cdot 10^{-5}$ for the `'simple'` algorithm.

CutRiv

The `cutRiv` function is used to create number of cuts specified in the input argument `nCuts` along the longitudinal coordinate of the rivulet. Each resulting cut is the result of mean values from 50 neighboring rows around the cut position.

The variable `YProfilPlatte` is both input and output variable. On input it is a vector of cells containing the complete liquid heights information for each processed image. On output, it is a vector of cells with the same number of elements as on input, but each cell contains the information about heights of the made cuts. This means that on output, `YProfilPlatte` is considerably smaller than on input.

Description of the algorithm: [6]

1. Calculate distance between two cuts in pixels.

2. If the distance between two cuts is, in pixels, lower than 50, issue a warning and ask for lower number of cuts to be made.

[6] For all the cells in `YProfilPlatte`

Function summary:

Name of the file	rivuletProcessing.m
Associated .fig file	–
Short description	Creation of the specified number of cuts along the rivulet
Inputs	`nCuts`
	`plateSize`
	`GR`
	`GRregime`
	`GRformat`
	`txtPars`
	`storDir`
	`rootDir`
	`[imNumber]`
Outputs	`XProfilPlatte`
In-Outs	`YProfilPlatte`

3. Made cuts at specified positions by taking the mean value of 50 neighboring rows around the specified position.
4. Rewrite input variable `YProfilPlatte` with these values
5. Create output variable `XProfilPlatte`, as linspace defining the width coordinate of the plate for each cut.
6. Optional: Plot results

Functions for saving data

The rest of the subfuntions of the `rivuletProcessing` are functions for saving calculated data both into the text files in specified `storDir` and into the fields of the output structure `OUT`.

These functions are:

- `saveProf` for saving rivulet profiles made in the cuts by the function `cutRiv`
- `saveMatSliced` for saving the `RivHeight`, `RivWidth` and `mSpeed` variables
- `saveCorrData` for saving the `IFArea` variable along with some other needed for the correlations.

All these function are very similar, at first, there is always created some output matrix of desired form and this matrix is then saved into the text file using DLMWRITE and returned as output of the function. The function `saveMatSliced` ads to the output variable also information about measured liquid volumetric flows – criterion for creating names of the files created by this function.

changeRPPars.m

Subprogram for showing and modifying the values of rivulet processing parameters. This function is a „sister“ function of `changeIMPars.m`, because their programming is almost the same. In the graphical user interface, the size of the plate and its inclination angle as well as some others parameters can be specified. These parameters are then used when calling the `rivuletProcessing.m` function.

Function summary:

Name of the file	changeRPPars.m
Associated .fig file	✓
Short description	Modification of rivulet processing parameters
Inputs	–/`'onlyshow'`
Outputs	`RivProcPars`

Note: Even if it is not used at the time, `changeRPPars.m` allows to specify also the parameters of the countercurrent gas flow and calculates its f-factor.

If is this function called with input parameter `'onlyshow'`, the OK pushbutton is disabled and there is no output from the function. Otherwise (called with no inputs), the output of the function is created during the call and variable `RivProcPars` is exported into the `handles.metricdata` of the main program.

Variable `RivProcPars` is the structure with fields specifying different rivulet processing parameters.

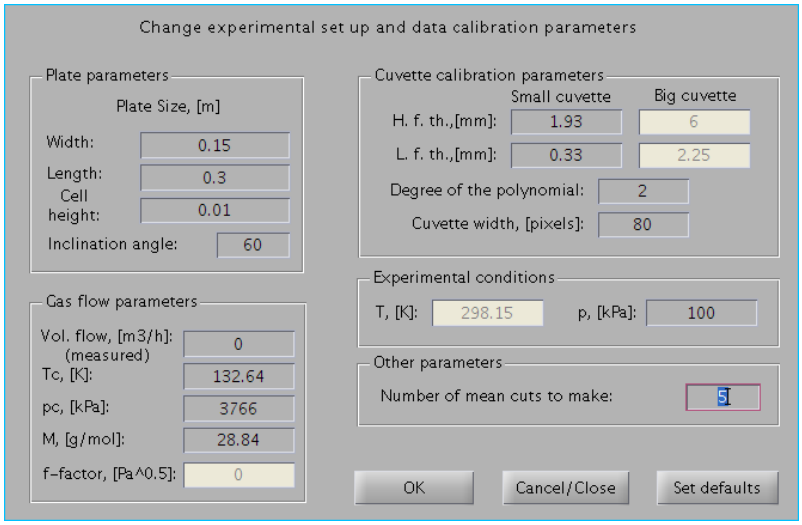

Figure D.12: GUI of the program for changing experimental set up parameters

The GUI of this function is shown in the Figure D.12.

D.3.3 Created files

The outputs of rivulet processing algorithms are saved into different text files for later use. There are created several text files and, if user selects to, also multiple plots. In the Table D.5 is list of created files and subdirectories where they are saved, as well as their short description.

More detailed description of the files is given in the following text.

Note: All the text files are delimited with tabulators to be loadable into different spreadsheets (MS Excel, Libreoffice/Openoffice Calc...).

[7]PRG stands for pump regime used during the measurement. It is a number in format `'%03D'`

[8]NEX stands for the number of experiment. It is a number in format `'%03D'`

[9]R stands for the rank of the image, FMT is the selectable file format(`'.png'`,`'.fig'`,`'.eps'`,`'tif'`)

Table D.5: Files created during the `rivuletProcessing` function execution

Filename	Folder	Description
IFACorr.txt	Correlation	Data usable in calculations of (g)–(l) interfacial area
ARhoCorr.txt	Correlation	Data usable in calculations of (g)–(l) interfacial area surface density
Height_PRG.txt[7]	Height	Rivulets heights in mean cuts One file for each pump regime
Speed_PRG.txt	Speed	Mean liquid speeds in cuts One file per pump regime
Width_PRG.txt	Width	Rivulets widths in mean cuts One file per pump regime
ARhoL_PRG.txt	Others	I-f. area surface density along the plate One file per pump regime
epsHR_PRG.txt	Others	Rivulet height to width ratio in cuts One file per pump regime
LocReA_PRG.txt	Others	Local Reynolds num. with respect to cap. length One file per pump regime
LocReW_PRG.txt	Others	Local Reynolds num. with respect to riv. width One file per pump regime
thetaApL_PRG.txt	Others	Apparent contact angle from the left One file per pump regime
thetaApR_PRG.txt	Others	Apparent contact angle from the right One file per pump regime
PRG_NEX[8].txt	Profiles	Mean profiles in cuts One file per measurement – image.
PRG_NEX.tif	Subtracted	Images with subtracted background One file per measurement – image.
PRG_NEX.tif	Subtracted/Smoothed	Images without random noise. One file per measurement – image.
rivRcomplprof.FMT[9]	Plots	Plots of the complete rivulet One file per image
rivRcutprof.FMT	Plots	Plots of the profiles in cuts One file per image
rivRfromtop.FMT	Plots	Contour plots of the rivulet One file per pump regime
rivRregrstate.FMT	Plots	Plots from `ImConv` function One file per image

Profiles

Files saved into *Profiles* subfolder of chosen data outputs storage directory contains data for later loading and visualizing the mean profiles created in cuts along the plate. There is one file created for each processed image. It contains the x (plate width) coordinates altering with the y (rivulet height appartening to corresponding x coordinate) coordinates organized into columns.

Thus for m made cuts along the plate length, the created files have $2m$ columns altering in a way $\vec{x}_1, \vec{y}_1, \vec{x}_2, \vec{y}_2, \ldots, \vec{x}_m, \vec{y}_m$, with $\vec{x}_i, \vec{y}_i$ being column vectors.

All the pairs of vectors that have to be written into the file have (presumably) different lengths, because the length of these vectors depends on the rivulet width which is changing

along the plate length coordinate. So these vectors have to be completed in the way that

$$\vec{x}_i, \vec{y}_i \in \mathbb{R}^l, i = 1,2,\ldots,m,$$

where

$$l = \max_{i=1,\ldots,m} |\dim(V_i); \vec{x}_i, \vec{y}_i \in V_i| \,.$$

This completion is done by adding according numbers of zeros at both sides of the too short vectors. Example of such file is on the Figure D.13.

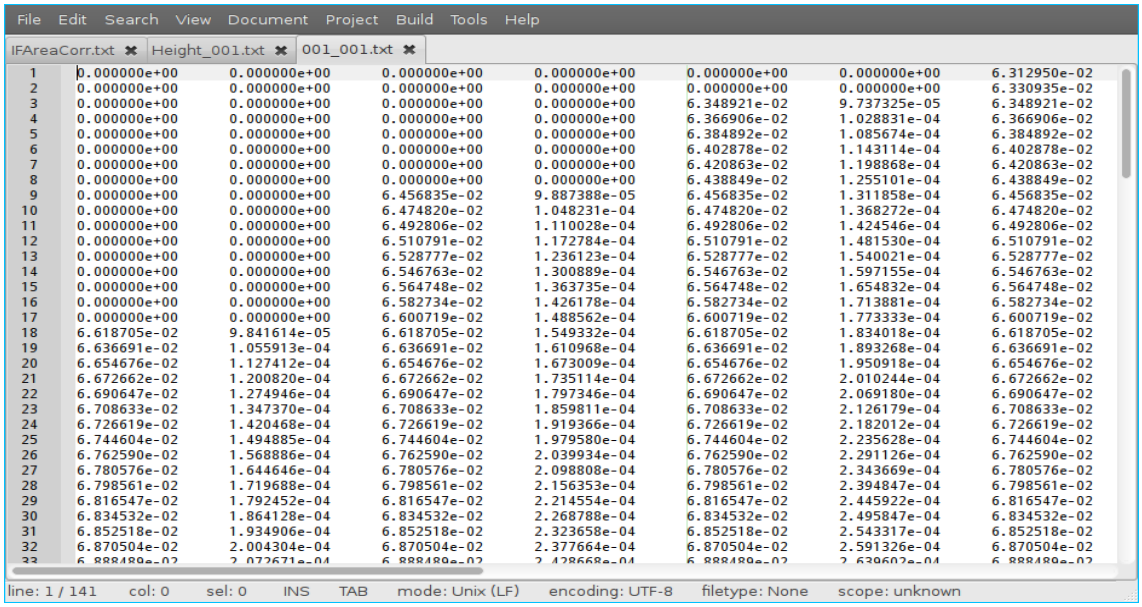

Figure D.13: Example of file created into *Profiles* folder

IFACorr.txt, ARhoCorr.txt

There is only one IFACorr.txt file created for all the processed images and it contains informations about experiment essential for creation of (g)–(l) interfacial area correlations. It contains number of rows corresponding to the number of processed images. Columns of this matrix are formed in the following order: liquid surface tension (σ), liquid density (ρ), liquid dynamic viscosity(η), liquid dimensionless flow rate ($\dot{M}$), plate inclination angle (α), gas F-Factor (F), and (g)–(l) interfacial area ($S_{g/l}$).

Written in symbols, each row of the file contains this informations about corresponding measurement:

$$(\gamma \ [\mathrm{N\,m^{-1}}], \rho \ [\mathrm{kg\,m^{-3}}], \eta \ [\mathrm{Pa\,s}], \dot{M} \ [-], \alpha \ [^\circ], F \ [\mathrm{Pa^{0.5}}], S_{g/l} \ [\mathrm{m^2}])$$

Other files

Rest of the files have all the same structure and are also created by the same function.

One of these files is created for each pump regime used during the experiment. It contains informations about measured variables along with some basic statistical calculations (mean values, μ and standard deviations, σ) and informations about the measurement (liquid flow rate in chosen form, M and gas F-Factor, F).

The files have number of rows corresponding to number of cuts made along the plate. The default number of these cuts is 5, which means that there is one cut taken every 5 cm of the plate, starting with 5 cm from the top and ending with 25 cm from the plate top.

Note: If you will change longitude dimension of the plate, these distances will be also changed.

First n columns of the file are corresponding to the n measurements taken for the current pump regime (usually $n = 4$). Then it follows a column containing zeros to distinguish between measured and calculated data. Next two columns are the mean value (μ) of measured variable at specified distance from the top of the plate and standard deviation (σ) of these values. Last three columns of the file are liquid flow rate (M, [−]), gas F-Factor (F, $[\mathrm{Pa}^{0.5}]$) and the distance from the top of the plate (d, [m]).

The example of such a file is in the Table D.6. There were m cuts made along the plate and for the studied pump regime were made n measurements.

`$VAR` stands for measured variable (width, height, speed, contact angles...) and `$D` for the distance from the top of the plate. Superscripts are for distinguishing between measurements and subscripts for distances from the top of the plate (in cm).

Table D.6: Example of file created in one of the *Height*, *Speed* or *Width* folders

Measured data						Zeros	μ	σ	$\dot{M}$	F	d
$\texttt{\$VAR}_1^1$	$\texttt{\$VAR}_1^2$	$\texttt{\$VAR}_1^3$	$\texttt{\$VAR}_1^4$	...	$\texttt{\$VAR}_1^n$	0	μ_1	σ_1	$\dot{M}$	F	$\texttt{\$D}_1$
$\texttt{\$VAR}_2^1$	$\texttt{\$VAR}_2^2$	$\texttt{\$VAR}_2^3$	$\texttt{\$VAR}_2^4$	...	$\texttt{\$VAR}_2^n$	0	μ_2	σ_2	0	0	$\texttt{\$D}_2$
⋮	⋮	⋮	⋮		⋮	⋮	⋮	⋮	⋮	⋮	⋮
$\texttt{\$VAR}_m^1$	$\texttt{\$VAR}_m^2$	$\texttt{\$VAR}_m^3$	$\texttt{\$VAR}_m^4$	...	$\texttt{\$VAR}_m^n$	0	μ_m	σ_m	0	0	$\texttt{\$D}_m$

Subtracted images

In the folder *Subtracted* are saved experimental images with background subtracted from them. These files are however created already during the Image loading (see the Figure D.2 on page 74).

Smoothed images

During execution of the `rivuletProcessing` function, parts of the experimental images with plate on them is cut out and the random noises are removed from it (for details, see subsection D.3.1, Description of the rivulet processing algorithm, on page 84).

Note: These images were created after the conversion of the grayscale values into distances, thus the contrasts of files are, compared to subtracted images, changed.

Exported plots

Numerous plots can be created during the runtime of `rivuletProcessing.m` function. It is possible to choose from GUI, which of these plots should be actually generated, if they are to be immediately shown or saved for the later use. Also, there is a possibility to select the format of created files.

These plots are of four different types. The first one are three dimensional plots of the whole rivulet, second are plots of the mean profiles made in cuts along the rivulet. Third type of graphics are the contour plots of the trickles and the last one is the calibration plot used for conversion of the grayscale values in distances for each image (for details on this conversion, see section D.3.2. Slightly modified examples of the first three types of the plots can be found in chapter 3, Experiments.

D.4 postProcPlotting.m

Function summary:	
Name of the file	postProcPlotting.m
Associated .fig file	–
Short description	Plotting of program outputs
Inputs	`Availible`
Outputs	–
Subfunctions	`showProcData`

The `postProcPlotting.m` function is a simple tool that can be used to plot and compare outputs of the program. After each run of the `rivuletProcessing.m` function, the output of this function is stored in new field of cell `Availible` which serves as storage space for all the processed data and also as input variable for `postProcPlotting` function.

User can display currently available data as well as load presaved ones from the *Post-processing* menu of the main program, using the subfunction of `postProcPlotting.m`, `showProcData.m`.

The function `postProcPlotting` is not linked with any graphical user interface, because its interface structure is simple enough to be created programatically. This approach also allows the main GUI window to be resizable.

D.4.1 Description of the algorithm

The data selection and plotting in postprocessing tool is based on three dynamically created lists. One of them contains available processed data distinguished by their ID strings, other one contains list of different variables usables for the postprocessing and the last one is optionally filled with data identification for each measurement or group of measurements.

Scheme of the algorithm of dynamic lists filling is on the Figure D.14 on page 100. As it can be seen, usable variables for the data postprocessing can be distinguished into three main groups.

First of them is consisted of `Profile`, variable containing data of profiles made in cuts through the rivulet (for details see section D.3.2). Second one of `IFACorr` and `ARhoCorr`, which are the variables containing data for creating correlations for size of (g)–(l) interfacial area of the rivulets. Last group then contains variables `mSpeed`, `RivHeight`, `RivWidth`, `ARhoL`, `epsHR`, `thetaApL`, `thetaApR`, `ReA` and `ReW`. In these variables are stored properties of the rivulets in cuts made along the plate (for details see section D.3.2).

The behavior of `postProcPlotting` function depends very strongly on chosen data group. Because of this, the following description will be divided into four parts: one for the common steps and one for each variable group.

Common steps:

1. Input processing: distinguishing different data groups in the `Availible` input variable.
2. GUI creation, the GUI is created programatically so it can be resizible.
3. Filling the list 1 (view Figure D.14) with ID string of available data groups. This string is created in format:

   `LiqType_F-Factor_InclAngle_DD_MM_YY-HH_MM_SS`,

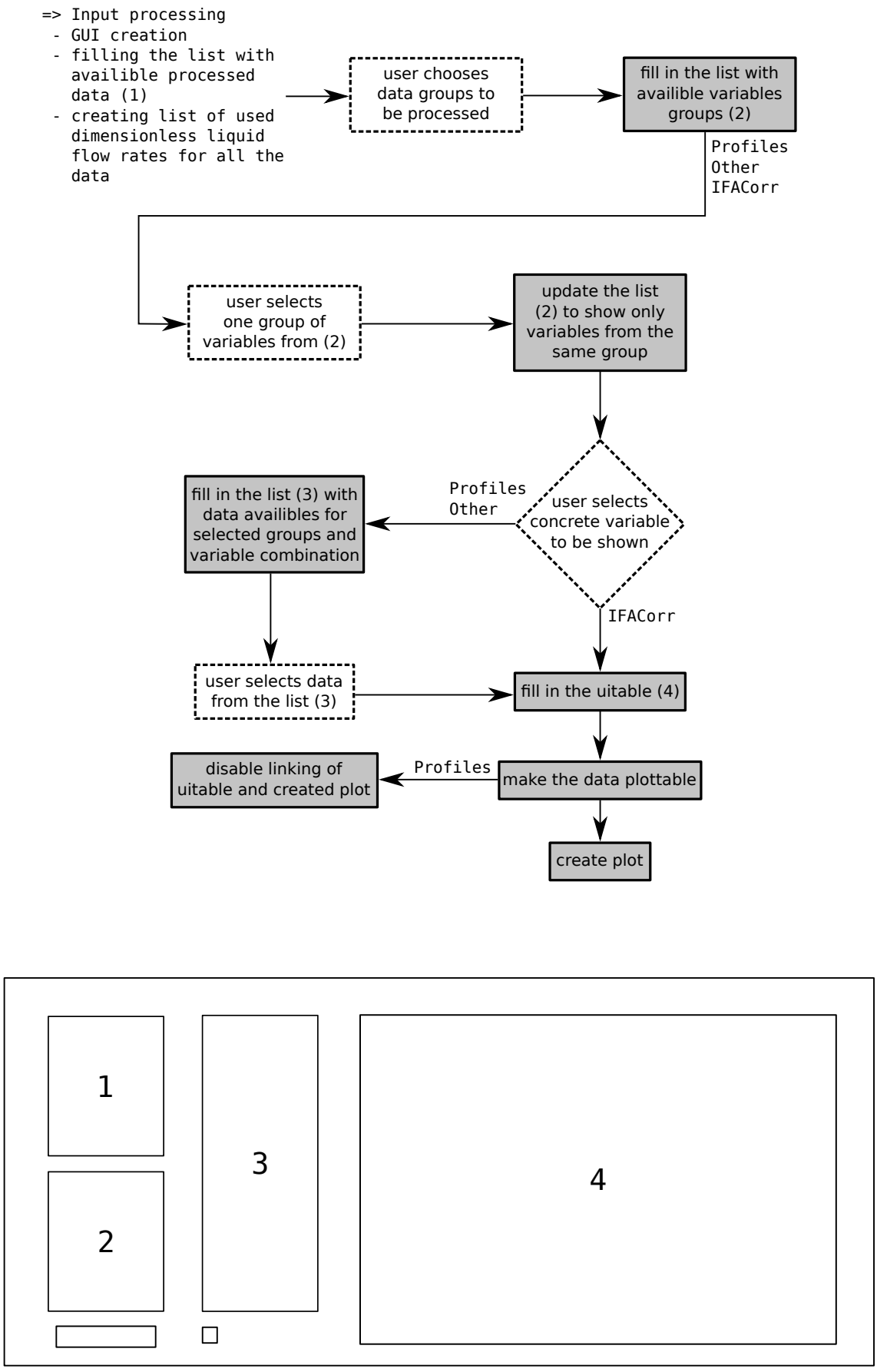

Figure D.14: Scheme of the `postProcPlotting` function algorithm and corresponding GUI elements

where `LiqType` is liquid type, `F-Factor` is gas f-factor in $Pa^{0.5}$, `InclAngle` is the plate inclination angle in degrees, `DD` is two digits date number, `MM` is for months in first mention and for minutes in second, `YY` is for the year, `HH` for hour and `SS` for seconds. Because the program execution time for one image is around 30 seconds, this format of ID string ensures that there never can be two measurements with the same ID string.

4. Filling the list 2 with different available variables: `Profiles`, `mSpeed`, `RivWidth`, `RivHeight` and `IFACorr`.

Following actions are dependable on the chosen variable from the list 2.

After choosing `Profiles` from the list 2:

This option is used to display profiles made along the plate length coordinate.

1. Reduce content of the list 2 only to compatible variables (`Profiles`).
2. In list 3, display all available measurements. User needs to choose from them. He may choose any number he wants, but if more than 4 different profiles are chosen, the program slows down and also the created plots are not very clear.
3. After choosing measurements, fill the uitable 4 with data corresponding to different profiles. In impair columns, there are plate width coordinates (X) and in pair ones, there are corresponding rivulet heights (Y). The values of rivulet height outside of specified rivulet borders are replaced by 0.
4. Disable option to link plot with data in the uitable 4.
5. Enable option to plot selected data.

After choosing `IFACorr` or `ARhoCorr` from the list 2:

This option is used display measured interfacial area in dependence of dimensionless liquid flow rate. In future releases (if any), options to plot these data also in dependence of other variables will be added.

1. Reduce content of the list 2 only to compatible variables.
2. Disable the list 3.
3. Fill in uitable 4 with available data. Structure of the shown data is the same as for the text files saved by function described in section D.3.2. For details, see section D.3.3.

After choosing one of the other variables from the list 2:

Using this option, the measured rivulet width, height and mean liquid velocity in cuts made along the plate length coordinate can be studied. All these variables were saved using the same function and they have the same structure, for details see section D.3.2 and section D.3.3.

1. Reduce content of the list 2 only to names of these variables.
2. Display different dimensionless liquid flow rates for each analyzed measurement in the list 3. User may choose any number of these data to be shown.
3. After choosing from the list 3, the corresponding measurements are displayed in uitable 4, with the same structure as have the saved text files described in section D.3.3.
4. Enable option for plotting the data. Created plot is linkable with the uitable data.

Note: The algorithm of `postProcPlotting.m` function is based on procedural programming principles. However, it could be significantly simplified with implementation of the object oriented code. The idea behind this approach is to implement three different custom object types (for profiles, correlation variables and the rest of the data) with all the necessary methods (for saving data, plotting them...) defined on them. Algorithms of the `RivuletExpDataProcessing.m` program were already partially modified to exploit advantages of object oriented programming, but the implementation is not yet fully functional. Even though, the length of the modified part of the `postProcPlotting.m` function source code was reduced by 150 lines (approximately 1/3 of the code).

D.4.2 Subfunctions

The postprocessing tool has only one subfunction. It is called `showProcData` and is used as data loader for the `postProcPlotting` function.

showProcData.m

Function summary:	
Name of the file	showProcData.m
Associated .fig file	✓
Short description	Data loader for the postprocessing tool
Inputs	`Availible`
Outputs	–

This function is used for showing available processed data saved into the `handles` structure and for working with them. User can load presaved data, save all present data or just a selection and start the postprocessing tool with selected data.

Function is controled through simple GUI. Availible data are presented in the list containing their ID strings.

D.5 Other functions

On top of up to now described functions, there are several others subprograms related to the data evaluation. The most important of them are `treshInflStudy.m` and `fitIFA.m`, both accessible from the *Other Function* menu of `RivuletExpDataProcessing.m` main window.

D.5.1 treshInflStudy.m

Function summary:	
Name of the file	treshInfStudy.m
Associated .fig file	✓
Short description	Study of the influence of `Treshold` on data evaluation
Inputs	metricdata prgmcontrol
Outputs	–

The key parameter for evaluation of experimental data is the threshold for distinction between the rivulet itself and background noise (for details, see section D.3.2). It is thus necessary to find optimal value of this parameter for each of the processed measurements.

The function `treshInflStudy.m` serves to plot the variables returned by `rivuletProcessing.m` which can be influenced by the threshold in dependence of it. These variables are: `IFACorr`, `ARhoCorr`, `mSpeed`, `RivWidth`, `epsHR`, `thetaApL`, `thetaApR` and `locReW`.

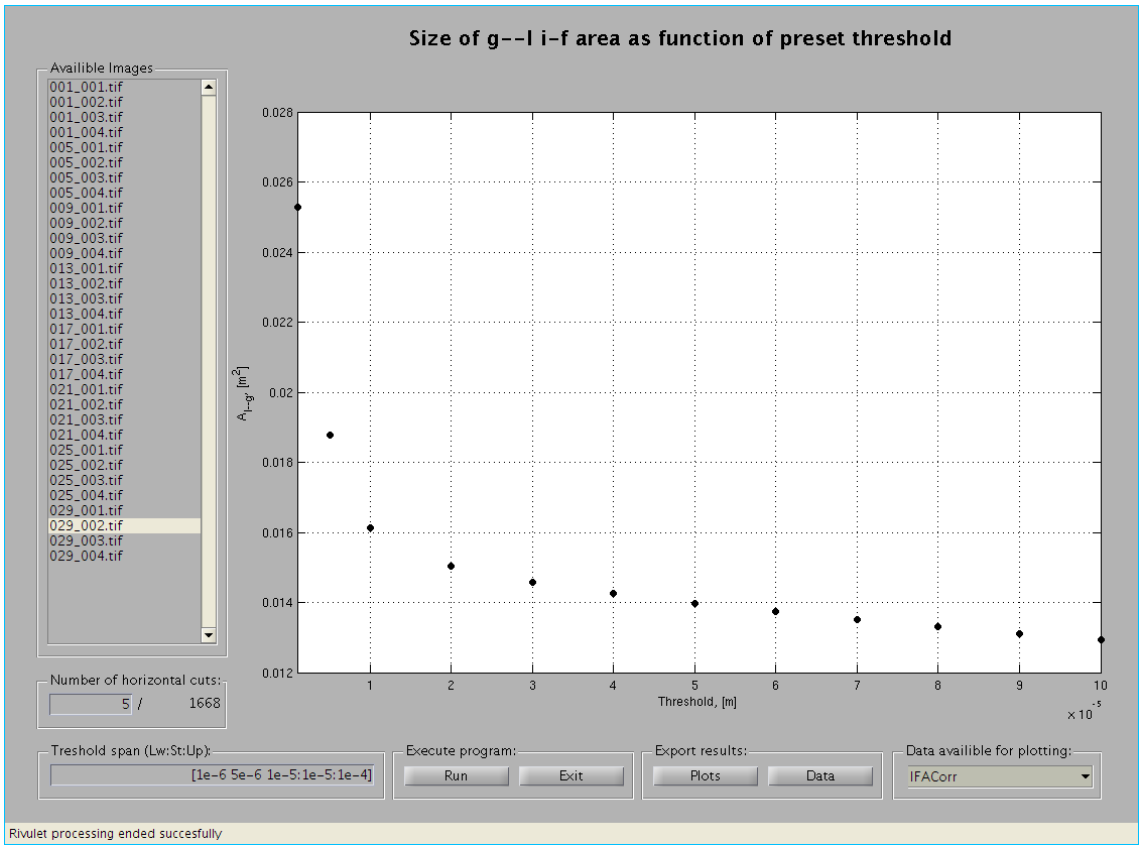

Figure D.15: Example of the threshold influence on results study

The window of this subprogram is shown in Figure D.15. As it is well visible, this function lets user to choose between the images loaded into the main program environment and to perform the threshold influence study on them. This is done by calling the `rivuletProcessing.m` function for each studied threshold and collecting the results. In the shown figure, there is shown the dependence of measured size of gas-liquid interfacial area in dependence on the threshold.

It is obvious that with the decrease of the threshold, the measured values of the interfacial area size will increase. The ideal threshold for the measurement is located approximately in the place, where the decrease of calculated values becomes more or less linear (in the case shown in Figure D.15 it would be between $2 \cdot 10^{-5}$ and $3 \cdot 10^{-5}$ m). For more accurate determination of threshold value, there is also possibility to plot any other of the calculated variables that might be influenced by it.

Note: There is also a possibility to export the results into the specified. In case of exporting the plots, there is eight images .png created in the specified directory, one for each calculated variable. Other option is to export the text file with results. Example of such a file can be found on the attached DVD, in folder */evalExpExample/treshInflStudy/*.

D.5.2 fitIFA.m

For the possibility of easy application of the model described in subsection 2.5.2 on page 19, a simple function providing option to do so from graphical user interface was

implemented.

Note: At the beginning, the initial contact angle was kept as an additional fitting parameter, but later on, it was replaced by the calculation based on equation (5.4) from page **??**. However, the corresponding fields were only disabled and not removed from the GUI to maintain easier applicability of the function to the problems with different geometry.

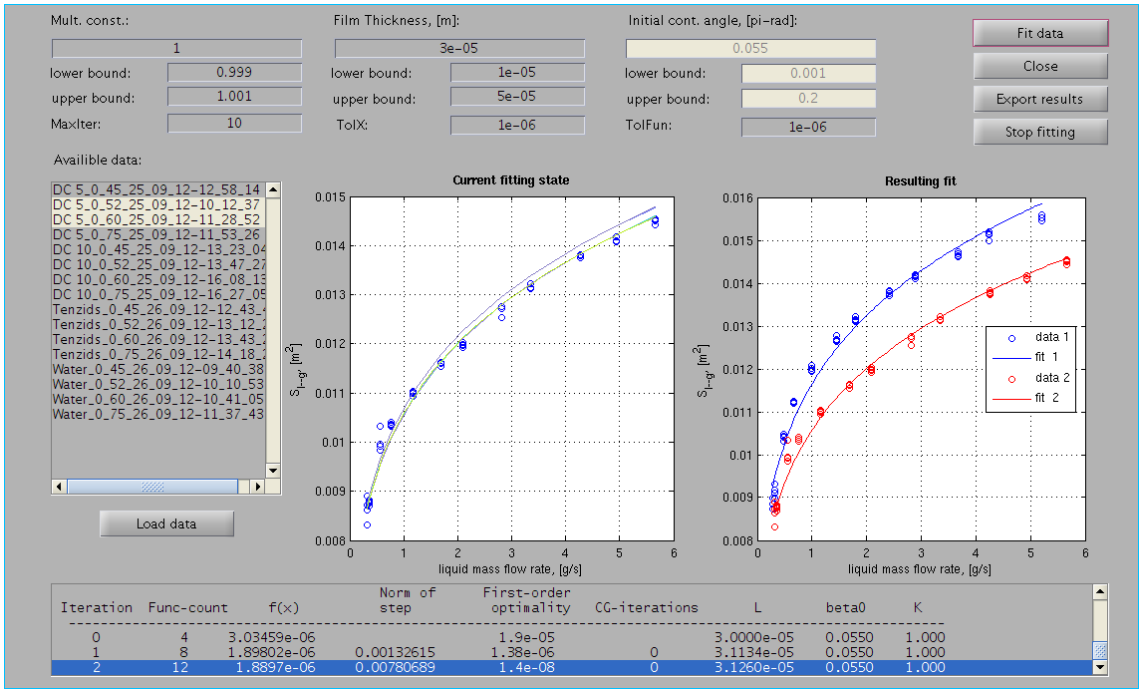

Figure D.16: Example of the current state of the `fitIFA.m` function

In the Figure D.16, there is shown an example of the GUI of the described function during a fitting session. All the results (including the description of the iteration process) can be exported to the text files.

The calculation of fitted parameters is based on the trust-reflective least square fitting algorithm. For the details on this procedure, see the help for LSQCURVEFIT function in [67].

The data can be fitted using two adjustable parameters, as it is described by equation (5.5). However, the multiplicative constant Φ (in the program denoted as `Mult. ... const.`) is by default disabled, as for the case of silicon oils the data can be fitted varying exclusively the guess of the underlying film thickness (also referred to as an intermediate length scale, l).

E. Experimental results

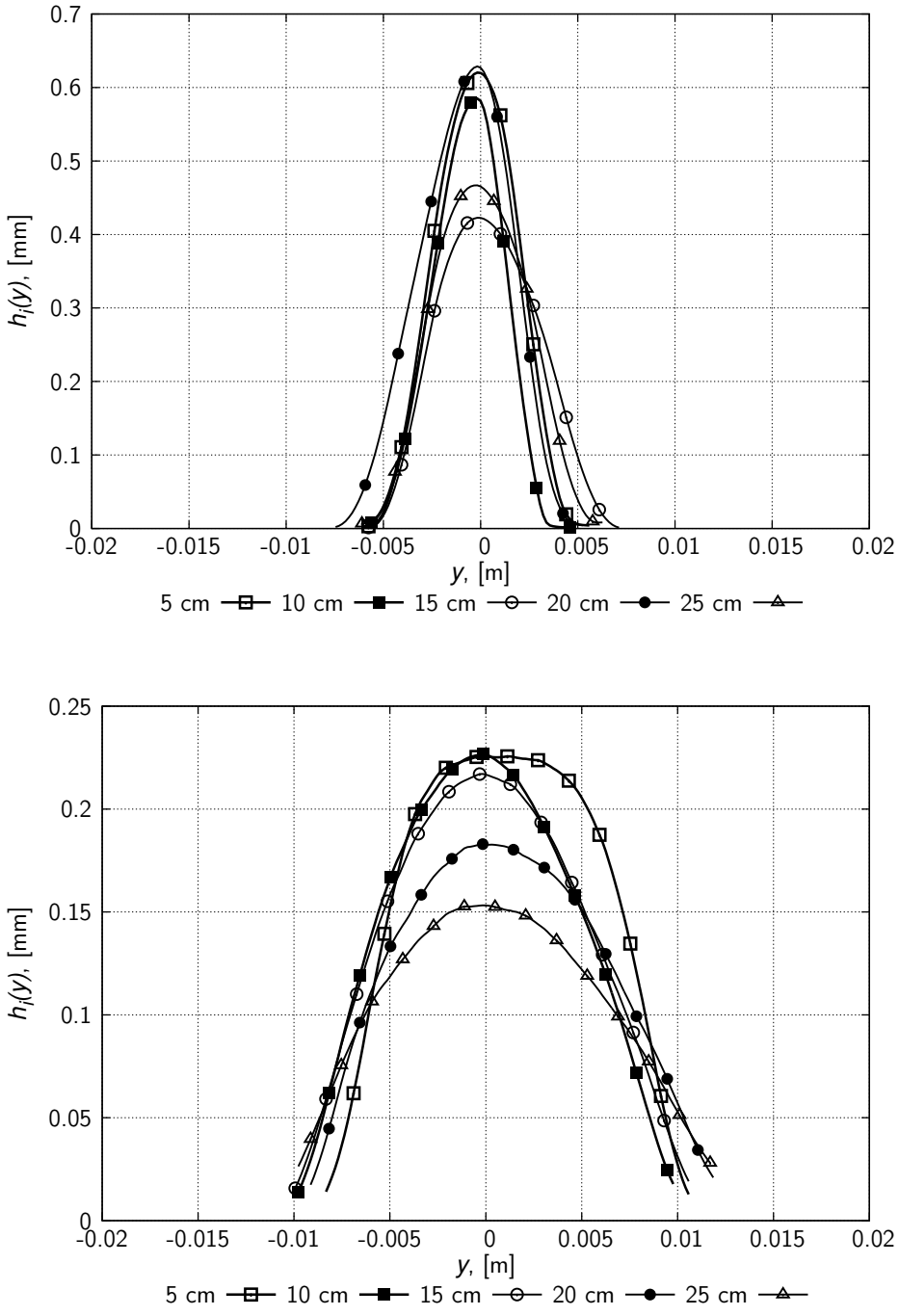

Figure E.1: Measured profile shapes along the plate for Water (upper) and tenzids, $\alpha = 60\,^\circ$ and $Q = 1.6 \cdot 10^{-6}\,\mathrm{m^3\,s^{-1}}$.

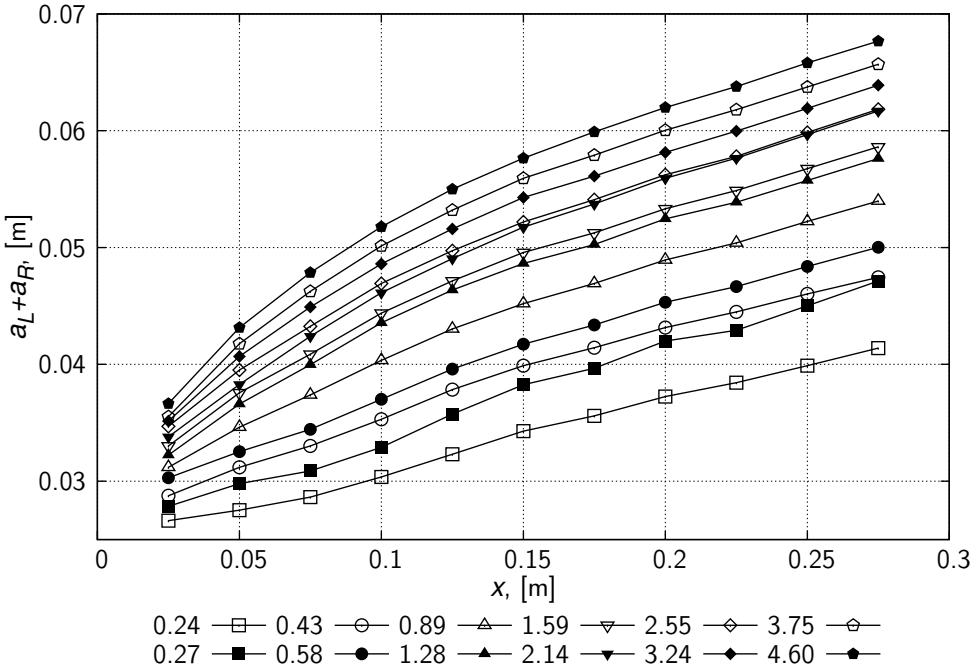

Figure E.2: Mean values of measured rivulet widths along the plate for DC 05 silicon oil, $\alpha = 45\,^\circ$. Liquid flow rates in $Q \cdot 10^{-6}\,\mathrm{m^3\,s^{-1}}$ are specified in graph legend.

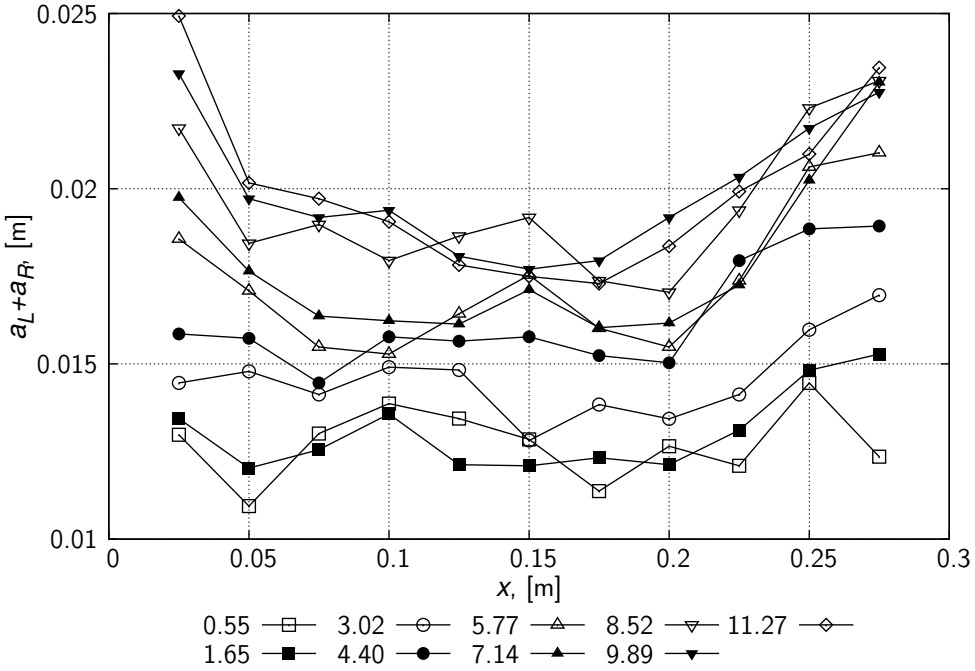

Figure E.3: Mean values of measured rivulet widths along the plate for water, $\alpha = 45\,^\circ$. Liquid flow rates in $Q \cdot 10^{-6}\,\mathrm{m^3\,s^{-1}}$ are specified in graph legend.

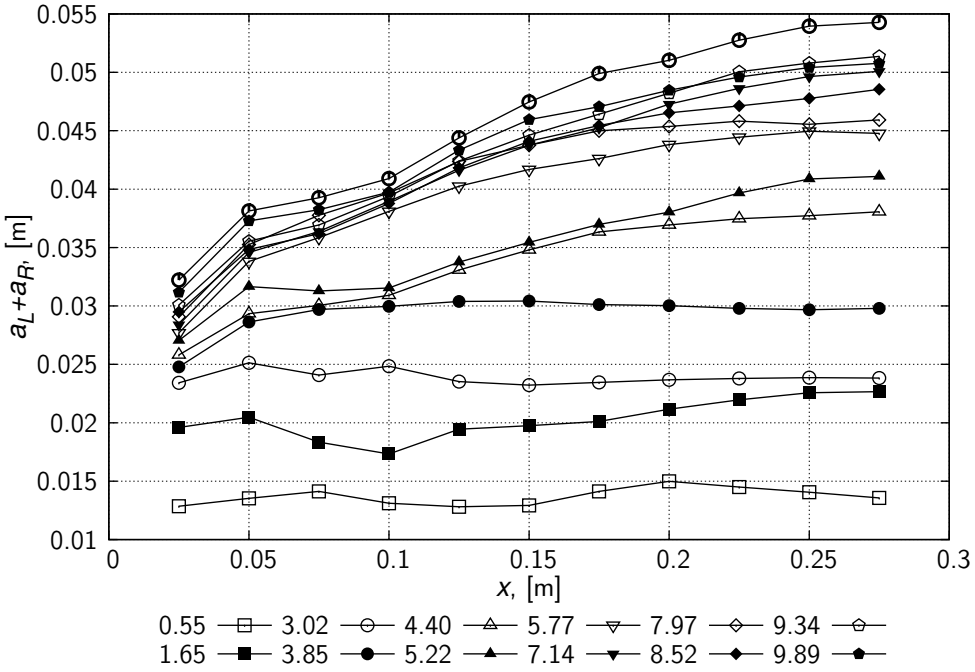

Figure E.4: Mean values of measured rivulet widths along the plate for tenzids, $\alpha = 45\,^\circ$. Liquid flow rates in $Q \cdot 10^{-6}\,\mathrm{m^3\,s^{-1}}$ are specified in graph legend.

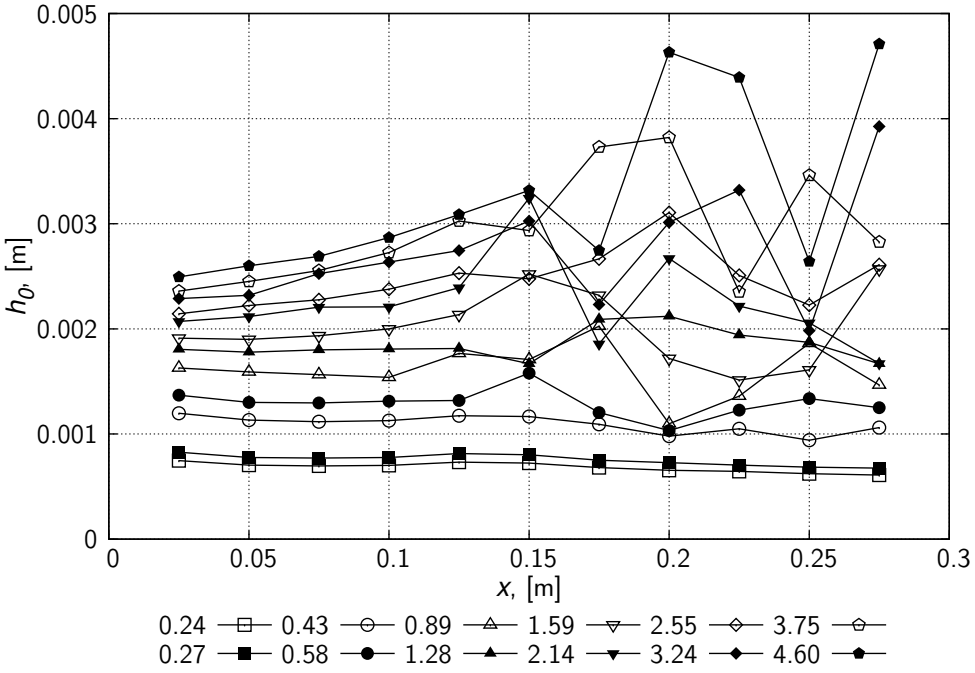

Figure E.5: Mean values of measured rivulet heights along the plate for DC 05 silicon oil, $\alpha = 45\,^\circ$. Liquid flow rates in $Q \cdot 10^{-6}\,\mathrm{m^3\,s^{-1}}$ are specified in graph legend.

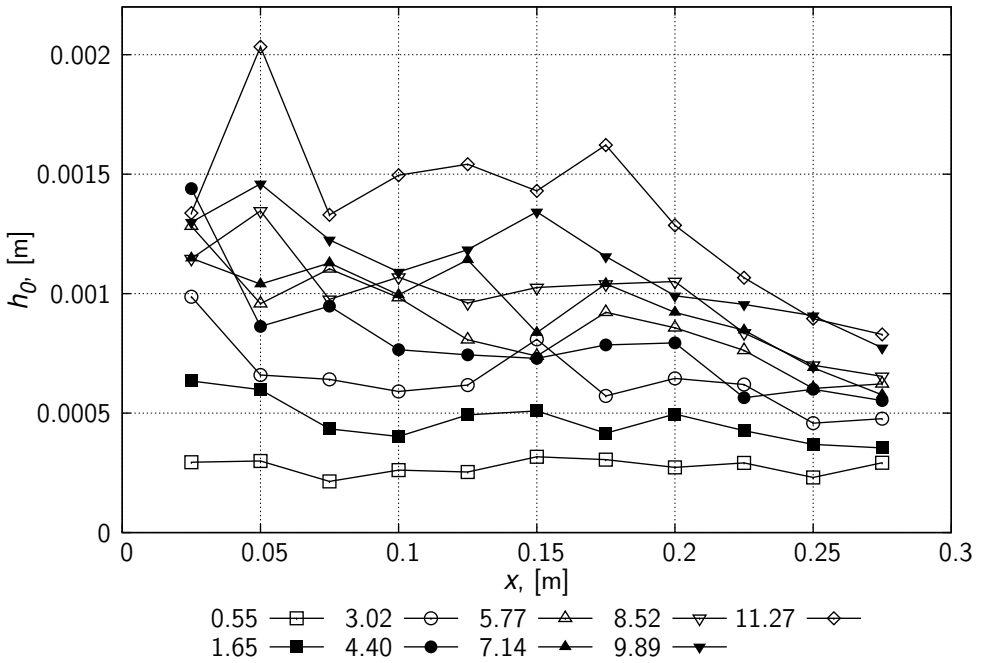

Figure E.6: Mean values of measured rivulet heights along the plate for water, $\alpha = 45\,^{\circ}$. Liquid flow rates in $Q \cdot 10^{-6}\,\mathrm{m^3\,s^{-1}}$ are specified in graph legend.

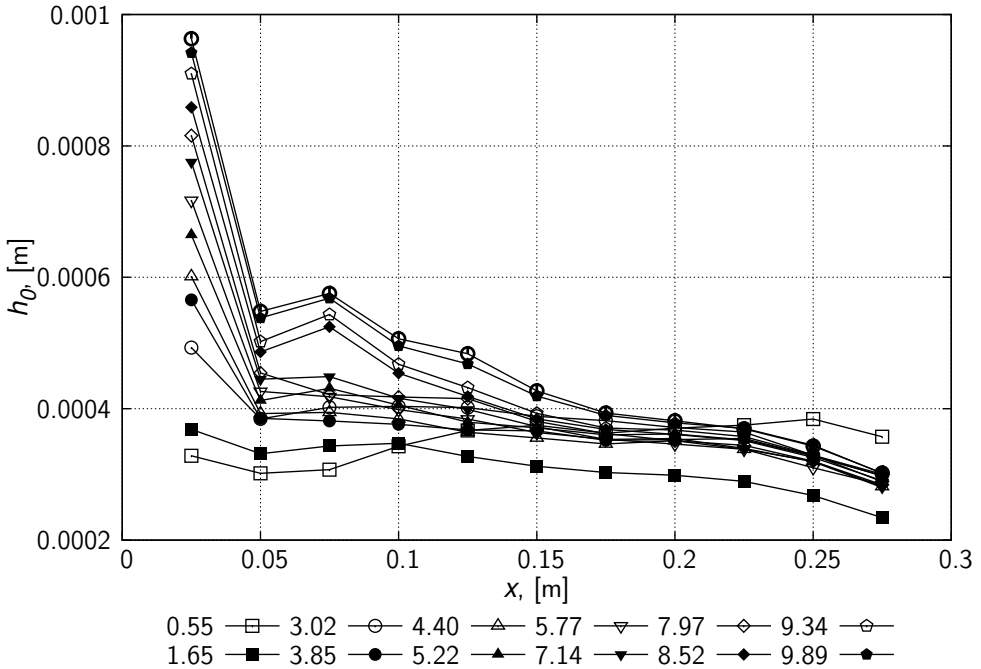

Figure E.7: Mean values of measured rivulet heights along the plate for tenzids, $\alpha = 45\,^{\circ}$. Liquid flow rates in $Q \cdot 10^{-6}\,\mathrm{m^3\,s^{-1}}$ are specified in graph legend.

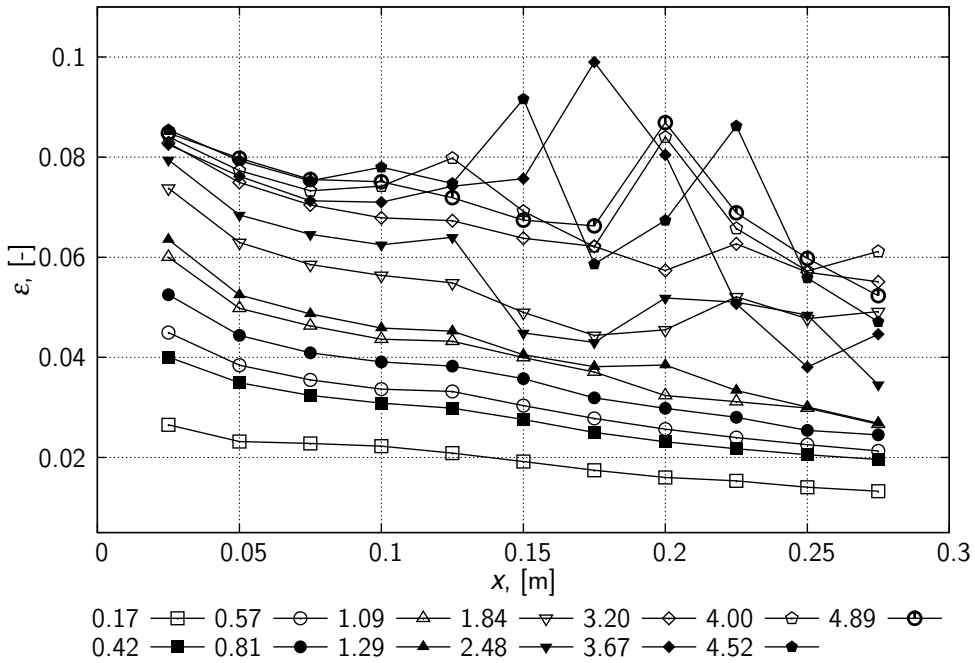

Figure E.8: Rivulet centerline height to width ratio for DC 10 silicon oil, $\alpha = 45\,°$. Liquid flow rates in $Q \cdot 10^{-6}\,\mathrm{m^3\,s^{-1}}$ are specified in graph legend.

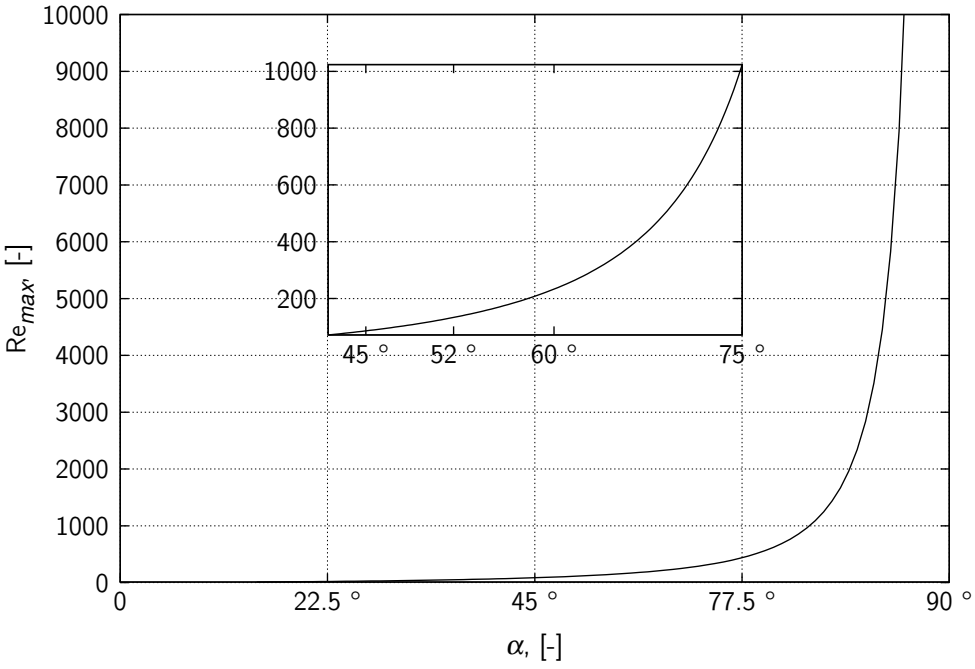

Figure E.9: Dependence of Re_{max} on the plate inclination angle, α, for DC 10 silicon oil. The part of the curve corresponding to measured α's is in the enhanced area.

F. Theoretical results

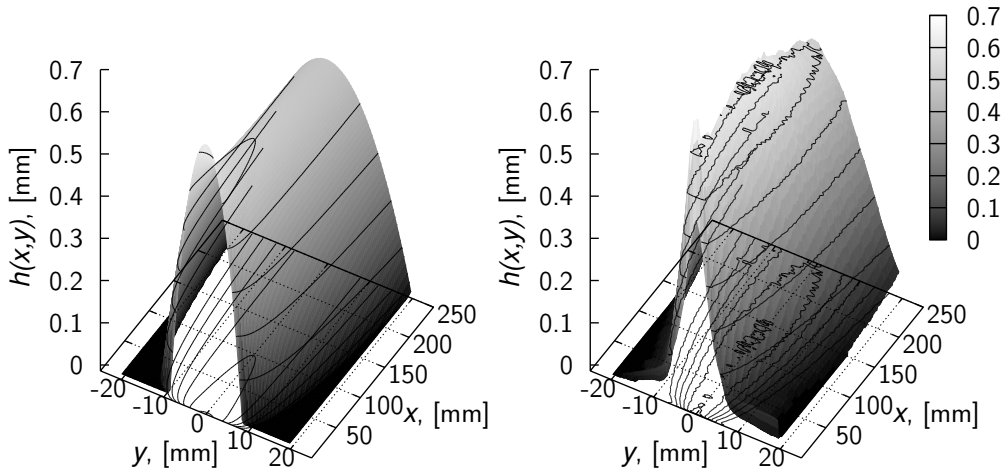

Figure F.1: Comparison of simulated (left) and measured gas-liquid interface of a DC 10 rivulet, $\alpha = 52\,^{\circ}$, $Q = 0.42 \cdot 10^{-6}\,\mathrm{m^3\,s^{-1}}$.

G. Contents of the attached DVD

There is a DVD distributed with this thesis. Its contents is divided in folders listed below.

Text

The folder containing the text of the thesis in .pdf

RivuletExpDataProcessing

Folder with the source codes to the program for experimental data evaluation. The program can be launched from MATLAB by running the file `RivuletExpDataProcessing.m`. Please note, that the program is own work of author of the thesis and is distributed freely, under MIT License [58], copy of which you should obtain with it.

Sample datasets

Examples with measured data for DC 05, $\alpha = 45\,^\circ$ and DC 10, $\alpha = 60\,^\circ$ silicon oils for testing of the data evaluation program.

Example of processed data

Folder with the various program outputs from processing the DC 05 sample dataset. The folder contains also the outputs from the `treshInflStudy.m` and `fitIFA.m` standalone functions.

Literature

The folder with literature concerning the studied problem divided in subfolders by their themes.